DNA 3921F

IMPACT AND PENETRATION TECHNOLOGY PROGRAM PARAMETRIC STUDY.

Avco Systems Division
201 Lowell Division
Wilmington, Massachusetts 01887

18 DNA, SBIE

19 3921F, AD-E300139

11 7 May 1976

12 138 p.

9 Final Report, [redacted] 18 Feb [redacted]–31 Dec [redacted]75;

CONTRACT No. DNA 001-75-C-0181

15

14 AVSD-0055-76-RR

APPROVED FOR PUBLIC RELEASE; DISTRIBUTION UNLIMITED.

10 D. Henderson

THIS WORK SPONSORED BY THE DEFENSE NUCLEAR AGENCY
UNDER RDT&E RMSS CODE B344075464 Y99QAXS04807 H2590D.

16

17 B048

Prepared for
Director
DEFENSE NUCLEAR AGENCY
Washington, D. C. 20305

404 788

Destroy this report when it is no longer needed. Do not return to sender.

UNCLASSIFIED

SECURITY CLASSIFICATION OF THIS PAGE *(When Data Entered)*

REPORT DOCUMENTATION PAGE		READ INSTRUCTIONS BEFORE COMPLETING FORM
1. REPORT NUMBER DNA 3921F	2. GOVT ACCESSION NO.	3. RECIPIENT'S CATALOG NUMBER
4. TITLE *(and Subtitle)* IMPACT AND PENETRATION TECHNOLOGY PROGRAM PARAMETRIC STUDY		5. TYPE OF REPORT & PERIOD COVERED Final Report for Period 18 Feb 75—31 Dec 75
		6. PERFORMING ORG. REPORT NUMBER AVSD-0055-76-RR
7. AUTHOR(s) D. Henderson		8. CONTRACT OR GRANT NUMBER(s) DNA 001-75-C-0181
9. PERFORMING ORGANIZATION NAME AND ADDRESS Avco Systems Division 201 Lowell Street Wilmington, Massachusetts 01887		10. PROGRAM ELEMENT, PROJECT, TASK AREA & WORK UNIT NUMBERS NWED Subtask Y99QAXSB048-07
11. CONTROLLING OFFICE NAME AND ADDRESS Director Defense Nuclear Agency Washington, D.C. 20305		12. REPORT DATE 7 May 1976
		13. NUMBER OF PAGES 142
14. MONITORING AGENCY NAME & ADDRESS*(if different from Controlling Office)*		15. SECURITY CLASS *(of this report)* UNCLASSIFIED
		15a. DECLASSIFICATION/DOWNGRADING SCHEDULE

16. DISTRIBUTION STATEMENT *(of this Report)*

Approved for public release; distribution unlimited.

17. DISTRIBUTION STATEMENT *(of the abstract entered in Block 20, if different from Report)*

18. SUPPLEMENTARY NOTES

This work sponsored by the Defense Nuclear Agency under RDT&E RMSS Code B344075464 Y99QAXSB04807 H2590D.

19. KEY WORDS *(Continue on reverse side if necessary and identify by block number)*

Terradynamic Impact and Penetration Performance
Influence of Media, Velocity, Orientation, W/A and L/D on Penetration Performance
Ricochet Predictions

20. ABSTRACT *(Continue on reverse side if necessary and identify by block number)*

A series of parametric studies are performed to predict the influence of variations in media, velocity, orientation, W/A and L/D on terradynamic impact and penetration performance for representative earth penetrator configuration. Ricochet predictions are also made for particular earth penetrator configurations.

→ next page

DD FORM 1 JAN 73 1473 EDITION OF 1 NOV 65 IS OBSOLETE

UNCLASSIFIED

SECURITY CLASSIFICATION OF THIS PAGE *(When Data Entered)*

20. ABSTRACT (Continued)

The parametric study was performed using an Avco-developed differential force law. The basic equations used are presented and discussed.

The results of the parametric studies are presented in summary form and the significance of the data discussed.

PREFACE

This final report documents the results of a parametric study conducted to determine the influence of pertinent parameters on the terradynamic impact and penetration performance of candidate earth penetrators. The results of the study are in the form of trajectory and loading environment histories plus graphs which summarize performance trends. The influence of media, orientation (i.e., obliquity and angle of attack), velocity, penetrator weight to cross sectional area ratio, and penetrator length to diameter ratio were investigated.

The program was conducted by Avco Systems Division under Contract DNA001-75-C-0181 for the Defense Nuclear Agency. The work was administered under the direction of Major T. Stong.

CONTENTS

ILLUSTRATIONS

ILLUSTRATIONS (Cont'd)

ILLUSTRATIONS (Cont'd)

ILLUSTRATIONS (Concl'd)

TABLES

1.0 SUMMARY

A Terradynamic Impact and Penetration Parametric study has been conducted in which the three principal parameters, i.e., impact conditions, earth penetrator configuration, and target media characteristics, were varied to establish their effect on the penetration events in question. The results of the study are in the form of trajectory and loading environment histories plus graphs which summarize performance trends. Performance trends refer to selected event characteristics such as:

- rigid body accelerations,
- penetration depths,
- local pressures and shears, and
- ricochet characteristics.

A brief description of the computer codes used to conduct this study is provided in Section 3.0.

A detailed discussion of the study and its results is provided in Sections 4 and 5. In Section 5.0, summary curves and tables are provided which convey the basic trends and results of the study. The detailed trajectory histories will be provided under separate cover to DNA.

2.0 INTRODUCTION

The main objectives of this study are:

1. Determine if the differential force law was capable of correctly accounting for variations in target media.
2. Establish, parametrically, a conceptual understanding of the loading environments imposed on an earth penetrator from impact through detonation.

The basic mission of an EP includes:

- delivery to the surface of the target with a given set of impact conditions, i.e., velocity, obliquity, and angle of attack.
- the impact phase during which peak structural design loads will usually be experienced.
- the penetration phase.
- detonation.

In order to evaluate and develop an EP weapon system, the TI&P performance characteristics must be well defined. TI&P characteristics are required for two important reasons. These are:

1. Impact Loading Environments
   These are necessary to EP structural design, component survival, and functioning.
2. EP Terradynamic Performance
   This information is required for overall system performance and effectiveness evaluation.

With a complete parametric data base (of which this study is only a part) consisting of the two performance characteristics, other aspects associated with the development of an EP weapon system can be addressed. These other aspects include:

- payload and component designation.
- EP packaging studies.
- EP structural design.
- component design.
- target selection.
- target vulnerability.
- EP effectiveness.

- collateral damage.
- delivery system considerations.

For this study, the TI&P characteristics were established through the 2D and 3D Terradynamic Impact and Penetration Simulator Computer Codes developed at Avco Systems Division. These codes are described in detail in Section 3.0.

The parametric study was divided into six parts, each part being selected for the purpose of investigating certain EP performance phenomena. The parts include the following series.

Series 1

To determine the sensitivity of media variations which are represented by resistance-to-penetration phenomena used in the 2D and 3D codes.

Series 2

To determine the effects of ballistic parameter (i.e., projectile weight/cross section area) and velocity on TI&P performance.

Series 3

To determine the effects of obliquity and angle of attack on TI&P performance.

Series 4

To determine the effects of L/D (i.e., EP length/diameter) on terradynamic stability.

Series 5

To investigate the relationships between basic media engineering properties and resistance-to-penetration phenomena, and to predict the performance of a specific impact event to be conducted at the Tonapa test site in New Mexico.

Series 6

To determine the ricochet performance characteristics of the Mk 82 and Mk 84 bomb warheads.

The specific matrix of runs for these series are provided in Section 4.0 along with example results from each series. The complete parametric study results are provided under separate cover to DNA. The parametric study results are summarized and discussed in Section 5.0.

3.0 IMPACT AND PENETRATION SIMULATOR

Avco's approach to the analytical simulation (or prediction) of a terradynamic impact and penetration event involves the use of a differential force law. The derived forces or pressures (both normal and tangential) are integrated over the surface of any specified body of revolution to establish resulting loads. The equations of motion are written (1, 2, or 3 dimensional) and are solved to obtain rigid body acceleration, velocity, and trajectory histories. The approach is basically the same as used in present aerodynamic trajectory analysis problems, except for the specific form of the force law, and the discontinuous nature of a typical impacted media.

Avco has developed these terradynamic trajectory programs for consideration of the unique characteristics of typical target media and to incorporate what we call Avco's General Resistance-to-Penetration Force Law. This force law simply states the assumed form of several possible resistance-to-penetration phenomena that can occur during a terradynamic impact event. These phenomena include:

- basic structural resistance to penetration.
- equivalent fluid flow.
- compressibility effects.
- surface effects.

The analytical form of this force law is:

$$\text{Normal Pressure} = \frac{dF}{dA} = \eta + 1/2\,\rho\,V^2\,C_N \sin^2\zeta + k\,V\epsilon^{-\alpha t}(t-\tau)$$

$$\text{Shear Pressure} = \frac{dF}{dA} = f_c\eta + 1/2\,\rho V^2\,C_\tau \sin\zeta\cos\zeta + f_c k\,V\epsilon^{-\alpha t}(t-\tau)$$

where:

η = Basic structural resistance to penetration

ρ = Media density

V = Local absolute velocity vector

C_N = Normal equivalent flow coefficient

ζ = Local incidence angle

k = Relative acoustic impedance between impacted media and penetrator

a = Exponential decay factor

$(t-\tau)$ = Mathematical control on the timing of compressibility effects

f_c = Coefficient of friction

C_τ = Shear equivalent flow coefficient.

The level of influence of these phenomena for any specific impact event is controlled by the values of the functional arguments which can vary with respect to time, velocity, or displacement.

Over the past several years, Avco has obtained values of these coefficients, empirically, for many representative media through laboratory and ballistic tests. The procedures used are equivalent to obtaining the lift drag coefficients of models in wind tunnels for the aerodynamic problem. The pertinent laboratory tests included:

- moisture content analysis.
- sieve analysis.
- wave velocity measurements in the media.
- static resistance to penetration tests.
- penetrometer tests.

The ballistic tests included:

- firing models and scale projectiles into instrumented media samples at varying impact velocities and impact angles, and measuring velocity and displacement (angular and translational) histories.
- firing instrumented full scale projectiles into hard (concrete) targets and measuring acceleration and structural strain histories, directly. These data were obtained through telemetry and recorded on high speed magnetic tape systems.
- performing reverse ballistic testing in which the target media was fired at instrumented EP's and distributed strain histories were obtained by conventional "hard lined" instrumentation systems.

The laboratory tests specifically yield the structural resistance-to-penetration terms, the degree of influence of compressibility effects, and a first estimate of the influence of the equivalent flow terms.

Through data reduction and analysis of the ballistic tests, specific dynamic values of η, f_c, C_N, and C_r have been obtained. This procedure has allowed Avco to characterize many target media and to simulate the behavior of many full scale projectiles impacting these media. Accurate simulations of the terradynamic performance of several rocket configurations, artillery rounds, EP's, etc., relative to trajectory, loads and critical ricochet angle have been made and agree well with actual field tests over the past several years.

This approach is relatively straightforward and, similar to aerodynamic loads and trajectory analysis techniques, gives reasonably accurate engineering solutions to complex problems which otherwise would remain unsolved. These codes were used exclusively to conduct the parametric study described in this report. This technique which represents the only capability for efficiently analyzing 3-D penetration problems is not without its limitations. Compared with the finite-difference technique now available, the force law approach cannot produce as much detail in a given calculation. But, it is important to note that the current finite-difference calculations are limited to axisymetric calculations and the cost is one to two orders of magnitude greater than a corresponding force law calculation.

The limitations of the present force law technique are associated with the simplification regarding media response, distributed pressures and shears are based upon the character of the formulations presented above, the direction and level of the assumed total velocity field (which is based solely upon rigid body motion of the projectile) and whether a given location on the projectile is in the shadow of the assumed parallel flow field or not. The finite-difference approach models the response of the media and therefore computes such phenomena as separation, compaction, etc.

4.0 EARTH PENETRATOR PARAMETRIC STUDY

As discussed in Section 2.0, the terradynamic parametric study was divided into six series, the purpose of and the specific conditions of which are listed in Tables 1-6 and 7-12.

Two sets of tables are provided: the first set being the initial proposed parametric study and the second (identified by "M" for modified) set consisting of the deletions and additions to the final matrix of runs to be conducted. Wherever possible, the original numbering system was retained to identify specific cases.

The principal target media for which this study was conducted was a particularly hard (i.e., high resistance-to-penetration) concrete. Concrete resistance-to-penetration can vary by as much as 200 percent depending on its age, basic unconfined compressive strength, and the type and size of the rock aggregate employed in the mix. The resistance-to-penetration parameter used in the general resistance-to-penetration force law (described in Section 3) is "η" and this parameter was assigned a value of 50,000 psi for the majority of the study. To relate this value to some equivalent homogeneous media of known physical characteristics, some conversion technique is required. The "η" term is representative of the local applied pressure exerted on the EP which causes media failure neglecting inertial effects. Any proven model which has been formulated to calculate this pressure can be used to relate the value of the "η" term to media physical properties. Such a method is the so-called "Cavity Expansion Theory" (first used for the penetration problem by J. N. Goodier of Stanford Research Institute). The basic terms in the "Cavity Expansion Theory" are similar to Avco's force law and include:

- basic media resistance-to-penetration.
- inertial effects.
- apparent mass effects.

There is, therefore, a one to one correspondence between the two models in at least the first terms.

TABLE 1

SERIES NO. 1 - PREL.
SENSITIVITY STUDY

Problem Number	Type 2D 3D	Projectile Data				Velocity (ft/sec)	Obliquity γ (deg)	Attack Angle α (deg)	Material Property
		W/A (psi)	D (in)	Nose Remarks CRH	Nose Remarks Weight (lb)				
1-1	2D	12.1	6.5	9.25	400	1500	0	0	Std σ_c = 5000 psi
1-2	2D	12.1	6.5	9.25	400	1500	0	3	Std σ_c = 5000 psi
1-3	2D	12.1	6.5	9.25	400	1500	0	0	Vary η +50%
1-4	2D	12.1	6.5	9.25	400	1500	0	3	Vary η +50%
1-5	2D	12.1	6.5	9.25	400	1500	0	0	Vary f +50%
1-6	2D	12.1	6.5	9.25	400	1500	0	3	Vary f +50%
1-7	2D	12.1	6.5	9.25	400	1500	0	0	Vary C_T +50%
1-8	2D	12.1	6.5	9.25	400	1500	0	3	Vary C_T =50%
1-9	2D	12.1	6.5	9.25	400	1500	0	0	Vary C_N =50%
1-10	2D	12.1	6.5	9.25	400	1500	0	3	Vary C_N +50%
1-11	2D	12.1	6.5	9.25	400	1500	0	0	Vary k +50%
1-12	2D	12.1	6.5	9.25	400	1500	0	3	Vary k +50%
1-13	2D	12.1	6.5	9.25	400	1500	0	0	Vary a +50%
1-14	2D	12.1	6.5	9.25	400	1500	0	3	Vary a +50%
1-15	DELETED								
1-16									
1-17	2D	12.1	6.5	9.25	400	1500	20	0	Std σ_c = 5000 psi
1-18	2D	12.1	6.5	9.25	400	1500	20	3	Std σ_c = 5000 psi
1-19	2D	12.1	6.5	9.25	400	1500	20	0	Most Sensitive Parameter Determined Above Varied 50%
1-20	2D	12.1	6.5	9.25	400	1500	20	3	

TABLE 2

SERIES NO. 2 - PREL.
VARIATIONS IN W/A AND VELOCITY

Problem Number	Type 2D or 3D	Projectile Data				Velocity (ft/sec)	Obliquity γ (deg)	Attack Angle α (deg)	Material Property Standard Concrete 5000 psi
		W/A (psi)	D (in)	Nose Remarks					
				CRH	Weight (lb)				
2-1	2D	12.1	6.5	9.25	400	500	0	0	Std
2-2	2D	12.1	6.5	9.25	400	1000	0	0	Std
2-3	3D	12.1	6.5	9.25	400	1500	0	0	Std
2-4	2D	12.1	6.5	9.25	400	2000	0	0	Std
2-5	2D	12.1	6.5	9.25	400	2500	0	0	Std
2-6	3D	12.1	6.5	9.25	400	3000	0	0	Std
2-7	2D	6.0	6.5	9.25	200	1000	0	0	Std
2-8	2D	6.0	6.5	9.25	200	2000	0	0	Std
2-9	2D	6.0	6.5	9.25	200	3000	0	0	Std
2-10	2D	18.0	6.5	9.25	600	1000	0	0	Std
2-11	2D	18.0	6.5	9.25	600	2000	0	0	Std
2-12	2D	18.0	6.5	9.25	600	3000	0	0	Std
2-13	2D	24.0	6.5	9.25	800	1000	0	0	Std
2-14	2D	24.0	6.5	9.25	800	2000	0	0	Std
2-15	2D	24.0	6.5	9.25	800	3000	0	0	Std
2-16	2D	30.0	6.5	9.25	1000	1000	0	0	Std
2-17	2D	30.0	6.5	9.25	1000	2000	0	0	Std
2-18	2D	30.0	6.5	9.25	1000	3000	0	0	Std
2-19	2D	31.8	4.0	9.25	400	1000	0	0	Std
2-20	2D	31.8	4.0	9.25	400	2000	0	0	Std
2-21	2D	31.8	4.0	9.25	400	3000	0	0	Std
2-22	2D	8.0	8.0	9.25	400	1000	0	0	Std
2-23	2D	8.0	8.0	9.25	400	2000	0	0	Std
2-24	2D	8.0	8.0	9.25	400	3000	0	0	Std

TABLE 3

SERIES NO. 3 - PREL.
VARIATIONS IN OBLIQUITY AND ANGLE OF ATTACK

Problem Number	Type 2D 3D	Projectile Data				Velocity (ft/sec)	Obliquity γ (deg)	Attack Angle α (deg)	Material Property Standard Concrete σ_c = 5000 psi
		W/A (psi)	D (in)	Nose Remarks CRH	Nose Remarks Weight (lb)				
3-1	3D	12.1	6.5	9.25	400	1500	0	0	Std
3-2	3D	12.1	6.5	9.25	400	1500	5	0	Std
3-3	3D	12.1	6.5	9.25	400	1500	10	0	Std
3-4	3D	12.1	6.5	9.25	400	1500	20	0	Std
3-5	3D	12.1	6.5	9.25	400	1500	30	0	Std
3-6	3D	12.1	6.5	9.25	400	1500	40	0	Std
3-7	3D	12.1	6.5	9.25	400	1500	50	0	Std
3-8	3D	12.1	6.5	9.25	400	1500	60	0	Std
3-9	2D	12.1	6.5	9.25	400	1500	0	+1	Std
3-10	3D	12.1	6.5	9.25	400	1500	0	+2	Std
3-11	2D	12.1	6.5	9.25	400	1500	0	+3	Std
3-12	2D	12.1	6.5	9.25	400	1500	0	+5	Std
3-13	2D	12.1	6.5	9.25	400	1500	0	-1	Std
3-14	3D	12.1	6.5	9.25	400	1500	0	-2	Std
3-15	2D	12.1	6.5	9.25	400	1500	0	-3	Std
3-16	2D	12.1	6.5	9.25	400	1500	0	-5	Std
3-17	2D	12.1	6.5	9.25	400	1500	20	+1	Std
3-18	3D	12.1	6.5	9.25	400	1500	20	+2	Std
3-19	2D	12.1	6.5	9.25	400	1500	20	+3	Std
3-20	2D	12.1	6.5	9.25	400	1500	20	+5	Std
3-21	2D	12.1	6.5	9.25	400	1500	20	-1	Std
3-22	3D	12.1	6.5	9.25	400	1500	20	-2	Std
3-23	2D	12.1	6.5	9.25	400	1500	20	-3	Std
3-24	2D	12.1	6.5	9.25	400	1500	20	-5	Std
3-25	2D	12.1	6.5	9.25	400	500	0	0	Std
3-26	2D	12.1	6.5	9.25	400	500	5	0	Std
3-27	2D	12.1	6.5	9.25	400	500	10	0	Std
3-28	2D	12.1	6.5	9.25	400	500	20	0	Std
3-29	2D	12.1	6.5	9.25	400	500	30	0	Std
3-30	2D	12.1	6.5	9.25	400	500	40	0	Std

TABLE 3 (Concl'd)

SERIES NO. 3

Problem Number	Type 2D 3D	Projectile Data				Velocity (ft/sec)	Obliquity α (deg)	Attack Angle a (deg)	Material Property Standard Concrete σ_c = 5000 psi
		W/A (psi)	D (in)	Nose Remarks					
				CRH	SLA Canadian				
3-31	2D	12.1	6.5	9.25	400	2500	0	0	Std
3-32	2D	12.1	6.5	With Tip	400	2500	5	0	Std
3-33	2D	12.1	6.5	With Tip	400	2500	10	0	Std
3-34	2D	12.1	6.5	With Tip	400	2500	20	0	Std
3-35	2D	12.1	6.5	With Tip	400	2500	30	0	Std
3-36	2D	12.1	6.5	With Tip	400	2500	40	0	Std
3-37	2D	12.1	6.5	With Tip	400	2500	50	0	Std
3-38	2D	12.1	6.5	With Tip	400	2500	60	0	Std
3-39	3D	12.1	6.5	Blunt	Same L/D Wt as SLA	1500	0	0	Std
3-40	3D	12.1	6.5	Blunt	Same L/D Wt as SLA	1500	0	+2	Std
3-41	3D	12.1	6.5	Blunt	Same L/D Wt as SLA	1500	0	-2	Std
3-42	3D	12.1	6.5	Blunt	Same L/D Wt as SLA	1500	20	0	Std
3-43	3D	12.1	6.5	Blunt	Same L/D Wt as SLA	1500	20	+2	Std
3-44	3D	12.1	6.5	Blunt	Same L/D Wt as SLA	1500	20	-2	Std
3-45	3D	12.1	6.5	Blunt	Same L/D Wt as SLA	1500	10	0	Std
3-46	3D	12.1	6.5	Blunt	Same L/D Wt as SLA	1500	40	0	Std
3-47	3D	12.1	6.5	Blunt	Same L/D Wt as SLA	1500	60	0	Std
3-48	2D	12.1	6.5	Biconic	Same L/D Wt as SLA	1500	0	0	Std
3-49	2D	12.1	6.5	Biconic	Same L/D Wt as SLA	1500	20	0	Std
3-50	2D	12.1	6.5	Biconic	Same L/D Wt as SLA	1500	20	+2	Std
3-51	2D	12.1	6.5	Biconic	Same L/D Wt as SLA	1500	20	-2	Std
3-52	2D	12.1	6.5	Biconic	Same L/D Wt as SLA	1500	40	0	Std
3-53	2D	12.1	6.5	Biconic	Same L/D Wt as SLA	1500	60	0	Std
3-54	2D	12.1	6.5	9.25	SLA Canadian 400 lb	1000	0	0	Std
3-55	2D	12.1	6.5	9.25	SLA Canadian 400 lb	1000	20	0	Std
3-56	2D	12.1	6.5	9.25	SLA Canadian 400 lb	1000	40	0	Std
3-57	2D	12.1	6.5	9.25	SLA Canadian 400 lb	1000	0	0	Std
3-58	2D	12.1	6.5	9.25	SLA Canadian 400 lb	1000	20	0	Std
3-59	2D	12.1	6.5	9.25	SLA Canadian 400 lb	1000	40	0	Std
3-60	2D	24.0	6.5	9.25	800	500	20	+2	Std
3-61	2D	24.0	6.5	9.25	800	1000	20	+2	Std
3-62	2D	24.0	6.5	9.25	800	1500	20	+2	Std
3-63	2D	24.0	6.5	9.25	800	2000	20	+2	Std
3-64	2D	24.0	6.5	9.25	800	2500	20	+2	Std

TABLE 4

SERIES NO. 4 - PREL.
EFFECT OF L/D ON STABILITY

Problem Number	Type 2D 3D	Projectile Data W/A (psi)	D (in)	Nose Remarks CRH	Nose Remarks Weight (lb)	L/D	Velocity (ft/sec)	Obliquity γ (deg)	Attack Angle α (deg)	Material Property
4-1	2D	VARIABLE	6.5	9.25	400	10	1500	10	+2	Till
4-2	2D		6.5	9.25	480	12	1500	10	+2	Till
4-3	2D		6.5	9.25	320	8	1500	10	+2	Till
4-4	2D		6.5	9.25	240	6	1500	10	+2	Till
4-5	2D		6.5	9.25	400	10	2500	10	+2	Till
4-6	2D		6.5	9.25	480	12	2500	10	+2	Till
4-7	2D		6.5	9.25	320	8	2500	10	+2	Till
4-8	2D		6.5	9.25	240	6	2500	10	+2	Till
4-9	2D		6.5	Blunt	400	10	1500	10	+2	Till
4-10	2D		6.5	Blunt	240	6	1500	10	+2	Till
4-11	2D		6.5	Blunt	400	10	2500	10	+2	Till
4-12	2D		6.5	Blunt	240	6	2500	10	+2	Till
4-13	DELETED									
4-14	TO BE PLANNED AT A LATER DATE									
4-15										
4-16										
4-17										
4-18										
4-19										
4-20										

TABLE 5

SERIES NO. 5 - PREL.
MEDIA VARIATIONS

Problem Number	Type 2D 3D	Projectile Data				Velocity (ft/sec)	Obliquity α (deg)	Attack Angle α (deg)	Material Property
		W/A (psi)	D (in)	Nose Remarks CRH	Nose Remarks SLA Canadian				
5-1	2D	12.1	6.5	9.25	400	1500	0	0	σ_c = 5000 psi concrete
5-2	2D	12.1	6.5	9.25	400	1500	20	+2	σ_c = 5000 psi concrete
5-3	2D	12.1	6.5	9.25	400	2500	0	0	σ_c = 5000 psi concrete
5-4	2D	12.1	6.5	9.25	400	1500	0	0	σ_c = 3000 psi concrete
5-5	2D	12.1	6.5	9.25	400	1500	20	+2	σ_c = 3000 psi concrete
5-6	2D	12.1	6.5	9.25	400	2500	0	0	σ_c = 3000 psi concrete
5-7	2D	12.1	6.5	9.25	400	1500	0	0	"Asphalt"
5-8	2D	12.1	6.5	9.25	400	1500	20	+2	"Asphalt"
5-9	2D	12.1	6.5	9.25	400	2500	0	0	"Asphalt"
5-10	2D	12.1	6.5	9.25	400	1500	0	0	"Till"
5-11	2D	12.1	6.5	9.25	400	1500	20	+2	"Till"
5-12	2D	12.1	6.5	9.25	400	2500	0	0	"Till"
5-13	2D	RESERVED FOR ATTEMPTED SIMULATION OF SELECTED ROCK PENETRATION TESTS TO BE CONDUCTED BY SLA IN SPRING OF FY75							
5-14	2D								
5-15	2D								
5-16	2D								
5-17	2D								
5-18	2D								
5-19	2D								
5-20	2D								
5-21	2D								
5-22	2D								
5-23	2D								
5-24	2D								
5-25	2D								
5-26	2D								
5-27	2D								
5-28	2D								
5-29	2D	RESERVED FOR SPECIAL ORDER OF DR. BOB ROHANI, WESSD							
5-30	2D								
5-31	2D								
5-32	2D								
5-33	2D								
5-34	2D								
5-35	2D								
5-36	2D								
5-37	2D								
5-38	2D								
5-39	2D								
5-40	2D								

TABLE 6

SERIES NO. 6 - PREL.
RICOCHET PREDICTIONS

Problem Number	Type 2D 3D	Projectile Data			Velocity (ft/sec)	Obliquity γ (deg)	Attack Angle α (deg)	Material Property Standard Concrete σ_c = 5000 psi
		W/A (psi)	D (in)	Nose Remarks				
6-1	2D	To Be Selected			1500	0	0	Std
6-2	2D	To Be Selected			1500	20	0	Std
6-3	2D	To Be Selected			1500	40	0	Std
6-4	2D	To Be Selected			1500	20	2	Std
6-5	2D	To Be Selected			2500	0	0	Std
6-6	2D	To Be Selected			2500	20	2	Std
6-7	2D	To Be Selected			1500	0	0	Std
6-8	2D	To Be Selected			1500	20	0	Std
6-9	2D	To Be Selected			1500	40	0	Std
6-10	2D	To Be Selected			1500	20	2	Std
6-11	2D	To Be Selected			2500	0	0	Std
6-12	2D	To Be Selected			2500	20	2	Std
6-13	2D	To Be Selected			1500	0	0	Std
6-14	2D	To Be Selected			1500	20	0	Std
6-15	2D	To Be Selected			1500	40	0	Std
6-16	2D	To Be Selected			1500	20	2	Std
6-17	2D	To Be Selected			2500	0	0	Std
6-18	2D	To Be Selected			2500	20	2	Std
6-19	2D	To Be Selected			1500	0	0	Std
6-20	2D	To Be Selected			1500	20	0	Std
6-21	2D	To Be Selected			1500	40	0	Std
6-22	2D	To Be Selected			1500	20	2	Std
6-23	2D	To Be Selected			2500	0	0	Std
6-24	2D	To Be Selected			2500	20	2	Std

TABLE 7

SERIES NO. 1 - FINAL SENSITIVITY STUDY

Problem Number	Type 2D 3D	Projectile Data				Velocity (ft/sec)	Obliquity γ (deg)	Attack Angle α (deg)	Material Property	Run Number	Summary Figure No.
		W/A (psi)	D (in)	Nose Remarks: CRH	Nose Remarks: Weight (lb)						
1-1	2D	12.1	6.5	9.25	400	1500	0	0	Std σ_c = 5000 psi	1-1-1 to 1-1-5	19,21
1-2	2D	12.1	6.5	9.25	400	1500	0	3	Std σ_c = 5000 psi	1-2-1 to 1-2-5	20,22,23,24
1-3	2D	12.1	6.5	9.25	400	1500	0	0	Vary η +50%	1-3-1 to 1-3-5	19,21
1-4	2D	12.1	6.5	9.25	400	1500	0	3	Vary η +50%	1-4-1 to 1-4-5	20,22,23,24
1-5	2D	12.1	6.5	9.25	400	1500	0	0	Vary f +50%	1-5-1 to 1-5-5	19,21
1-6	2D	12.1	6.5	9.25	400	1500	0	3	Vary f +50%	1-6-1 to 1-6-5	20,22,23,24
1-7	2D	12.1	6.5	9.25	400	1500	0	0	Vary C_T +50%	1-7-1 to 1-7-5	19,21
1-8	2D	12.1	6.5	9.25	400	1500	0	3	Vary C_T +50%	1-8-1 to 1-8-5	20,22,23,24
1-9	2D	12.1	6.5	9.25	400	1500	0	0	Vary C_N +50%	1-9-1 to 1-9-5	19,21
1-10	2D	12.1	6.5	9.25	400	1500	0	3	Vary C_N +50%	1-10-1 to 1-10-5	20,22,23,24
1-11	2D	12.1	6.5	9.25	400	1500	0	0	Vary k +50%	1-11-1 to 1-11-5	
1-12	2D	12.1	6.5	9.25	400	1500	0	3	Vary k +50%	1-12-1 to 1-12-5	
1-13	2D	12.1	6.5	9.25	400	1500	0	0	Vary α +50%	1-13-1 to 1-13-5	
1-14	2D	12.1	6.5	9.25	400	1500	0	3	Vary α +50%	1-14-1 to 1-14-5	
1-15	DELETED										
1-16											
1-17	2D	12.1	6.5	9.25	400	1500	20	0	Std σ_c = 5000 psi	1-17-1 to 1-17-5	21
1-18	2D	12.1	6.5	9.25	400	1500	20	3	Std σ_c = 5000 psi	1-18-1 to 1-18-5	22
1-19	2D	12.1	6.5	9.25	400	1500	20	0	Most Sensitive Parameter Determined Above Varied 50% (found to be η)	1-19-1 to 1-19-5	
1-20	2D	12.1	6.5	9.25	400	1500	20	3		1-20-1 to 1-20-5	
1-2A	3D	12.1	6.5	9.25	400	1500	180*	3		1-2A-1 to 1-2A-10	
1-2AI	3D	12.1	6.5	9.25	400	1500	180*	3		1-2AI-1 to 1-2AI-11	Table 15
1-17A	3D	12.1	6.5	9.25	400	1500	200*	0		1-17A-1 to 1-17A-10	
1-18A	3D	12.1	6.5	9.25	400	1500	200*	3		1-18A-1 to 1-18A-10	

*Note: The 3-D code utilizes a different reference system than the 2-D code. See Figure 17 and 18 and Tables 13 and 14.

TABLE 8

SERIES NO. 2 - FINAL
VARIATIONS IN W/A AND VELOCITY

Problem Number	Type 2D or 3D	Projectile Data				Velocity (ft/sec)	Obliquity γ (deg)	Attack Angle α (deg)	Material Property Standard Concrete 5000 psi	Run Number	Summary Curve No.
		W/A (psi)	D (in)	Nose Remarks							
				CRH	Weight (lb)						
2-1	2D	12.1	6.5	9.25	400	500	0	0	Std	2-1-1 to 2-1-5	
2-2	2D	12.1	6.5	9.25	400	1000	0	0	Std	2-2-1 to 2-2-5	
2-3	3D	12.1	6.5	9.25	400	1500	0	0	Std	2-3-1 to 2-3-10	Table 16
2-4	2D	12.1	6.5	9.25	400	2000	0	0	Std	2-4-1 to 2-4-5	
2-5	2D	12.1	6.5	9.25	400	2500	0	0	Std	2-5-1 to 2-5-5	
2-6	3D	12.1	6.5	9.25	400	3000	0	0	Std	2-6-1 to 2-6-25	
2-7	2D	6.0	6.5	9.25	200	1000	0	0	Std	2-7-1 to 2-7-5	25
2-8	2D	6.0	6.5	9.25	200	2000	0	0	Std	2-8-1 to 2-8-5	
2-9	2D	6.0	6.5	9.25	200	3000	0	0	Std	2-9-1 to 2-9-5	26
2-10	2D	18.0	6.5	9.25	600	1000	0	0	Std	2-10-1 to 2-10-5	
2-11	2D	18.0	6.5	9.25	600	2000	0	0	Std	2-11-1 to 2-11-5	
2-12	2D	18.0	6.5	9.25	600	3000	0	0	Std	2-12-1 to 2-12-5	
2-13	2D	24.0	6.5	9.25	800	1000	0	0	Std	2-13-1 to 2-13-5	
2-14	2D	24.0	6.5	9.25	800	2000	0	0	Std	2-14-1 to 2-14-5	
2-15	2D	24.0	6.5	9.25	800	3000	0	0	Std	2-15-1 to 2-15-5	
2-16	2D	30.0	6.5	9.25	1000	1000	0	0	Std	2-16-1 to 2-16-5	
2-17	2D	30.0	6.5	9.25	1000	2000	0	0	Std	2-17-1 to 2-17-5	
2-18	2D	30.0	6.5	9.25	1000	3000	0	0	Std	2-18-1 to 2-18-5	
2-19	2D	31.8	4.0	9.25	400	1000	0	0	Std	2-19-1 to 2-19-5	
2-20	2D	31.8	4.0	9.25	400	2000	0	0	Std	2-20-1 to 2-20-5	
2-21	2D	31.8	4.0	9.25	400	3000	0	0	Std	2-21-1 to 2-21-5	
2-22	2D	8.0	8.0	9.25	400	1000	0	0	Std	2-22-1 to 2-22-5	
2-23	2D	8.0	8.0	9.25	400	2000	0	0	Std	2-23-1 to 2-23-5	
2-24	2D	8.0	8.0	9.25	400	3000	0	0	Std	2-24-1 to 2-24-5	
2-25	2D	21.1	5.0	9.25	400	1000	0	0	Std	2-25-1 to 2-25-5	
2-26	2D	21.1	5.0	9.25	400	1500	0	0	Std	2-26-1 to 2-26-5	
2-27	2D	21.1	5.0	9.25	400	2000	0	0	Std	2-27-1 to 2-27-5	
2-28	2D	21.1	5.0	9.25	400	3000	0	0	Std	2-28-1 to 2-28-5	
2-29	2D	12.1	6.5	0.5	400	500	0	0	Std	2-29-1 to 2-29-5	27
2-30	2D	12.1	6.5	0.5	400	1000	0	0	Std	2-30-1 to 2-30-5	28
2-31	2D	12.1	6.5	0.5	400	1500	0	0	Std	2-31-1 to 2-31-5	29
2-32	2D	12.1	6.5	0.5	400	2000	0	0	Std	2-32-1 to 2-32-5	
2-33	2D	12.1	6.5	0.5	400	2500	0	0	Std	2-33-1 to 2-33-5	
2-34	2D	12.1	6.5	0.5	400	3000	0	0	Std	2-34-1 to 2-34-5	
2-35	2D	18.0	6.5	0.5	600	1000	0	0	Std	2-35-1 to 2-35-5	
2-36	2D	18.0	6.5	0.5	600	2000	0	0	Std	2-36-1 to 2-36-5	27
2-37	2D	18.0	6.5	0.5	600	3000	0	0	Std	2-37-1 to 2-37-5	30
2-38	2D	30.0	6.5	0.5	1000	1000	0	0	Std	2-38-1 to 2-38-5	31
2-39	2D	30.0	6.5	0.5	1000	2000	0	0	Std	2-39-1 to 2-39-5	
2-40	2D	30.0	6.5	0.5	1000	3000	0	0	Std	2-40-1 to 2-40-5	
2-41	2D	12.1	6.5	2.25	400	500	0	0	Std	2-41-1 to 2-41-5	28
2-42	2D	12.1	6.5	2.25	400	1000	0	0	Std	2-42-1 to 2-42-5	32
2-43	2D	12.1	6.5	2.25	400	1500	0	0	Std	2-43-1 to 2-43-5	33

TABLE 8 (Concl'd)

Problem Number	Type 2D or 3D	Projectile Data				Velocity (ft/sec)	Obliquity γ (deg)	Attack Angle α (deg)	Material Property Standard Concrete 5000 psi	Run Number	Summary Curve No.
		W/A (psi)	D (in)	Nose Remarks: CRH	Nose Remarks: Weight (lb)						
2-44	2D	12.1	6.5	2.25	400	2000	0	0	Std	2-44-1 to 2-44-5	
2-45	2D	12.1	6.5	2.25	400	2500	0	0	Std	2-45-1 to 2-45-5	
2-46	2D	12.1	6.5	2.25	400	3000	0	0	Std	2-46-1 to 2-46-5	
2-47	2D	18.0	6.5	2.25	600	1000	0	0	Std	2-47-1 to 2-47-5	
2-48	2D	18.0	6.5	2.25	600	2000	0	0	Std	2-48-1 to 2-48-5	
2-49	2D	18.0	6.5	2.25	600	3000	0	0	Std	2-49-1 to 2-49-5	
2-50	2D	30.0	6.5	2.25	1000	1000	0	0	Std	2-50-1 to 2-50-5	
2-51	2D	30.0	6.5	2.25	1000	2000	0	0	Std	2-51-1 to 2-51-5	
2-52	2D	30.0	6.5	2.25	1000	3000	0	0	Std	2-52-1 to 2-52-5	
2-53	2D	12.1	6.5	6.0	400	500	0	0	Std	2-53-1 to 2-53-5	29
2-54	2D	12.1	6.5	6.0	400	1000	0	0	Std	2-54-1 to 2-54-5	34
2-55	2D	12.1	6.5	6.0	400	1500	0	0	Std	2-55-1 to 2-55-5	
2-56	2D	12.1	6.5	6.0	400	2000	0	0	Std	2-56-1 to 2-56-5	
2-57	2D	12.1	6.5	6.0	400	2500	0	0	Std	2-57-1 to 2-57-5	
2-58	2D	12.1	6.5	6.0	400	3000	0	0	Std	2-58-1 to 2-58-5	
2-59	2D	18.0	6.5	6.0	600	1000	0	0	Std	2-59-1 to 2-59-5	
2-60	2D	18.0	6.5	6.0	600	2000	0	0	Std	2-60-1 to 2-60-5	
2-61	2D	18.0	6.5	6.0	600	3000	0	0	Std	2-61-1 to 2-61-5	
2-62	2D	30.0	6.5	6.0	1000	1000	0	0	Std	2-62-1 to 2-62-5	
2-63	2D	30.0	6.5	6.0	1000	2000	0	0	Std	2-63-1 to 2-63-5	
2-64	2D	30.0	6.5	6.0	1000	3000	0	0	Std	2-64-1 to 2-64-5	
				L/D=1							
2-1A	2D	12.1	6.5	Blunt	43.36	500	0	0	Std	2-1A-1	
2-2A	2D	12.1	6.5	Blunt	43.36	1000	0	0	Std	2-2A-1 to 2-2A-5	
2-3A	2D	12.1	6.5	Blunt	43.36	1500	0	0	Std	2-3A-1 to 2-3A-5	
2-4A	2D	12.1	6.5	Blunt	43.36	2000	0	0	Std	2-4A-1 to 2-4A-5	
2-5A	2D	12.1	6.5	Blunt	43.36	2500	0	0	Std	2-5A-1 to 2-5A-5	
2-6A	2D	12.1	6.5	Blunt	43.36	3000	0	0	Std	2-6A-1 to 2-6A-5	
				L/D=2							
2-1B	2D	12.1	6.5	Blunt	86.71	500	0	0	Std	2-1B-1 to 2-1B-5	
2-2B	2D	12.1	6.5	Blunt	86.71	1000	0	0	Std	2-2B-1 to 2-2B-5	
2-3B	2D	12.1	6.5	Blunt	86.71	1500	0	0	Std	2-3B-1 to 2-3B-5	
2-4B	2D	12.1	6.5	Blunt	86.71	2000	0	0	Std	2-4B-1 to 2-4B-5	
2-5B	2D	12.1	6.5	Blunt	86.71	2500	0	0	Std	2-5B-1 to 2-5B-5	
2-6B	2D	12.1	6.5	Blunt	86.71	3000	0	0	Std	2-6B-1 to 2-6B-5	
				L/D=3							
2-1C	2D	12.1	6.5	Blunt	130.06	500	0	0	Std	2-1C-1 to 2-1C-5	
2-2C	2D	12.1	6.5	Blunt	130.06	1000	0	0	Std	2-2C-1 to 2-2C-5	
2-3C	2D	12.1	6.5	Blunt	130.06	1500	0	0	Std	2-3C-1 to 2-3C-5	
2-4C	2D	12.1	6.5	Blunt	130.06	2000	0	0	Std	2-4C-1 to 2-4C-5	
2-5C	2D	12.1	6.5	Blunt	130.06	2500	0	0	Std	2-5C-1 to 2-5C-5	
2-6C	2D	12.1	6.5	Blunt	130.06	3000	0	0	Std	2-6C-1 to 2-6C-5	
2-18	3D	12.1	6.5	2.25	130.06	3000	0	0	Std	2-18-1 to 2-18-18	

TABLE 9

SERIES NO. 3 - FINAL
VARIATIONS IN OBLIQUITY AND ANGLE OF ATTACK

Problem Number	Type 2D 3D	Projectile Data				Velocity (ft/sec)	Obliquity γ (deg)	Attack Angle α (deg)	Material Property Concrete (psi)	Run Number	Summary Curve No.
		W/A (psi)	D (in)	Nose Remarks CRH	Nose Remarks Weight (lb)						
3-1	3D	12.1	6.5	9.25	400	1500	180	0	σ_c = 5000	3-1-1 to 3-1-10	
3-2	3D	12.1	6.5	9.25	400	1500	185	0	σ_c = 5000	3-2-1 to 3-2-10	
3-3	3D	12.1	6.5	9.25	400	1500	190	0	σ_c = 5000	3-3-1 to 3-3-10	37
3-4	3D	12.1	6.5	9.25	400	1500	200	0	σ_c = 5000	3-4-1 to 3-4-10	38
3-5	3D	12.1	6.5	9.25	400	1500	210	0	σ_c = 5000	3-5-1 to 3-5-10	39
3-6	3D	12.1	6.5	9.25	400	1500	220	0	σ_c = 5000	3-6-1 to 3-6-11	
3-7	3D	12.1	6.5	9.25	400	1500	230	0	σ_c = 5000	3-7-1 to 3-7-11	
3-8	3D	12.1	6.5	9.25	400	1500	240	0	σ_c = 5000	3-8-1 to 3-8-12	
3-9 to 3-11	DELETED										
3-12	2D	12.1	6.5	9.25	400	1500	0	+5	σ_c = 5000	3-12-1 to 3-12-5	
3-13 to 3-16	DELETED										
3-17	2D	12.1	6.5	.5	400	1500	20	+1	σ_c = 5000	3-17-1 to 3-17-5	
3-18	3D	12.1	6.5	9.25	400	1500	200	+2	σ_c = 5000	3-18-1 to 3-18-10	40
3-19	2D	12.1	6.5	9.25	400	1500	20	+3	σ_c = 5000	3-19-1 to 3-19-5	41
3-20	2D	12.1	6.5	9.25	400	1500	20	+5	σ_c = 5000	3-20-1 to 3-20-5	42
3-21	2D	12.1	6.5	9.25	400	1500	20	-1	σ_c = 5000	3-21-1 to 3-21-5	43
3-22	3D	12.1	6.5	9.25	400	1500	200	-2	σ_c = 5000	3-22-1 to 3-22-10	44
3-23	2D	12.1	6.5	9.25	400	1500	20	-3	σ_c = 5000	3-23-1 to 3-23-5	
3-24	2D	12.1	6.5	9.25	400	1500	20	-5	σ_c = 5000	3-24-1 to 3-24-5	
3-25 to 3-30	DELETED										
3-31	2D	12.1	6.5	9.25	400	2500	0	0	σ_c = 5000	3-31-1 to 3-31-5	
3-32	2D	12.1	6.5	with	400	2500	5	0	σ_c = 5000	3-32-1 to 3-32-5	45
3-33	2D	12.1	6.5	slightly	400	2500	10	0	σ_c = 5000	3-33-1 to 3-33-5	46
3-34	2D	12.1	6.5	conic	400	2500	20	0	σ_c = 5000	3-34-1 to 3-34-5	
3-35	2D	12.1	6.5	tip	400	2500	30	0	σ_c = 5000	3-35-1 to 3-35-5	
3-36	2D	12.1	6.5	of	400	2500	40	0	σ_c = 5000	3-36-1 to 3-36-5	
3-37	2D	12.1	6.5	45°	400	2500	50	0	σ_c = 5000	3-37-1 to 3-37-5	
3-38	2D	12.1	6.5		400	2500	60	0	σ_c = 5000	3-38-1 to 3-38-5	
3-39 to 3-47	DELETED										

TABLE - 10

SERIES NO. 4 - FINAL
EFFECT OF L/D ON STABILITY

Problem Number	Type 2D 3D	Projectile Data					Velocity (ft/sec)	Obliquity γ (deg)	Attack Angle α (deg)	Material Property	Run Number	Summary Curve No.
		W/A (psi)	D (in)	Nose Remarks								
				CRH	L/D	Weight (lb)						
4-1	2D	Variable	6.5	9.25	10	400	1500	10	+2	Till	4-1-1 to 4-1-5	55
4-2	2D	Variable	6.5	9.25	8	320	1500	10	+2	Till	4-2-1 to 4-2-5	56
4-3	2D	Variable	6.5	9.25	6	240	1500	10	+2	Till	4-3-1 to 4-3-5	57
4-4	2D	Variable	6.5	9.25	4	160	1500	10	+2	Till	4-4-1 to 4-4-5	58
4-5	2D	Variable	6.5	9.25	10	400	2500	10	+2	Till	4-5-1 to 4-5-5	59
4-6	2D	Variable	6.5	9.25	8	320	2500	10	+2	Till	4-6-1 to 4-6-5	
4-7	2D	Variable	6.5	9.25	6	240	2500	10	+2	Till	4-7-1 to 4-7-5	
4-8	2D	Variable	6.5	9.25	4	160	2500	10	+2	Till	4-8-1 to 4-8-5	
4-9	2D	Variable	6.5	Blunt	3	320	1500	10	+2	Till	4-9-1 to 4-9-5	
4-10	2D	Variable	6.5	Blunt	4	160	1500	10	+2	Till	4-10-1 to 4-10-5	
4-11	2D	Variable	6.5	Blunt	8	320	2500	10	+2	Till	4-11-1 to 4-11-5	
4-12	2D	Variable	6.5	Blunt	4	160	2500	10	+2	Till	4-12-1 to 4-12-5	

TABLE - 11

SERIES NO. 4 - FINAL
MEDIA VARIATIONS

Problem Number	Type 2D 3D	Projectile Data				Velocity (ft/sec)	Obliquity γ (deg)	Attack Angle α (deg)	Material Property	Run Number	Summary Curve No.
		W/D (psi)	D (in)	Nose Remarks							
				CRH	Weight (lb)						
5-4	2D	12.1	6.5	9.25	400	1500	0	0	σ_c = 3000 psi Concrete	5-4-1 to 5-4-5	
5-5	2D	12.1	6.5	9.25	400	1500	20	+2	σ_c = 3000 psi Concrete	5-5-1 to 5-5-5	60
5-6	2D	12.1	6.5	9.25	400	2500	0	0	σ_c = 3000 psi Concrete	5-6-1 to 5-6-5	61
5-10	2D	12.1	6.5	9.25	400	1500	0	0	Till	5-10-1 to 5-10-5	60
5-11	2D	12.1	6.5	9.25	400	1500	20	+2	Till	5-11-1 to 5-11-5	61
5-12	2D	12.1	6.5	9.25	400	2500	0	0	Till	5-12-1 to 5-12-5	
TONAPA TEST PREDICTIONS											
5-1A	2D	12.1	6.5	9.25	517	1500	0	0	Till	5-1A-1 to 5-1A-5	66
5-2A	2D	12.1	6.5	9.25	517	2000	0	0	Till	5-2A-1 to 5-2A-5	67
5-3A	2D	12.1	6.5	9.25	517	1640	0	0	Till	5-3A-1 to 5-3A-5	

TABLE 12

SERIES NO. 6 - FINAL
RICOCHET PREDICTIONS

Problem Number	Type 2D 3D	Projectile Data				Velocity (ft/sec)	Obliquity γ (deg)	Attack Angle α (deg)	Material Property	Run Number	Summary Curve No.
		W/A (psi)	D (in)	Nose Remarks Mk	Weight (lb)						
6-1A	DELETED										
6-2A	2D			82	500	700	40	0	Target Layered Media	6-2A-1 to 6-2A-3	
6-3A	2D			82	500	700	50	0	Target Layered Media	6-3A-1 to 6-3A-3	71
6-4A	2D			82	500	700	55	0	Target Layered Media	6-4A-1 to 6-5A-3	73
6-5A	2D			82	500	700	60	0	Target Layered Media	6-5A-1 to 6-5A-3	75
6-6A	2D			82	500	700	65	0	Target Layered Media	6-6A-1 to 6-6A-3	
6-7A	2D			82	500	700	70	0	Target Layered Media	6-7A-1 to 6-7A-3	
6-8A	2D			84	2000	700	30	0	Target Layered Media	6-8A-1 to 6-8A-3	
6-9A	2D			84	2000	700	40	0	Target Layered Media	6-9A-1 to 6-9A-3	72
6-10A	2D			84	2000	700	50	0	Target Layered Media	6-10A-1 to 6-10A-3	74
6-11A	2D			84	2000	700	55	0	Target Layered Media	6-11A-1 to 6-11A-3	76
6-12A	2D			84	2000	700	60	0	Target Layered Media	6-12A-1 to 6-12A-3	
6-13A	2D			84	2000	700	65	0	Target Layered Media	6-13A-1 to 6-13A-3	
6-14A	2D			84	2000	700	70	0	Target Layered Media	6-14A-1 to 6-14A-3	
6-15A	2D			84	2000	700	75	0	Target Layered Media	6-15A-1 to 6-15A-3	
6-16A	DELETED										
6-4	3D			82	500	700	235	0	Target Layered Media	6-4-1 to 6-4-10	
6-5	3D			82	500	700	240	0	Target Layered Media	6-5-1 to 6-5-12	
6-12	3D			84	2000	700	240	0	Target Layered Media	6-12-1 to 6-12-6	
6-13	3D			84	2000	700	245	0	Target Layered Media	6-13-1 to 6-13-10	
6-1B	2D			82	500	700	30	+5	Target Layered Media	6-1B-1 to 6-1B-3	
6-2B	2D			82	500	700	40	+5	Target Layered Media	6-2B-1 to 6-2B-3	
6-3B	2D			82	500	700	50	+5	Target Layered Media	6-3B-1 to 6-3B-3	71
6-4B	DELETED										
6-5B	2D			82	500	700	60	+5	Target Layered Media	6-5B-1 to 6-5B-3	75
6-7B	2D			82	500	700	70	+5	Target Layered Media	6-7B-1 to 6-7B-3	
6-8B	2D			84	2000	700	30	+5	Target Layered Media	6-8B-1 to 6-8B-3	72
6-9B	2D			84	2000	700	40	+5	Target Layered Media	6-9B-1 to 6-9B-3	74
6-10B	2D			84	2000	700	50	+5	Target Layered Media	6-10B-1 to 6-10B-3	76
6-12B	2D			84	2000	700	60	+5	Target Layered Media	6-12B-1 to 6-12B-3	
6-14B	2D			84	2000	700	70	+5	Target Layered Media	6-14B-1 to 6-14B-3	
6-1C	2D			82	500	700	30	-5	Target Layered Media	6-1C-1 to 6-1C-3	71
6-2C	2D			82	500	700	40	-5	Target Layered Media	6-2C-1 to 6-2C-3	73
6-3C	2D			82	500	700	50	-5	Target Layered Media	6-3C-1 to 6-3C-3	75
6-4C	DELETED										
6-5C	2D			82	500	700	60	-5	Target Layered Media	6-5C-1 to 6-5C-3	
6-7C	2D			82	500	700	70	-5	Target Layered Media	6-7C-1 to 6-7C-3	
6-8C	2D			84	2000	700	30	-5	Target Layered Media	6-8C-1 to 6-8C-3	72
6-9C	2D			84	2000	700	40	-5	Target Layered Media	6-9C-1 to 6-9C-3	74
6-10C	2D			84	2000	700	50	-5	Target Layered Media	6-10C-1 to 6-10C-3	76
6-12C	2D			84	2000	700	60	-5	Target Layered Media	6-12C-1 to 6-12C-3	
6-14C	2D			84	2000	700	70	-5	Target Layered Media	6-14C-1 to 6-14C-3	

The equation of motion used to describe the terradynamic trajectory of a penetrator based on the Cavity Expansion technique is:

$$M \frac{d^2z}{dt^2} + \frac{\pi D^2}{4} \left\{ \phi_3 + \frac{2}{3} \rho_p \left[\phi_1 \frac{D}{2} \left(\frac{d^2z}{dt^2} \right) + \phi_2 \left(\frac{dz}{dt} \right)^2 \right] \right\} \quad (1)^*$$

The parameters in Eq. (1) are given in terms of target properties by the following relations:

$$\phi_1 = 1 - \delta^{1/3} \quad (2)$$

$$\phi_2 = \left[\frac{3}{2} - (1 + \alpha_p) \delta^{1/3} + \frac{1}{2} \delta^{4/3} \right] f_N \quad (3)$$

$$\phi_3 = \frac{4}{9} E \left[1 - \exp(-3\beta) \right] - \frac{2}{3} Y \ell n \, \delta + \frac{2}{27} \pi^2 E_t - \frac{4}{9} E_t \eta \quad (4)$$

$$\delta = 1 - \frac{\rho_o}{\rho_p} \exp(-3\beta) \quad (5)$$

$$\alpha_p = 1 - \frac{\rho_o}{\rho_p} \quad (6)$$

$$\eta = \sum_{n=1}^{\infty} \delta \frac{n}{n^2} \quad (7)$$

$$\beta = \frac{Y}{2E} - \frac{e_i}{3} \quad (8)$$

$$\rho_p = \rho_o \exp(e_p) \quad (9)$$

where:

ρ_o = initial density of target material, slugs/ft^3

Y = yield strength of target material, psf

E = Young's modulus of elasticity, corresponding to locked elastic region, psf = 3G

E_t = strain-hardening modulus, corresponding to locked plastic region, psf = $3G_t$

*Rohani, R., Waterways Experiment Paper, S-73-58, June 1973.

e_i = volumetric strain related to the elastic region of the pressure-volumetric strain curve

e_p = volumetric strain related to plastic region of the pressure-volumetric strain curve

π = 3.1416

f_N = $\sin\theta + 1/3 \cos^2\theta$

θ = nose angle

The equation of motion using Avco's force law approach for one dimensional motion is:

$$-M \frac{d^2z}{dt^2} = \int \{\eta (1 + f_c) + 1/2\, \rho V^2 (C_N \sin^2\zeta + C_f \sin\zeta \cos\zeta)\, dA \tag{10}$$

Equating similar terms:

$$2/3\, \rho_p f_N \phi_2 V^2 = 1/2\, \rho V^2 (C_N \sin^2\zeta + C_f \sin\zeta \cos\zeta) \tag{11}$$

$$2/3\, \rho_p \phi_1 \frac{D}{2} \frac{d^2z}{dt^2} = \begin{matrix}\text{modified nose shape} \\ + \text{ increased mass}\end{matrix} \tag{12}$$

$$\phi_3 = \eta (1 + f_c) \tag{13}$$

Referring to Eq. (11) both sides represent equivalent fluid flow terms. The Cavity Expansion Theory offers no direct or fundamental method of obtaining the correct values of the required coefficients, consequently, empirical evaluation of these are necessary unless a conversion process can be derived from, for example, trial finite difference calculations.

The Cavity Expansion term represented by Eq. (12) is representative of an equivalent mass of fluid entrapped by the nose of the penetrator and decelerating with it.

The conversion here is direct; however, in the case of a large sharp nose penetrator, the term becomes negligible.

In the Cavity Expansion Theory sliding friction between the media and the projectile surface is not represented. Consequently, Eq. (13) becomes:

$$\phi_3 = \eta \tag{14}$$

The "η" term used in Avco's force law approach is a measurable quantity established by conducting static penetration tests. "ϕ_3" is the analytically derived static resistance to penetration. Consequently, "η" can be obtained by evaluating the "ϕ_3" expression.

To summarize, only two of the penetrability terms for Avco's force law approach can be derived from the Cavity Expansion technique. These include the apparent mass term, which already has been included, and the normal pressure term associated with the media's static resistance-to-penetration. The sliding or Coulomb friction term used in Avco's force law technique is not currently present in the Cavity Expansion technique, and the equivalent fluid flow terms used in both techniques must be arrived at empirically.

This conversion or equivalency technique can therefore be used to describe the strength characteristics of the concrete used in the parametric study.

Performing the indicated operations suggested by Eq. (14) and assuming that Young's modulus remains that of typical concrete, i.e., 3×10^6 psi, the equivalent unconfined compressive strength is approximately 10,000 psi.

It is apparent that if the above procedure can be used to arrive at and describe an equivalent strength media, it can also be used to find the approximate "η" term given the properties of the media. This technique has been used in the past to aid in predicting penetration events into "uncharacterized" media and an example of this procedure and outcome is described in Section 5.0 in which a prediction was made for the Tonapa Test Series conducted in the Spring of 1975.

The following sections describe the results of the parametric studies for Series 1.0 through 6.0.

5.0 IMPACT AND PENETRATION PARAMETRIC STUDY RESULTS

In this section each series of runs is described and summarized to allow the reader to quickly grasp the more significant aspects of the particular area of investigation. Under conditions where a more in-depth review is desired, the reader is referred to the detailed time histories of the event. When specific runs are referred by run number (i.e., 3.8, 3.60 etc.) the variables are defined in the appropriate table of this report and the complete run data is available under separate cover through DNA.

5.1 SERIES 1 -- SENSITIVITY STUDY

The matrix of runs conducted for Series 1 is presented in Table 7. The EP used in this study is shown in Figure 1. The EP weighs 400 pounds, is 60 inches long with a diameter of 6.5 inches. The nose shape is described by the parameter "CRH" which represents the ratio between the tangent ogive radius and the EP diameter.

The nominal media for this series is the "hard concrete" described in Section 4.0 and variations from the nominal are given in percent. In each of the series, there are generally two types of runs made; i.e., 2-D and 3-D. All the impact conditions are described in a plane and because none of the EP's is spinning, no out of plane motion is incurred. Consequently, the impact event can be described in the 2-D plane of symmetry which they are. The purpose of the 3-D runs is to provide three dimensional distribution plots of the local pressures and shears.

Examples of the 2-D and 3-D plots for Runs 3.60 and 3.8 are presented in Figures 2 through 6 and 7 through 16, respectively. The output format for these plots is described in detail in Tables 13 and 14.

There are generally five separate graphs for each 2-D run consisting of:

- a pictorial description of the event. (See Figure 2.)
- the rigid body resulting loading environments. (See Figure 3.)
- the basic trajectory data. (See Figure 4.)
- the rigid body axial accelerations. (See Figure 5.)
- the rigid body lateral accelerations. (See Figure 6.)

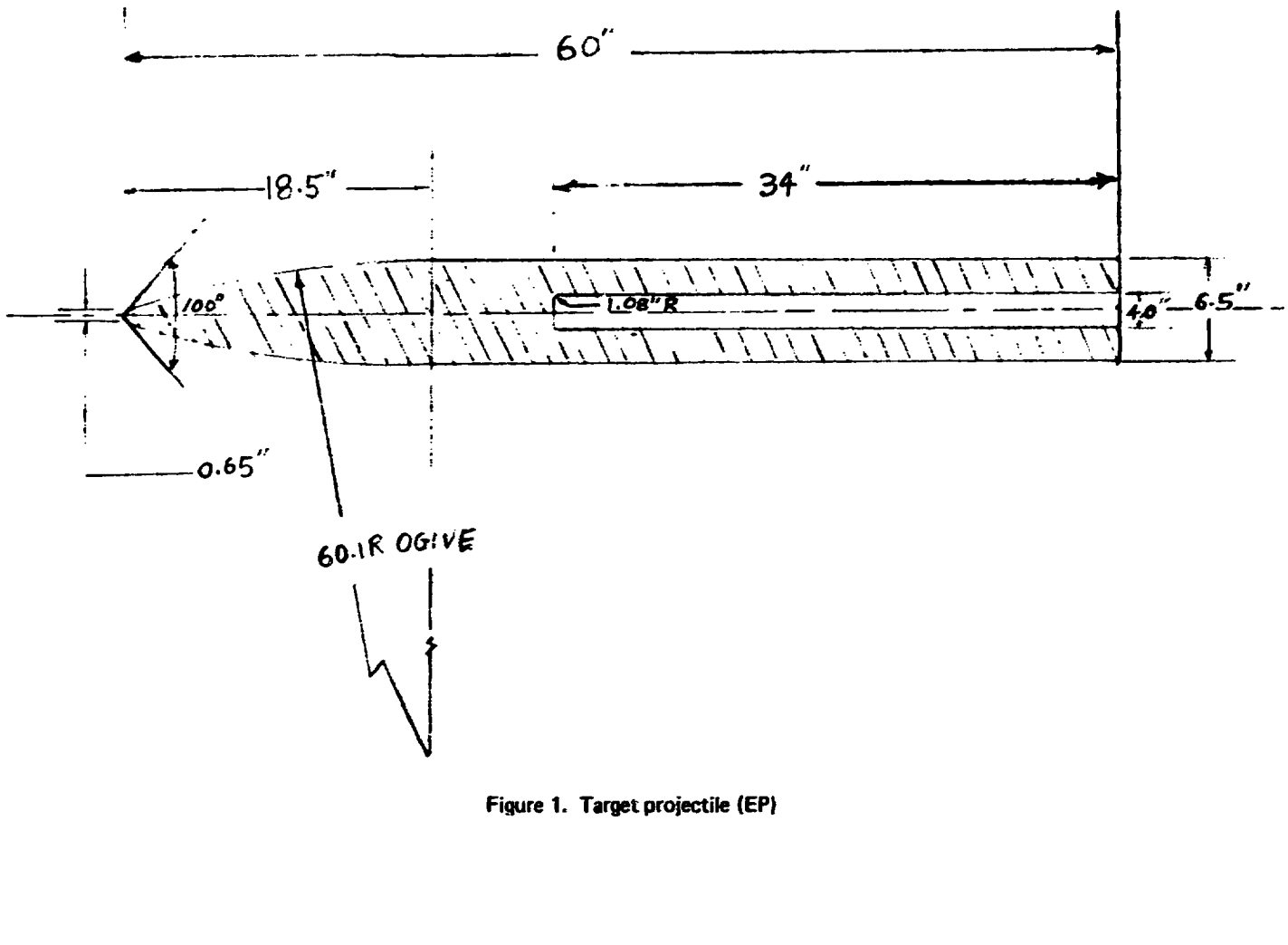

Figure 1. Target projectile (EP)

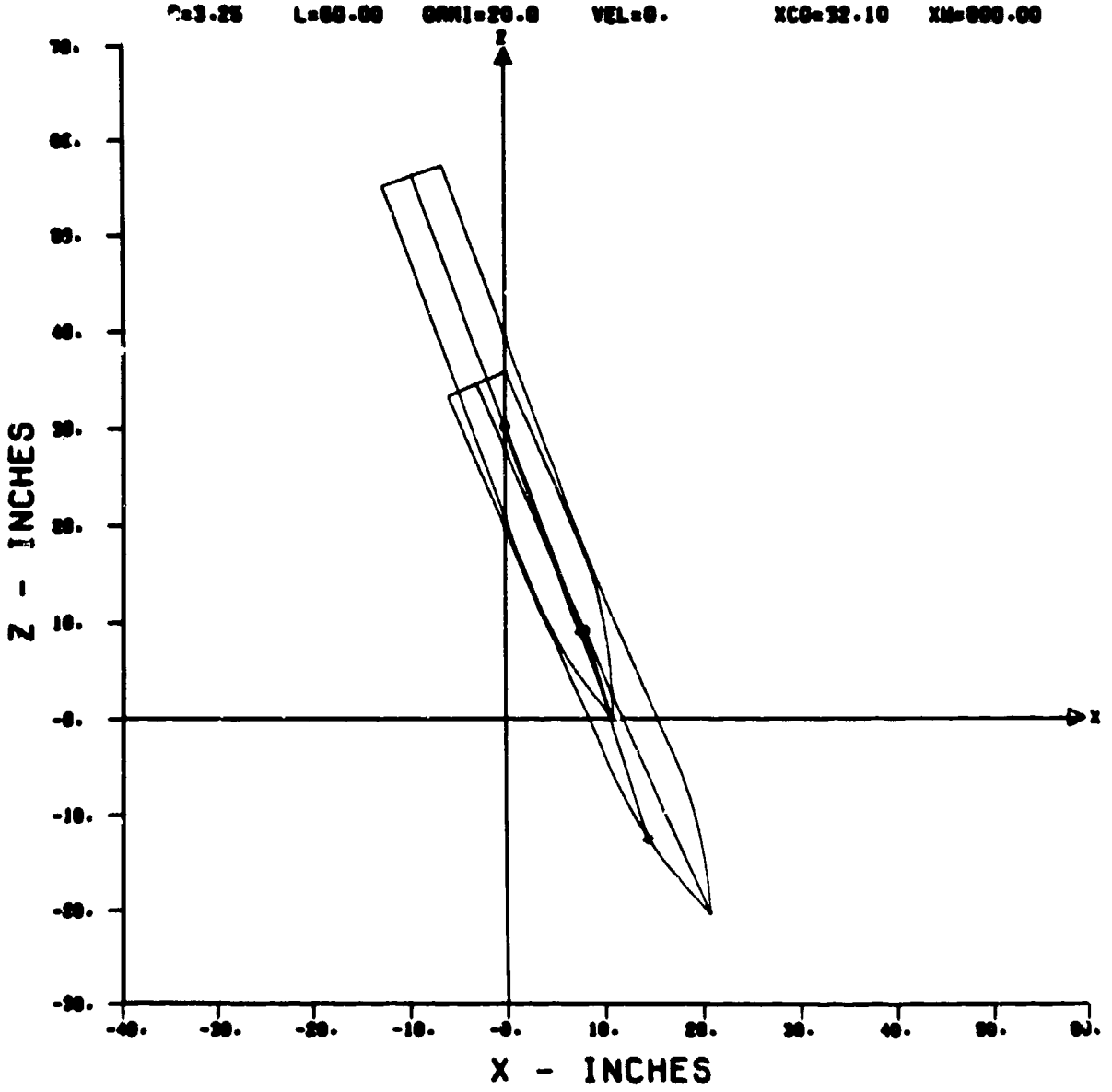

Figure 2. Trajectory

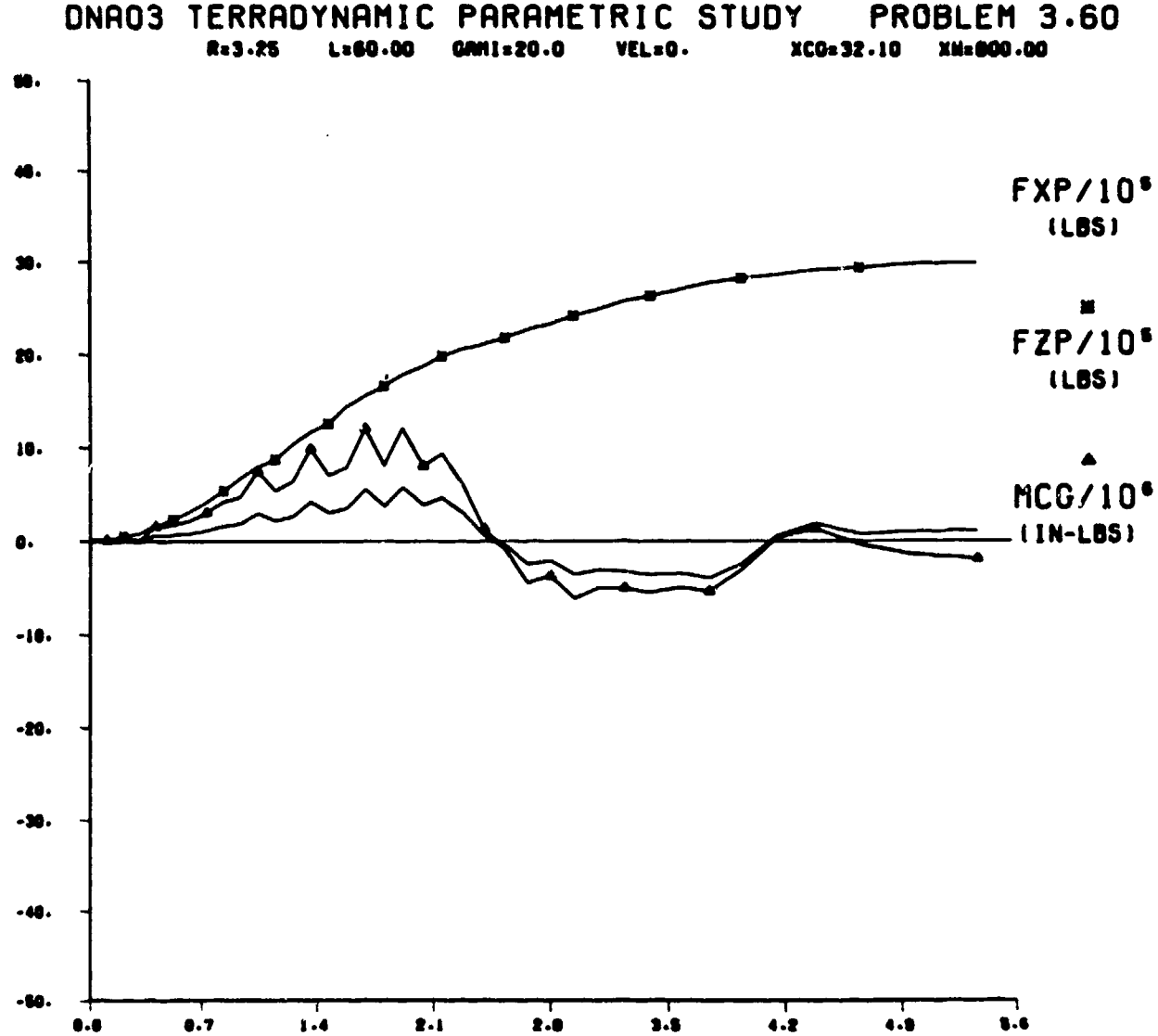

Figure 3. Loads

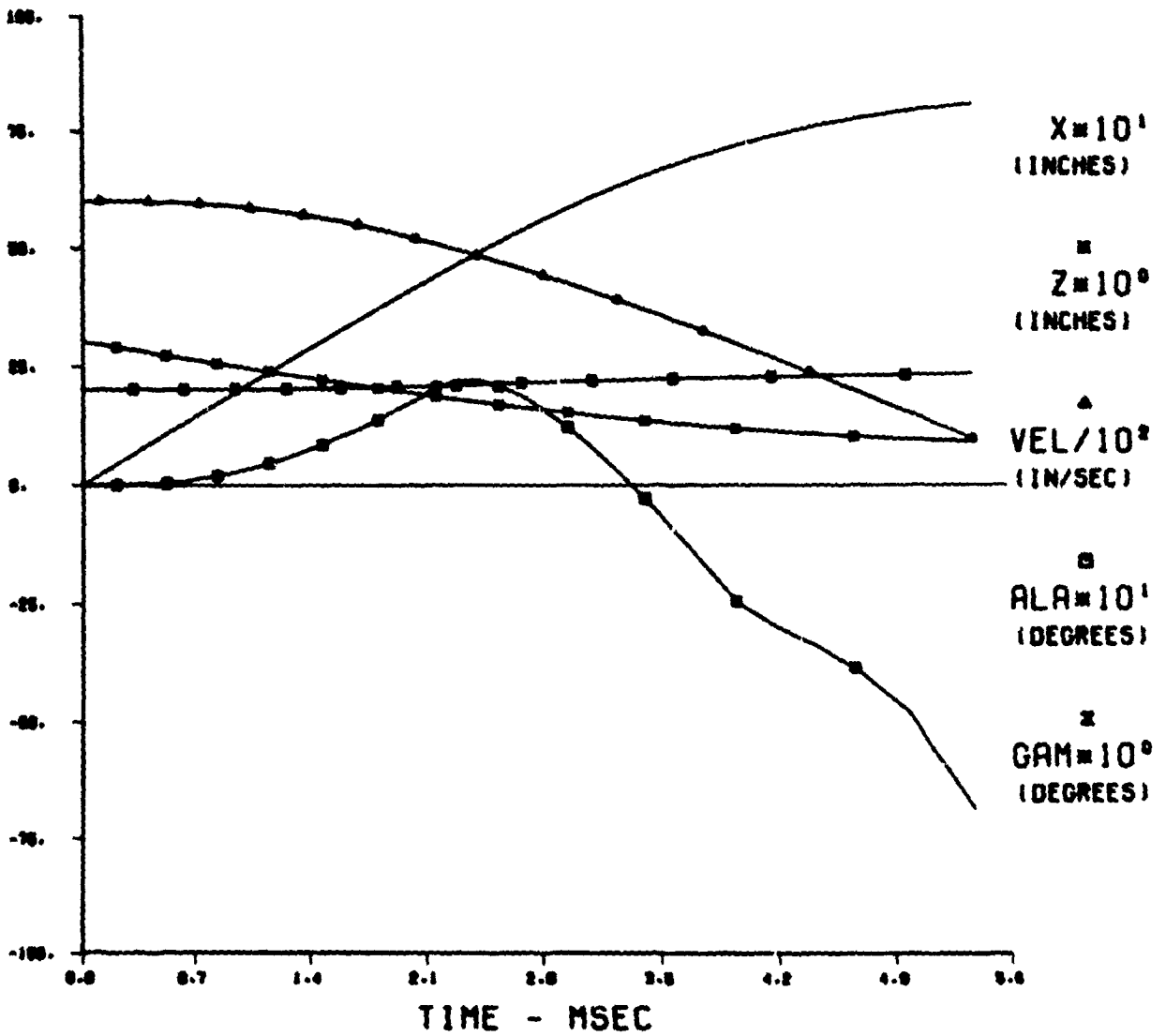

Figure 4. Trajectory data

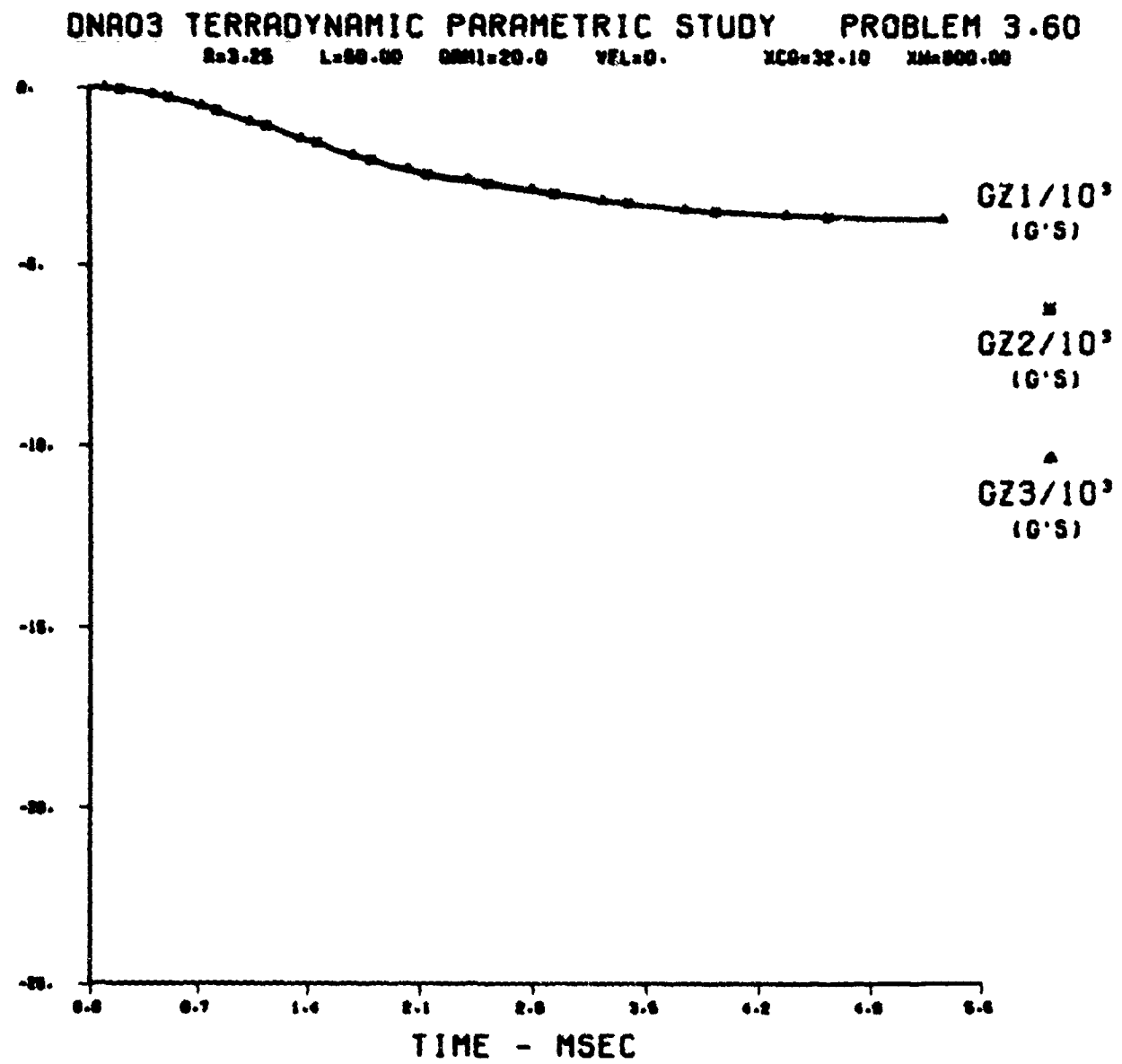

Figure 5. Axial acceleration

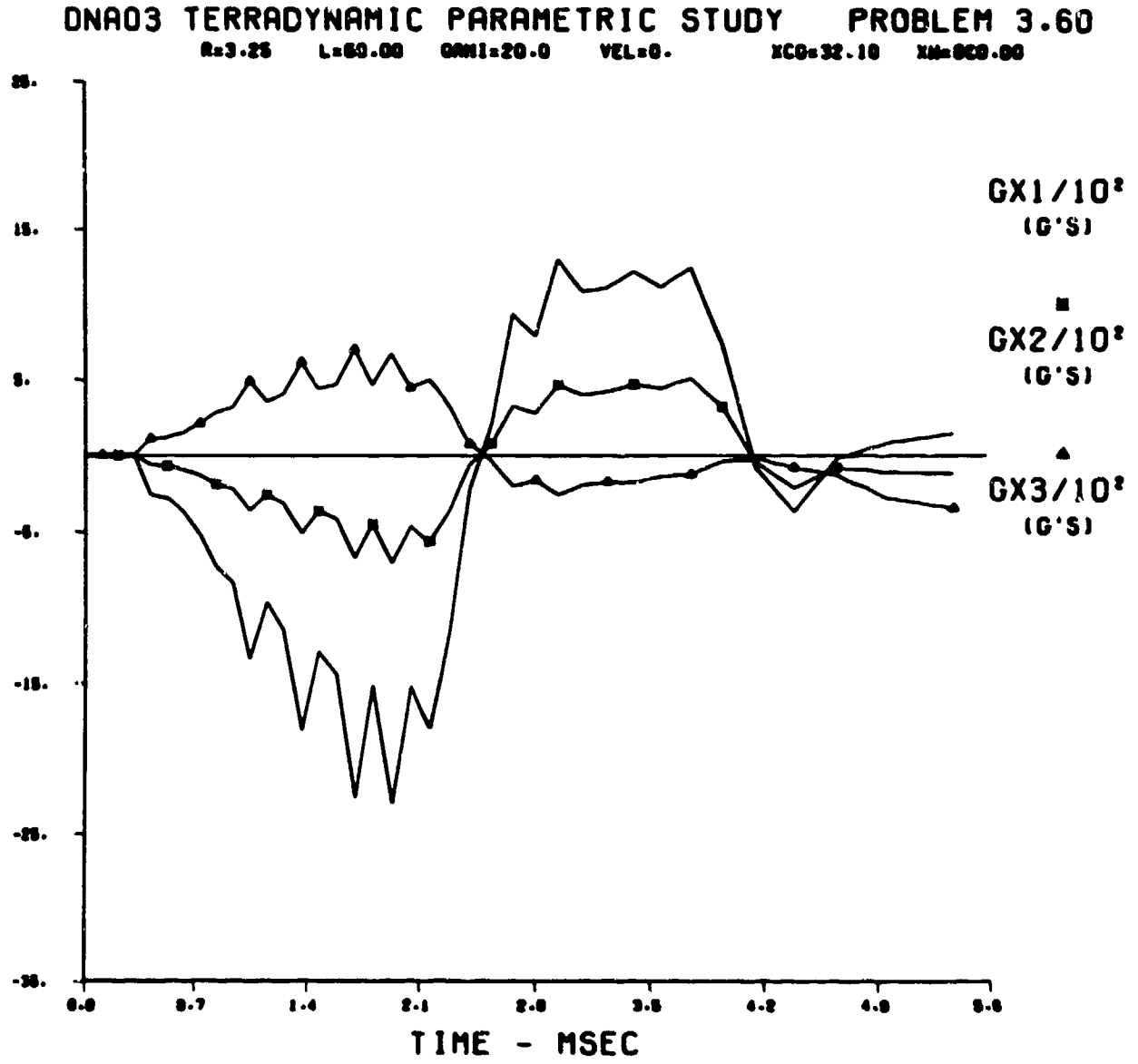

Figure 6. Lateral acceleration

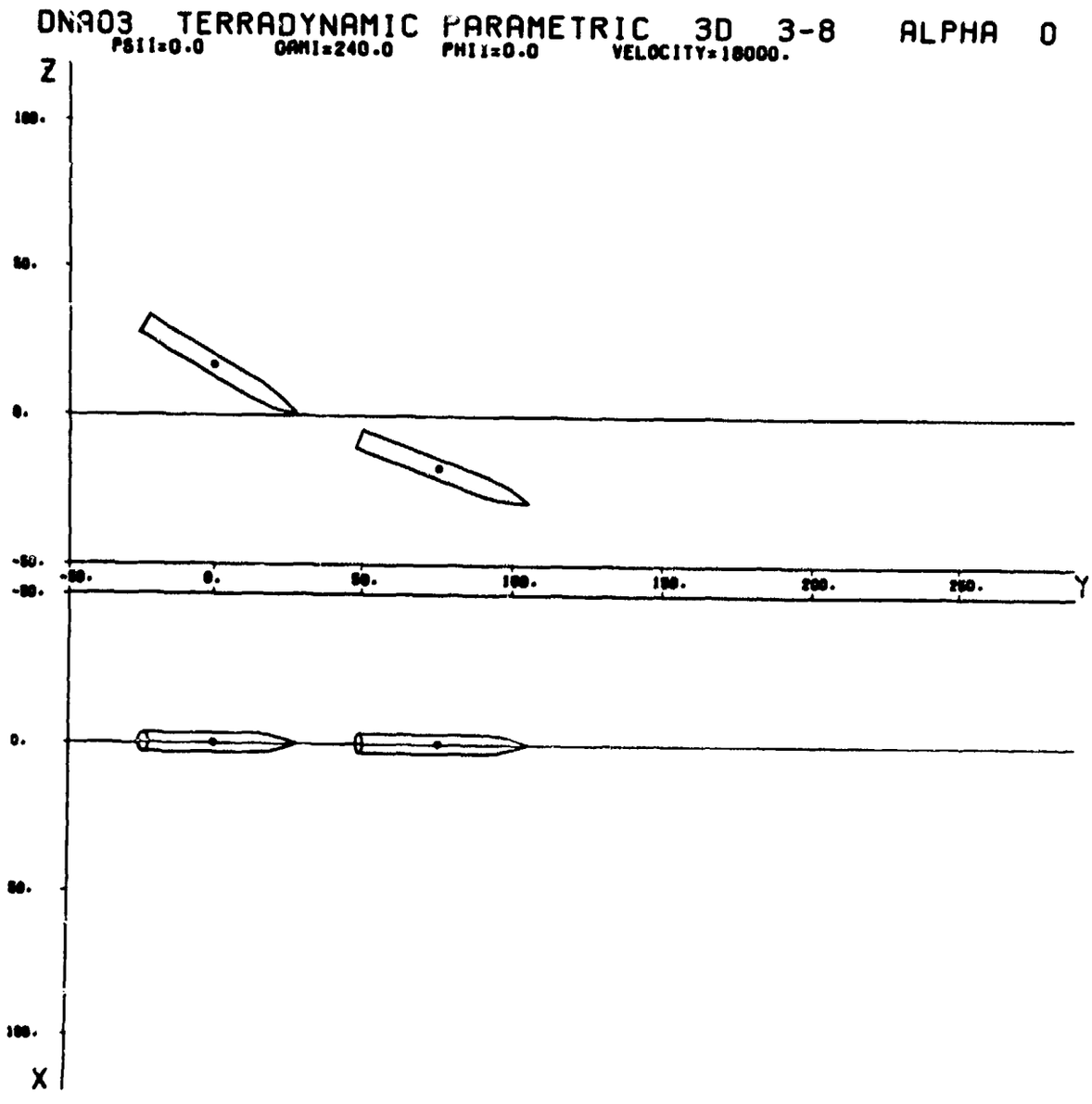

Figure 7. (3D) Trajectory

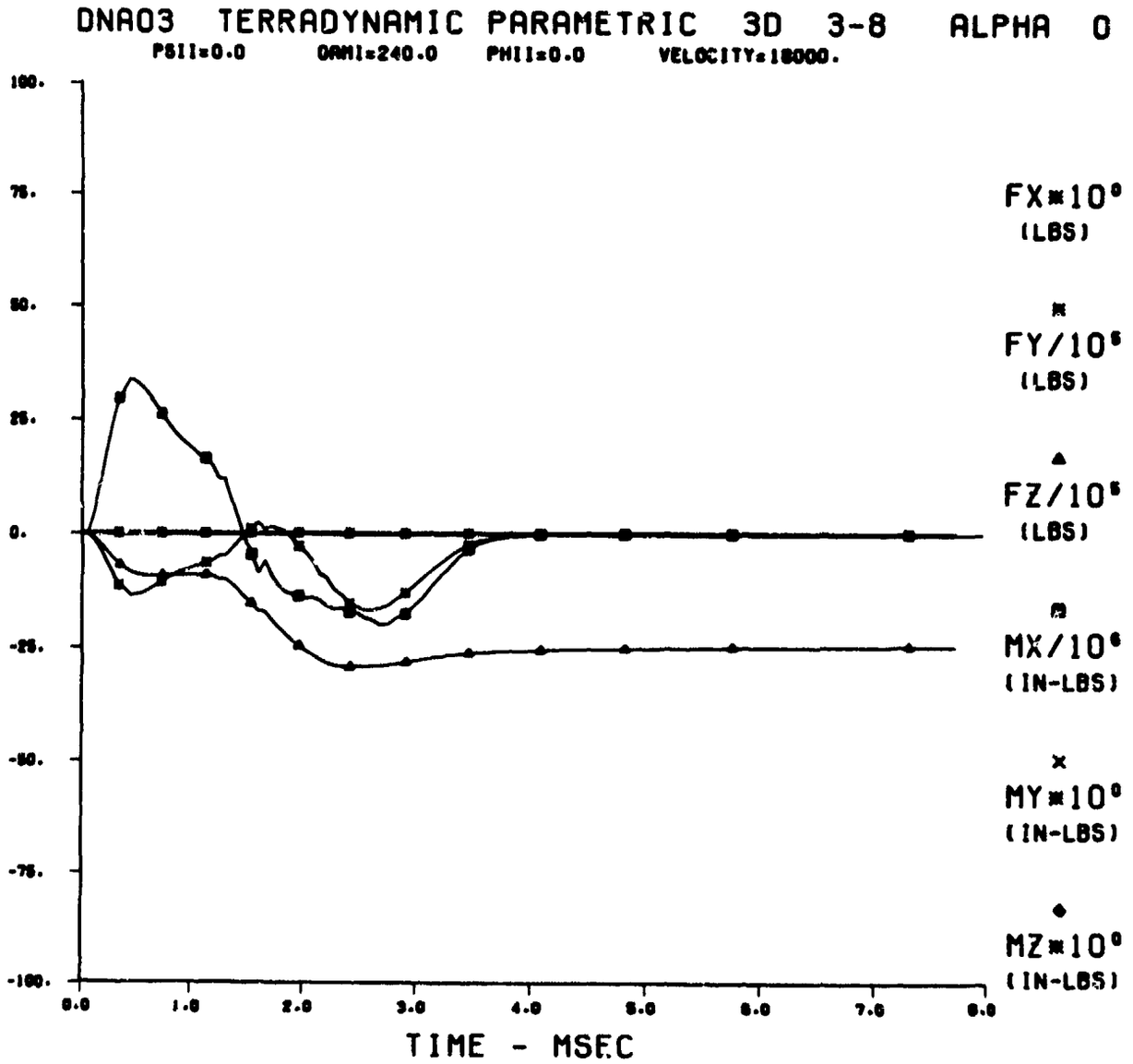

Figure 8. (3D' Loads

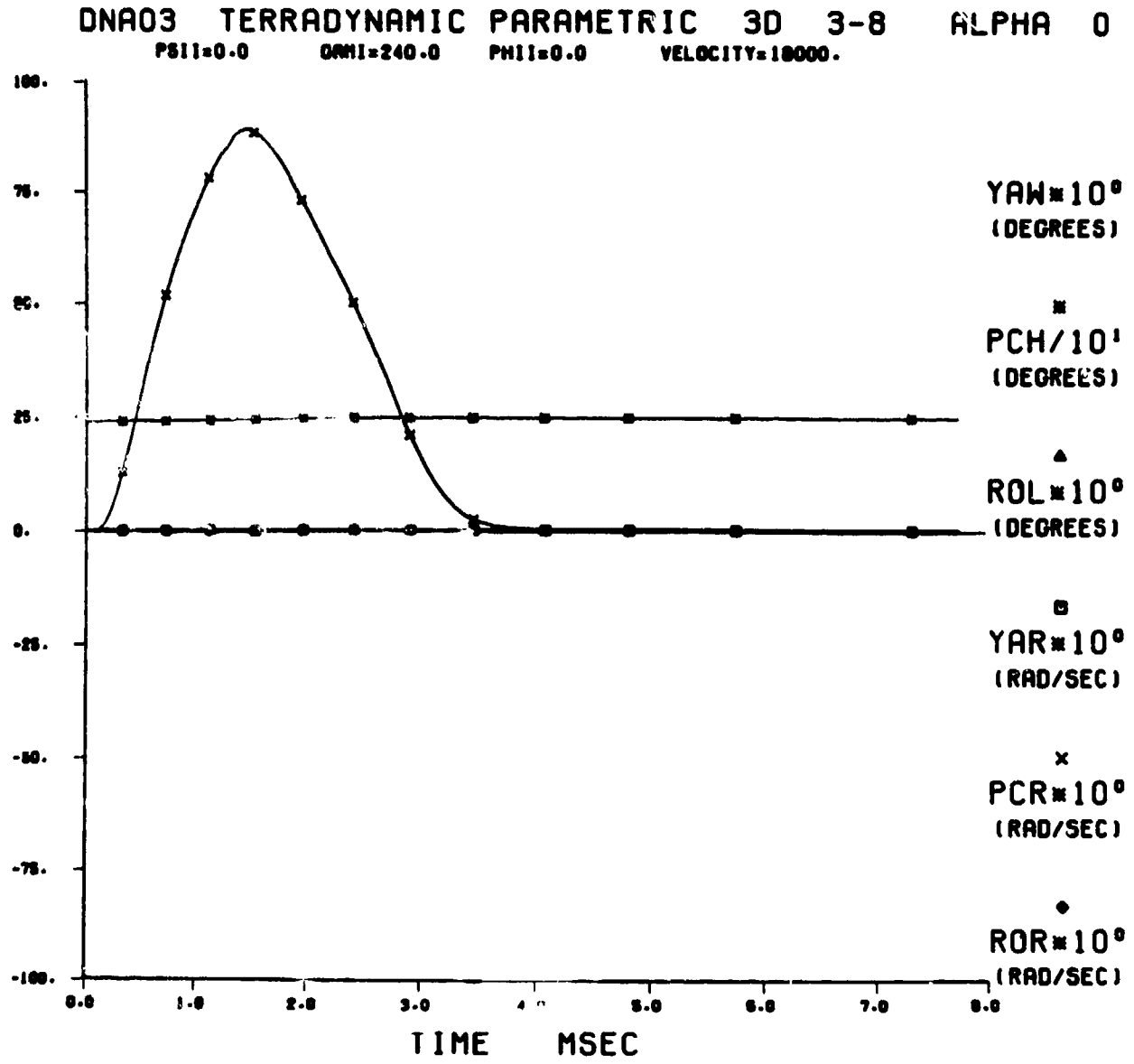

Figure 9. (3D) Rotational data

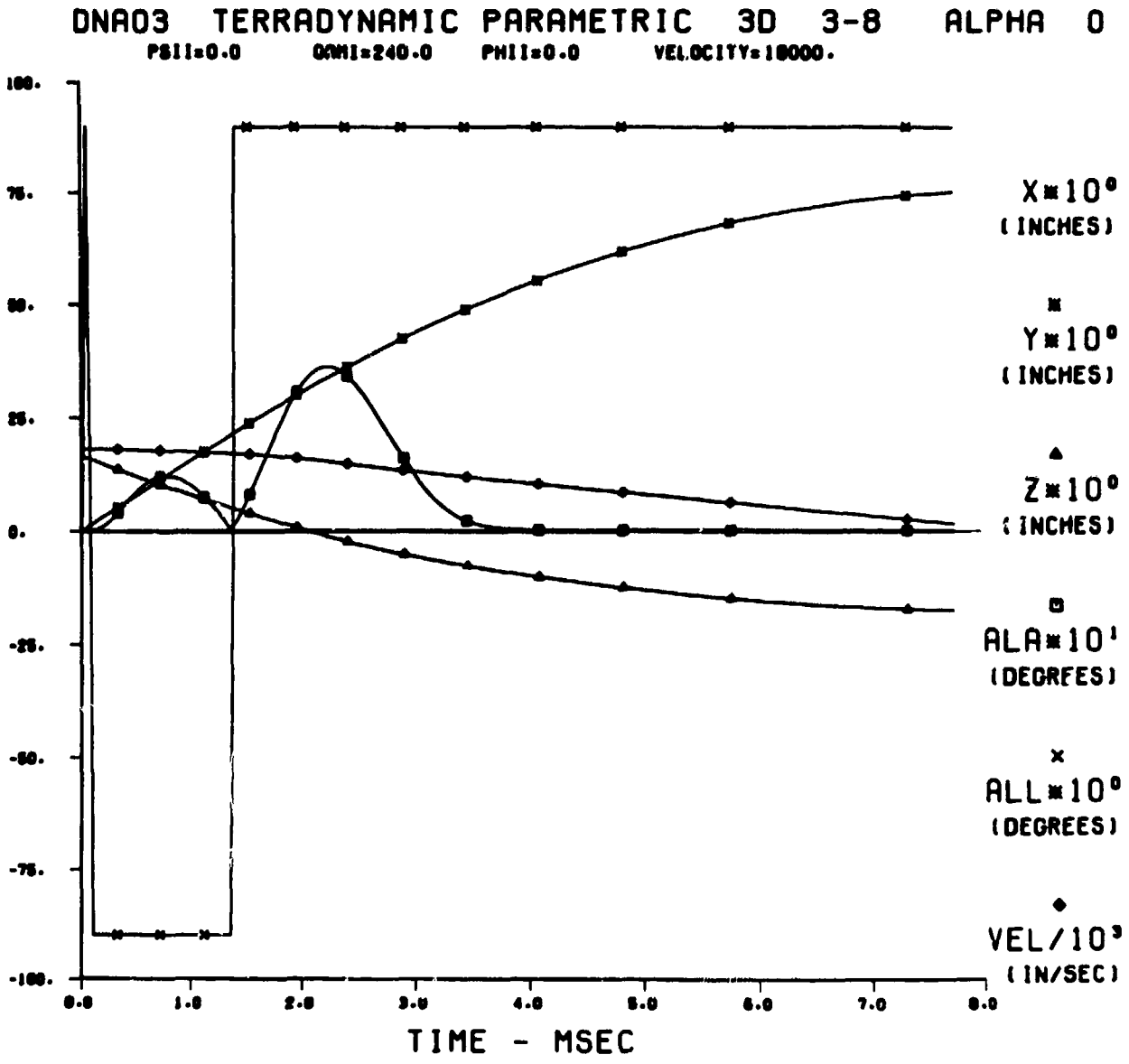

Figure 10. (3D) Translational data

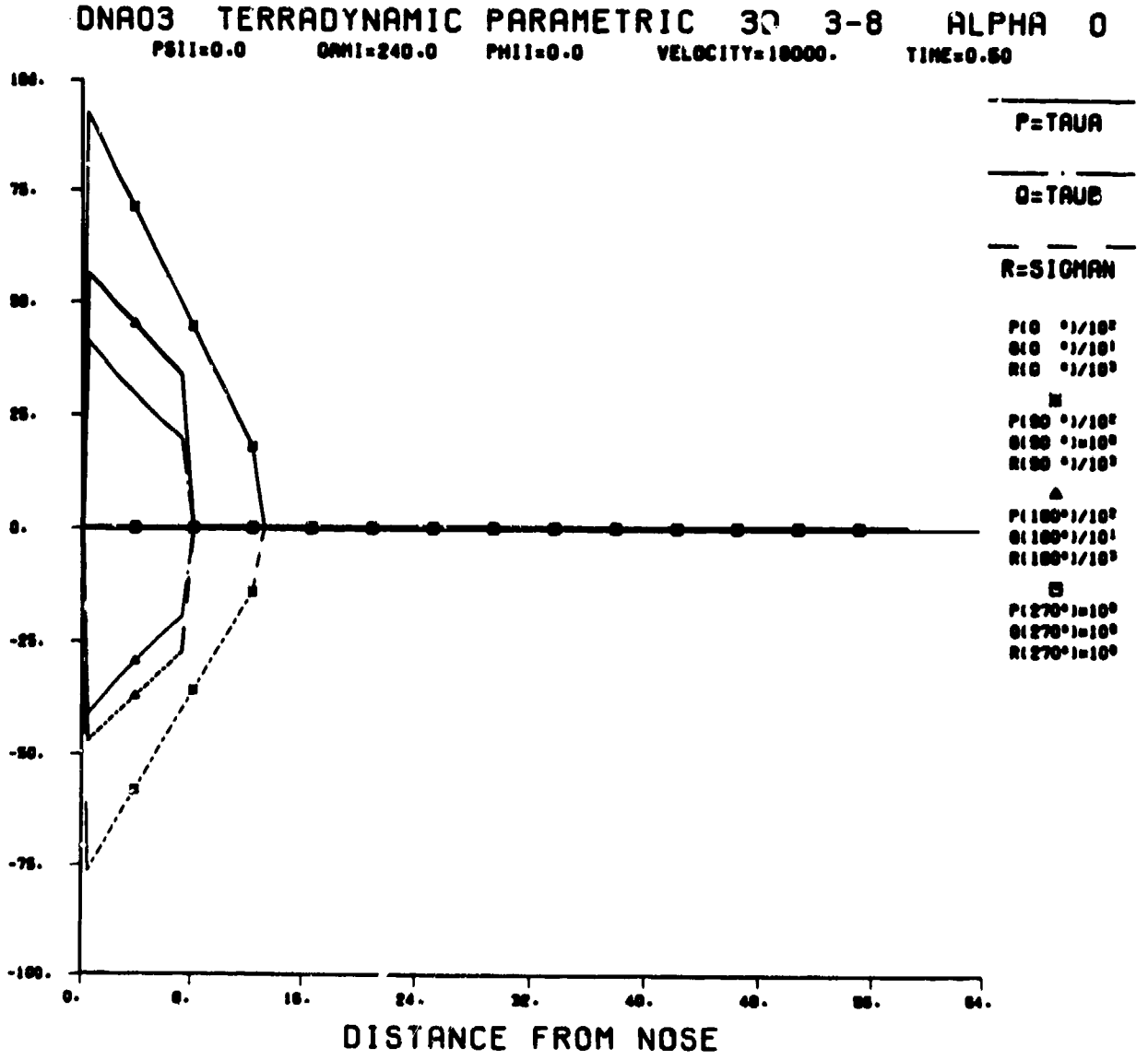

Figure 11. (3D) Stress data

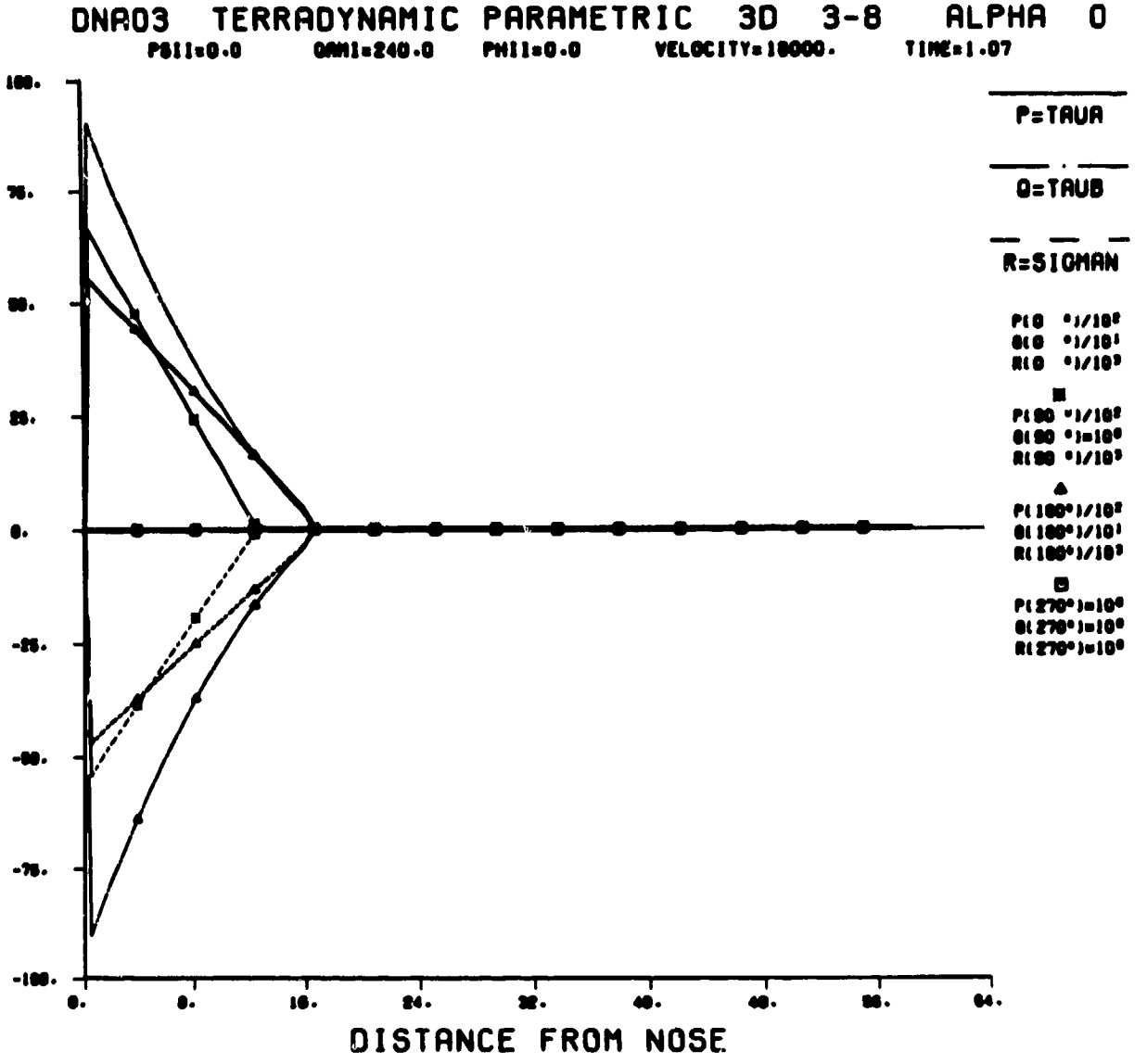

Figure 12. (3D) Stress data

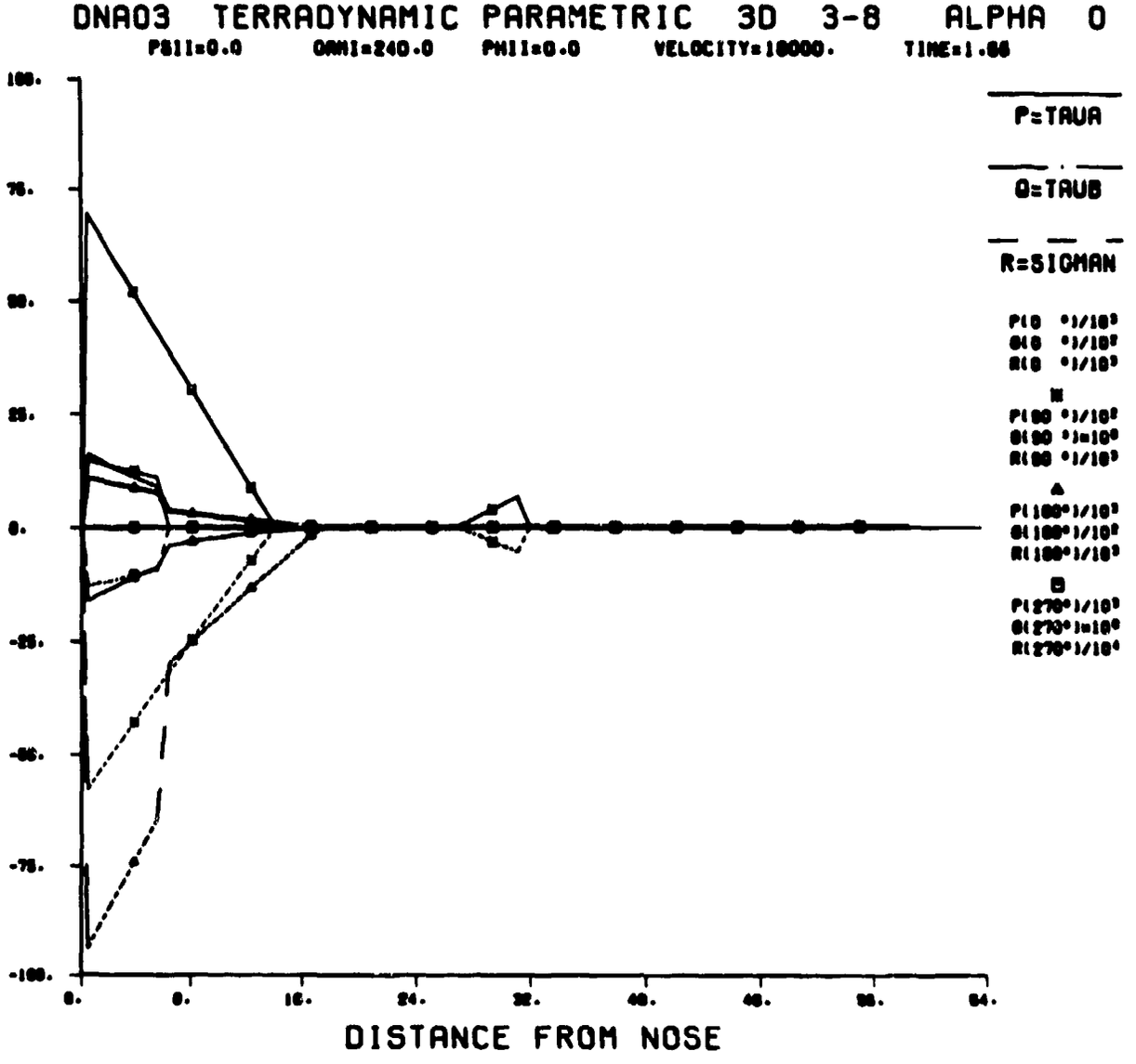

Figure 13. (3D) Stress data

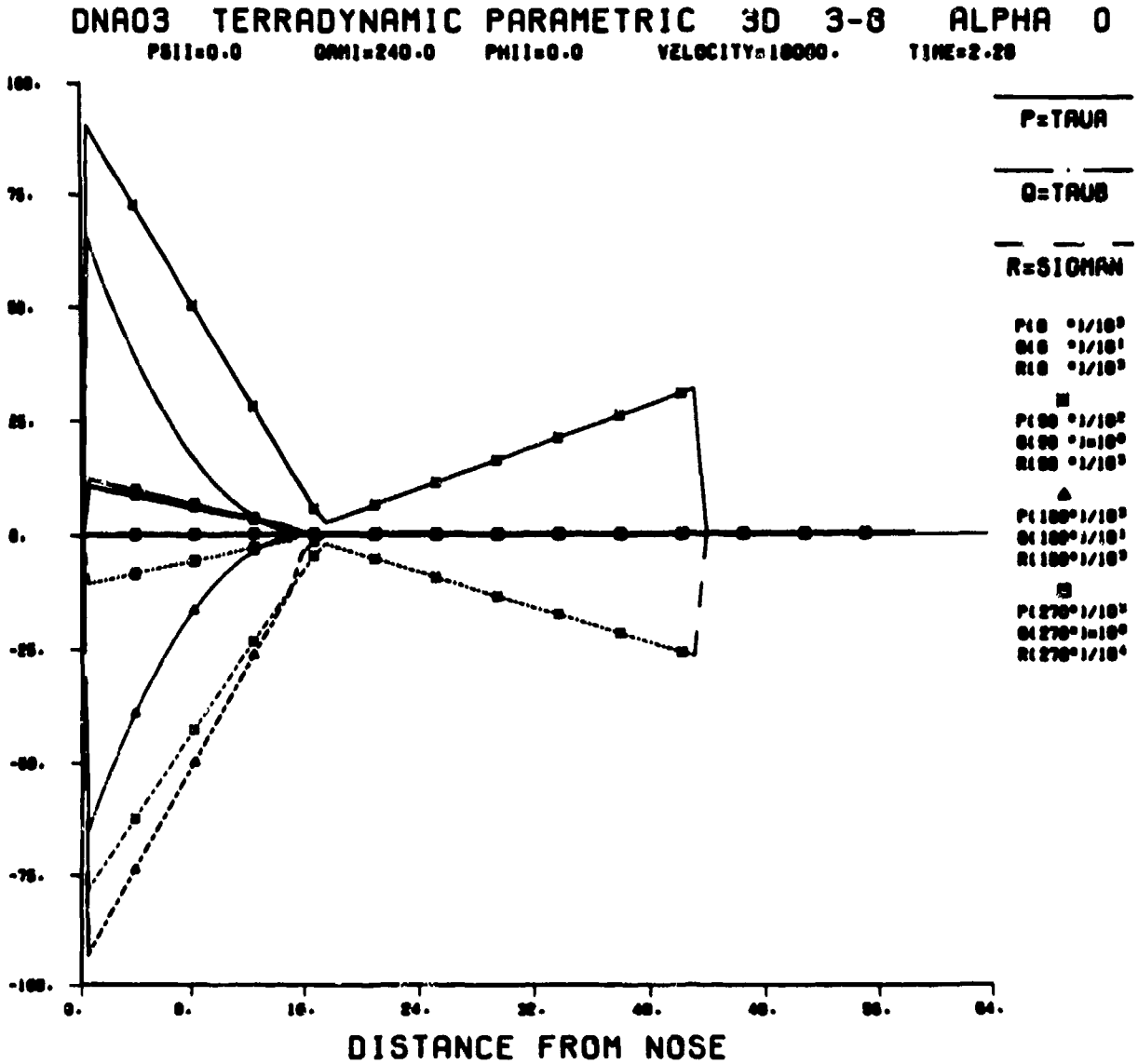

Figure 14. (3D) Stress data

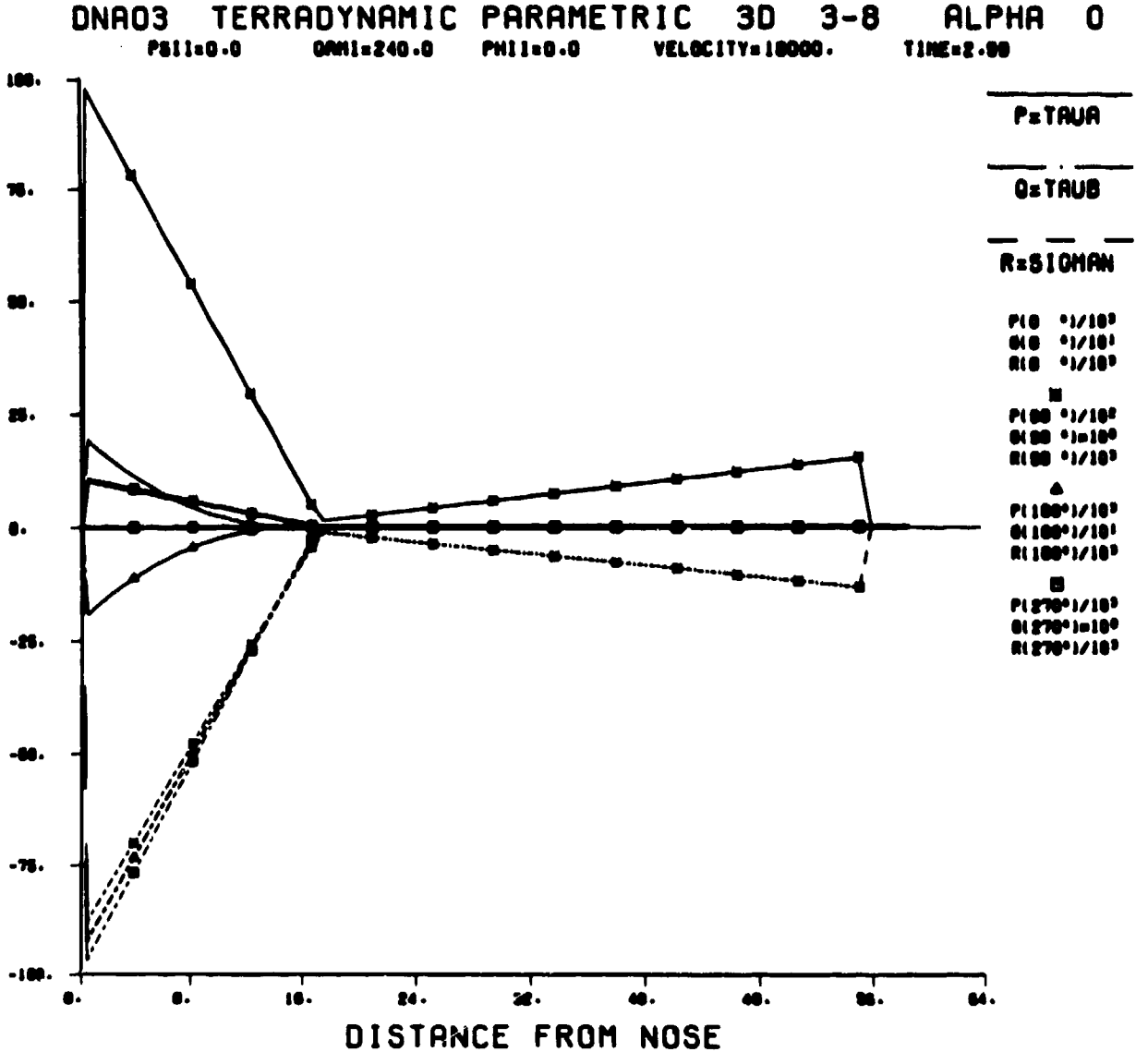

Figure 15. (3D) Stress data

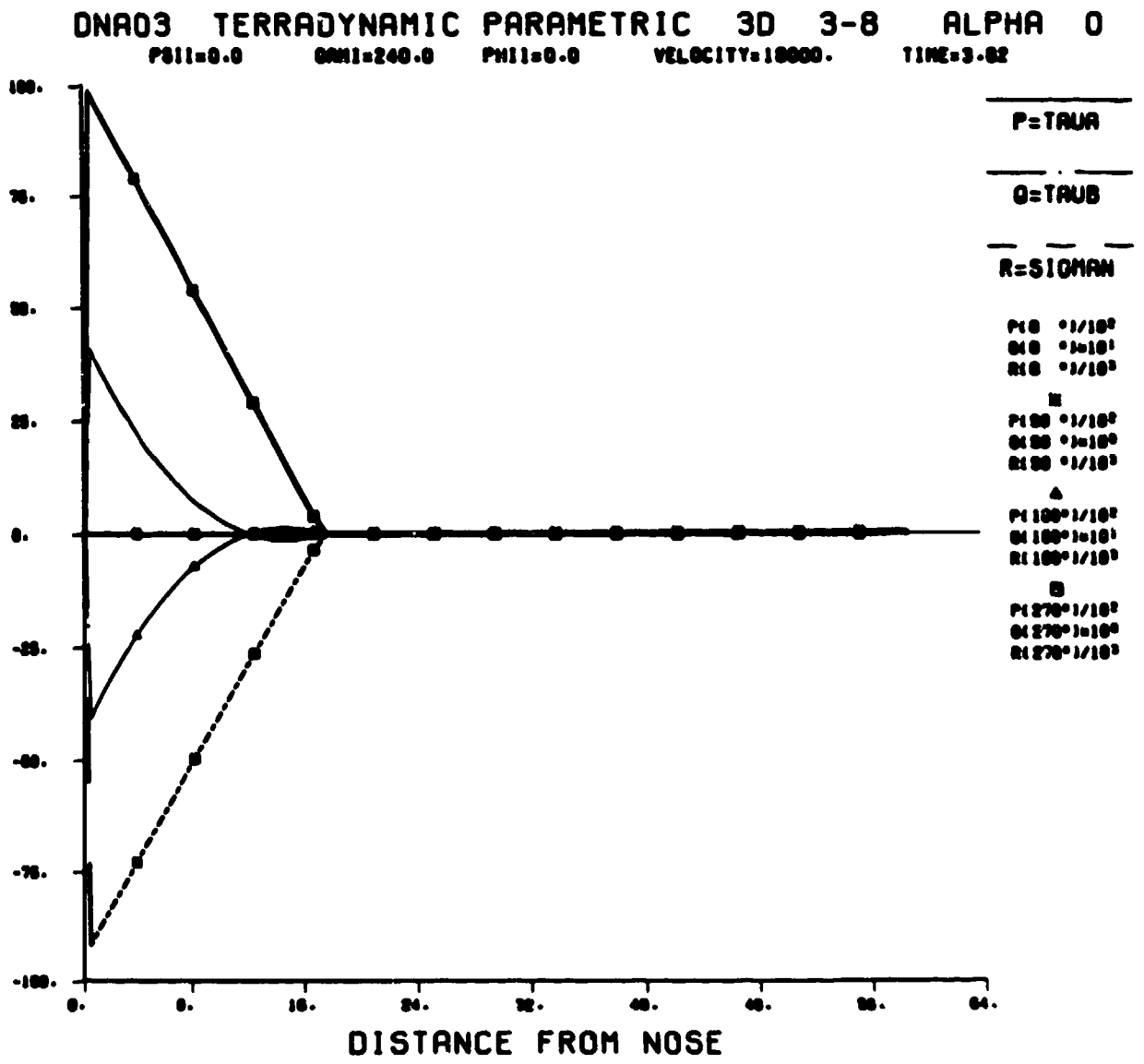

Figure 10. (3D) Stress data

TABLE 13

PURPOSE: To give the output format for 2D plots.

GENERAL FORMAT: At the top of each graph directly under the main title specific data on the penetrator characteristics and impact conditions are included.

Symbol	Characteristics	Units
R	Cylindrical radius	inches
L	Cylindrical length	inches
GAMI	Impact obliquity angle plus angle attack	degrees
VEL	Impact velocity of the penetrator, while it is zero when the angle of attack is not zero.	inches/sec
XCG	Center of gravity acceleration	ft/sec^2
XW	Weight of the penetrator	pounds

1. Graph 1: Trajectory Schematic

The penetrator axis lies in the XZ plane. Velocity of the penetrator is shown as an arrow from the center of gravity and point along the axis of the penetrator, Alpha is the angle of attack which is defined as follows:

$$\alpha = \gamma - \theta'$$

where γ is obliquity angle measured from the normal of the target to the axis of the penetrator as shown below:

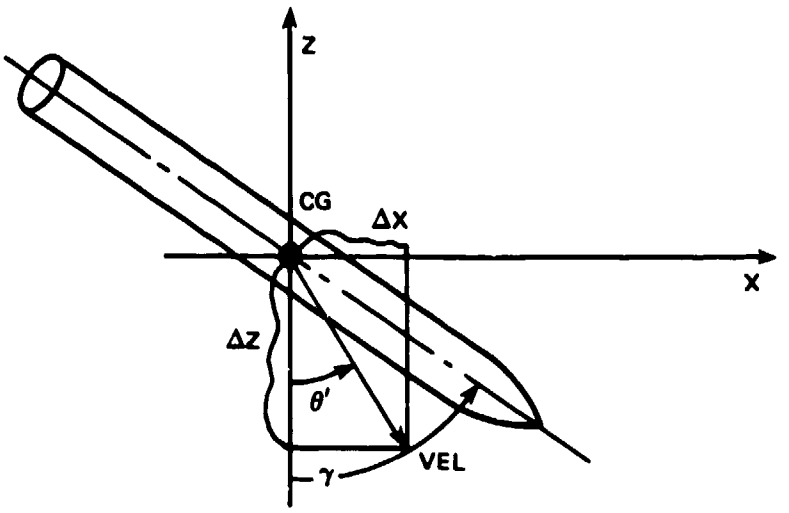

TABLE 13 (Cont'd)

and θ' is defined as

$$\theta' = \tan^{-1}\left|\frac{\Delta X}{\Delta Z}\right|$$

therefore α is positive when $\gamma > \theta'$

α is negative when $\gamma < \theta'$

2. Graph 2: The Loading History of the Penetration

Symbol	Characteristics	Units
FXP	The lateral loads	pounds
FZP	The axial loads	pounds
MCG	The applied moment (or torque) acting about the center of gravity.	in-pounds

3. Graph 3: The Trajectory History of the Penetration

Symbol	Characteristics	Units
X	The lateral displacement	inches
Z	The axial displacement	inches
VEL	The velocity at the center of gravity	inches/sec
ALA	The angle of attack amplitude	radians
GAM	The angle of obliquity (orientation of the penetrator measured from the target normal)	degrees

4. Graph 4: The Axial Acceleration History of the Penetration

Symbol	Characteristics	Units
GZ1 ' · '	The axial acceleration at point 1	g
GZ2 ' * '	The axial acceleration at point 2	g
GZ3 ' ▲ '	The axial acceleration at point 3	g

and the three points are referred to the positions on the penetrator selected by the user. (For this study at the cg).

TABLE 13 (Concl'd)

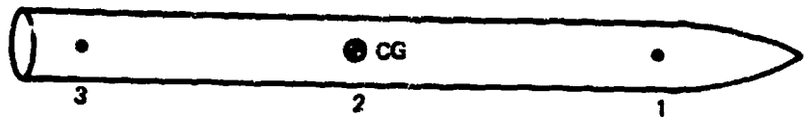

5. Graph 5: The Lateral Acceleration History of the Penetration

Symbol	Characteristics	Units
GX1	The lateral acceleration at point 1	g
GX2	The lateral acceleration at point 2	g
GX3	The lateral acceleration at point 3	g

TABLE 14

PURPOSE: To give the output format for 3D plots:

GENERAL FORMAT: At the top of each graph directly under the main title specific data on the penetrator characteristics and impact conditions are included.

Symbol	Characteristics	Units
PSII 'ψ'	Initial rotational displacement in yaw of the flight path frame with respect to inertia frame.	degrees
GAMI 'γ'	Initial rotational displacement in pitch of the flight path frame with respect to inertia frame.	degrees
PHII 'ϕ'	Initial rotational displacement of body fixed frame with respect to flight path frame.	degrees
VELOCITY	Impact velocity of the penetrator, while it is zero when the angle of attack is not zero.	in/sec
TIME	Time at which the plot is taken.	sec.

For further reference see Figure 17.

1. Graph 1: Penetrator Orientations in ZY Plane and XY Plane

   Velocity of the penetrator is not shown on this graph, but the definition of obliquity angle is a little different (by adding 180°) from the one defined in 2D cases.

2. Graph 2: The Loading History of the Penetrator

Symbol	Characteristics	Units
FX ' . '	The lateral loads in X-direction	pounds
FY ' * '	The lateral loads in Y-direction	pounds
FZ ' ▲ '	The axial loads in Z-direction	pounds
MX '⊔'	The shear-moment in X-direction	in-pounds
MY ' X '	The shear-moment in Y-direction	in-pounds
MZ ' ♦ '	The bent-moment in Z-direction	in-pounds

3. Graph 3: Rotational History of the Penetrator

Symbol	Characteristics	Units
YAW ' . '	Angular displacement with respect to local non-spinning frame of Z_1.	degrees

TABLE 14 (Cont'd)

Symbol	Characteristics	Units
PCH '*'	Angular displacement with respect to local non-spinning frame of Z_2.	degrees
ROL '▲'	Angular displacement with respect to local non-spinning frame of Z_3.	degrees
YAR '□'	Rate of change of angular displacement with respect to Z_1 along the direction of Z_3.	rad/sec
PCR 'X'	Rate of change of angular displacement with respect to Z_2 along the direction of Z_1.	rad/sec
ROR '♦'	Rate of change of angular displacement with respect to Z_3 along the direction of Z_2.	rad/sec

NOTE: All rotations were made using right-hand rule.

4. Graph 4: Translational History of the Penetrator

Symbol	Characteristics	Units
X '.'	The lateral displacement in X-direction	inches
Y '*'	The lateral displacement in Y-direction	inches
Z '▲'	The axial displacement in Z-direction	inches
ALA '□'	The axial amplitude of angle of attack	degrees
ALL 'X'	The lateral amplitude of angle of attack	degrees
VEL '♦'	The resultant translational velocity	in/sec

5. Graph 5 to Graph 10: Stress History of the Penetrator

Symbol		Characteristics	Units
P		Axial shear at a local surface	psi
Q		Lateral shear at a local surface	psi
R		Normal pressure at a local surface	psi
$P(0^o)$	'.'	Axial shear at 0^o	psi
$Q(0^o)$	'.'	Lateral shear at 0^o	psi
$R(0^o)$	'.'	Normal pressure at 0^o	psi
$P(90^o)$	'*'	Axial shear at 90^o	psi
$Q(90^o)$	'*'	Lateral shear at 90^o	psi
$R(90^o)$	'*'	Normal pressure at 90^o	psi

TABLE 14 (Concl'd)

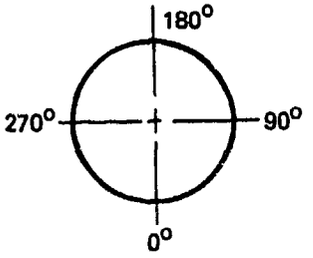

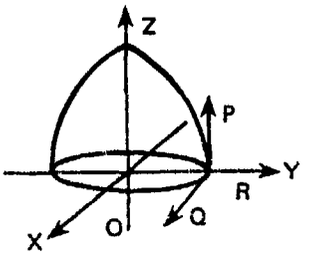

For further reference see Figure 18.

The 3-D graphical output format is similar to the 2-D except that the rotational and translational trajectory data are separated (to avoid confusion) and several additional graphs (the number depending upon the times during the trajectory of interest) are generally provided to define the pressure and shear distribution on the body.

The 3-D graphical displays include:

- a pictorial representation of the impact and penetration event. (See Figure 7.)
- the total rigid body applied loads and moments. (See Figure 8.) (The center of gravity accelerations can be obtained through division of these quantities by the EP weight or rotational inertias.)
- the rotational motion and rate histories. (See Figure 9.)
- the translational trajectory histories. (See Figure 10.)
- local pressure and shear distribution plots. (See Figures 11 through 16.)

For specific definition of these displayed quantities, the reader is referred to Tables 13 and 14.

The 2-D output information is readily understood as to the manner of the quantities in question. In order to understand the output quantities of a 3-D event, it is necessary to understand the reference frames in which the data is provided. The 3-D data is specified in three separate reference frames.

- Inertial.
- Flight path.
- Local non-spinning.

These reference frames and the coordinate transformation sequence are presented and defined in Figures 17 and 18. Referring to these figures:

- the translational state vectors are specified in the inertial reference frame X, Y, and Z.
- the rotational state vectors are Eulerian rotational displacements and rates.

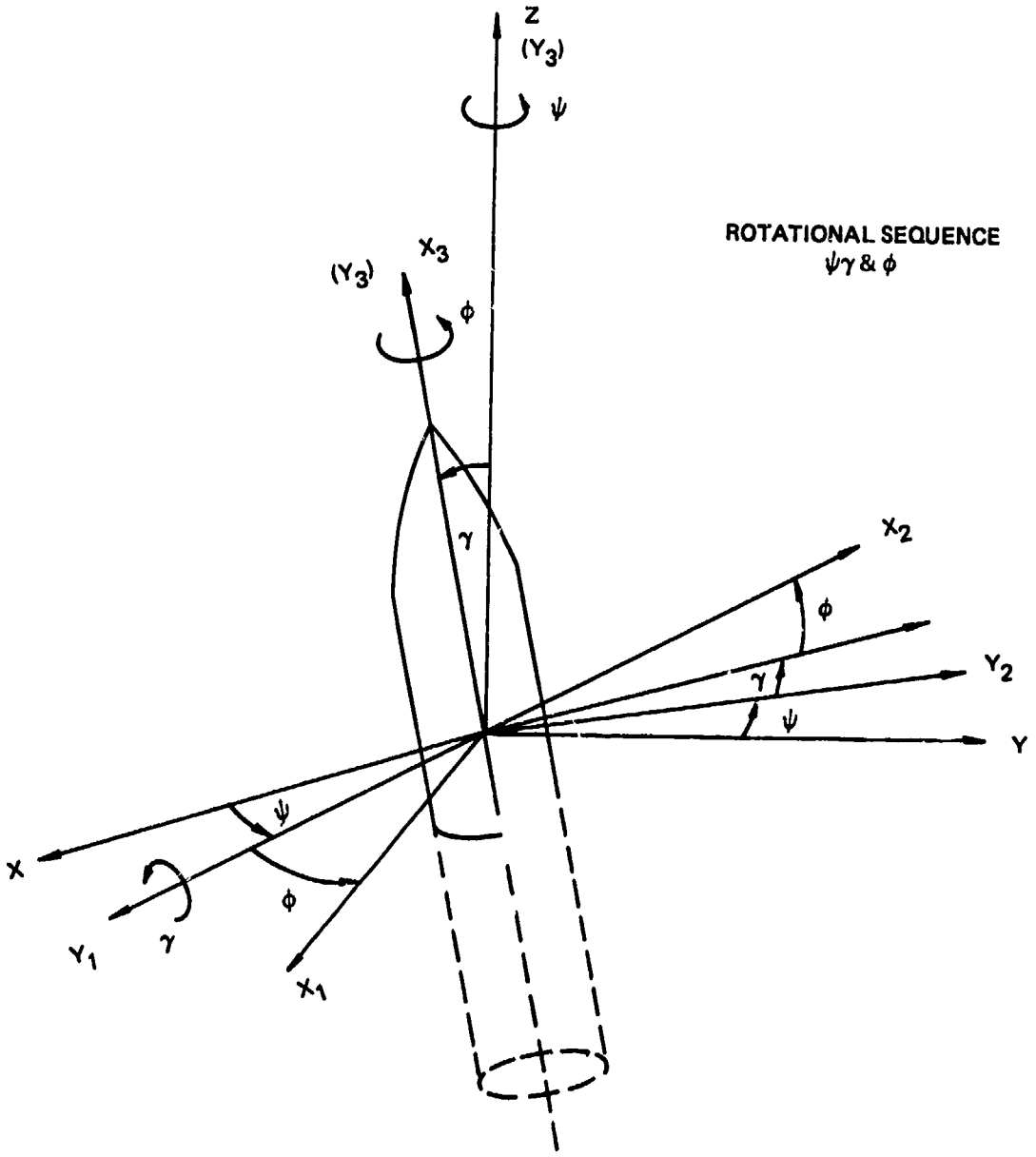

X Y Z ~ Inertia frame (right handed coordinate system)
X & Y are in the plane of target surface

$Y_1Y_2Y_3$ ~ Flight path frame (fixed in the body of projectile but not spinning with it)

$X_1X_2X_3$ ~ Body fixed frame (spinning with it)

Figure 17. Reference coordinate systems

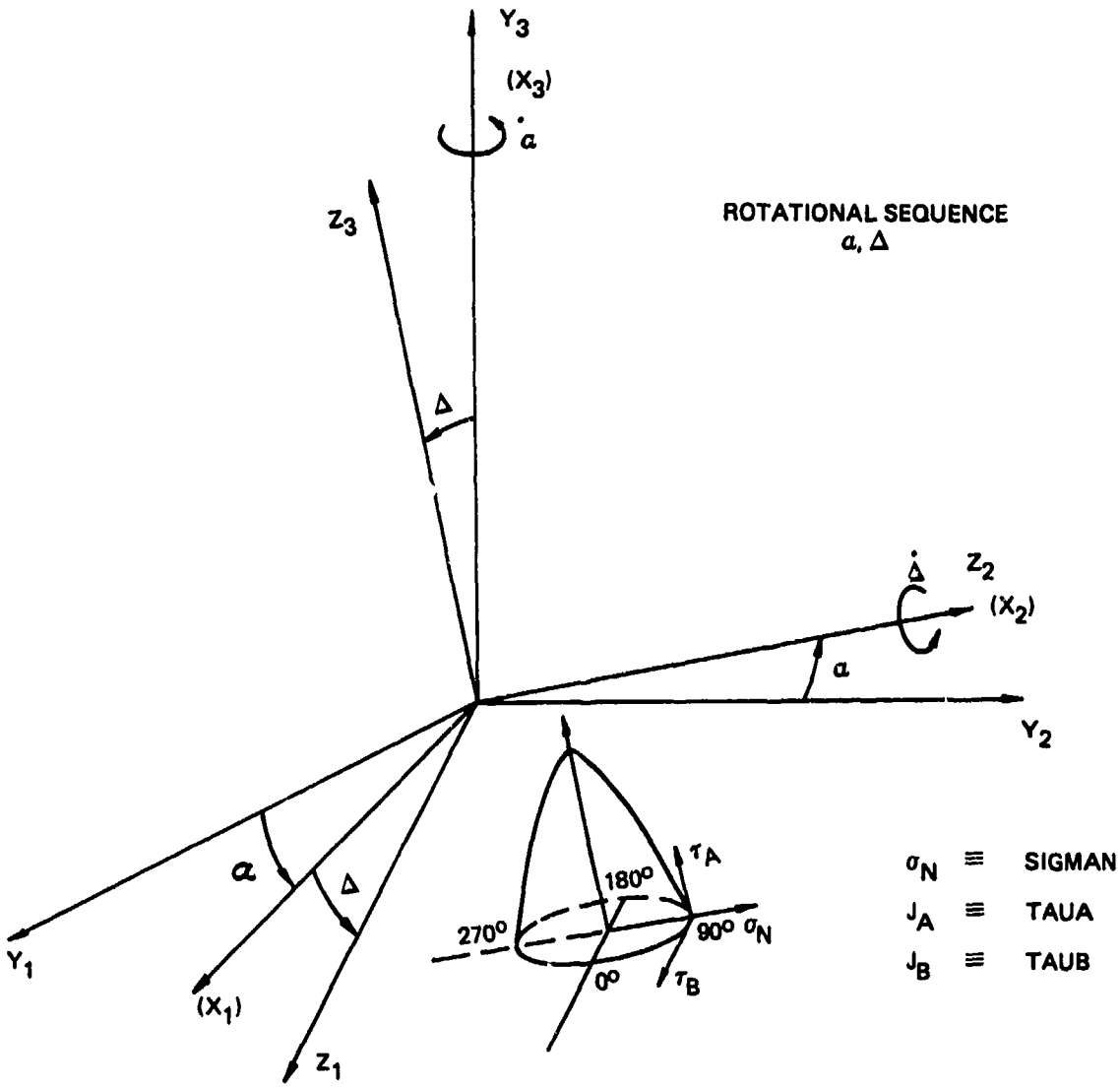

$Y_1Y_2Y_3$ ~ Flight path frame

$X_1X_2X_3$ ~ Body fixed frame (spinning)

$Z_1Z_2Z_3$ ~ Local non-spinning frame

Figure 18. Local non-spinning frames

- the resulting forces and moments are specified in the flight path frame ($\bar{Y}_1$, $\bar{Y}_2$, and $\bar{Y}_3$).
- the pressures and shears are defined in the local non-spinning reference frame (Z_1, Z_2, and Z_3). (See Figure 18.)

In order to obtain the body fixed rotational vectors (ω_1, ω_2, and ω_3) which lie along the X_1, X_2, and X_3 axis respectively in Figure 17, the following relationships are provided:

$$\omega_3 = \dot{\phi} + \dot{\psi}\cos\gamma$$

$$\omega_2 = (\sin\gamma\,\dot{\psi} - \dot{\gamma}\sin\phi/\cos\phi)/(\sin^2\phi + \cos\phi)$$

$$\omega_1 = (\dot{\gamma} + \omega_2\sin\phi)/\cos\phi$$

When studying the stress distribution data (i.e., Figures 11 through 16), it should be noted that each of these graphs provides surface traction information (lb/in^2):

- at a specific time during the penetration event.
- at specific locations around the periphery of the EP.
- distributed along the length of the vehicle (the nosetip being the zero station) and after stations along the abscissa.
- consisting of three components, SIGMAN - normal to the surface, TAUB - perpendicular to the body longitudinal axis in the plane of the surface, and TAUA - also in the plane of the surface directed aft.

Some discussion relative to the shape of these surface tractions distributions is in order. The specific value of the pressure or shear is of course the direct vectoral sum of the force law terms described in Section 3.0.

In the majority of runs conducted for this study, these terms consisted of the media resistance terms (i.e., η and $f_c\eta$) and the equivalent fluid flow terms ($C_N q$, and $C_\tau q$, where q is the dynamic pressure). Because of the shape of these EP's (mostly sharp nosed) little compressibility effects were noted

and only for high obliquity cases (i.e., 45° and above) were surface effects introduced. As a result, the surface traction data appear, in general, as steady-state conditions. This requires some explanation. Avco theorizes that there are three penetration regions for a normal impact event into a semi-infinite target half space.

1. Initial region -- where the presence of the free surface significantly effects distributed surface tractions.
2. The transition region -- where the free surface is becoming less influential.
3. The steady state region -- where the presence of free surfaces no longer effects the surface tractions.

Little real test data is available which quantitatively describes the first two phases or the transition between Phases 1 and 3. In addition, these phases vary significantly depending upon target media, EP nose configuration, and velocity. Fortunately, the resulting (integrated) loads experienced by an EP during this phase of the vent do not appear to alter subsequent steady state loading environments or penetration performance significantly. For the majority of runs therefore, the steady-state (i.e., third phase) force law theory was used. This accounts for the somewhat square appearance of the surfact tractions distributions. Recently, finite difference calculations of the initial phase of the penetration event have been made and these surface tractions are more triangular in shape. In this parametric study, where the initial phase of the penetration event significantly effects subsequent penetration performance, the initial phase theory is used. The effect of this is to produce surface traction distributions more similar to those predicted by the finite difference techniques.

The detailed trajectory and loads history data for the Series 1, Sensitivity Study, was indicated in Runs 1.1.1 through 1.20.5 as defined in Table 7. These data have been analyzed, reduced, and summarized in Figures 19 through 24 of this report.

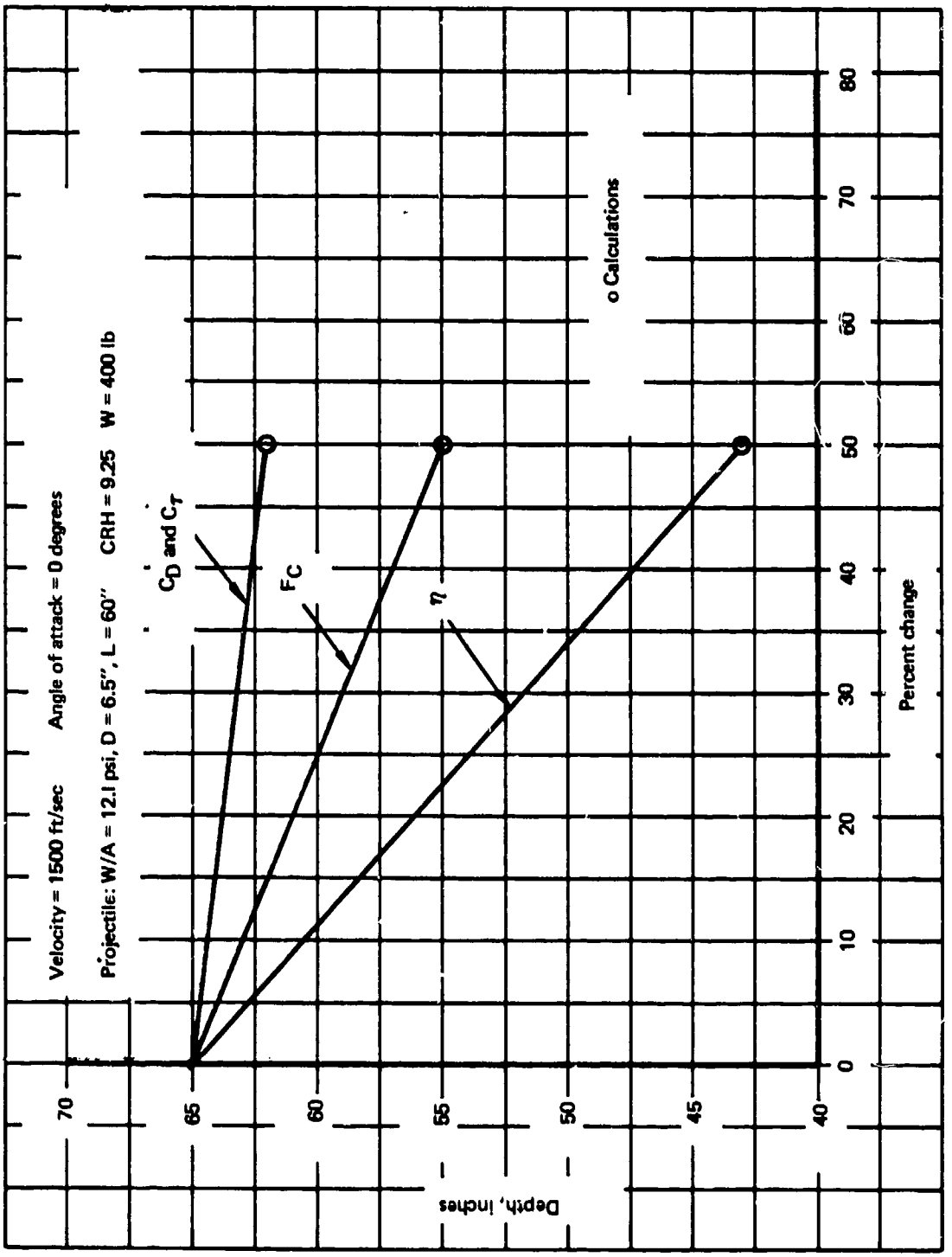

Figure 19. Performance sensitivity, $\alpha = 0^0$

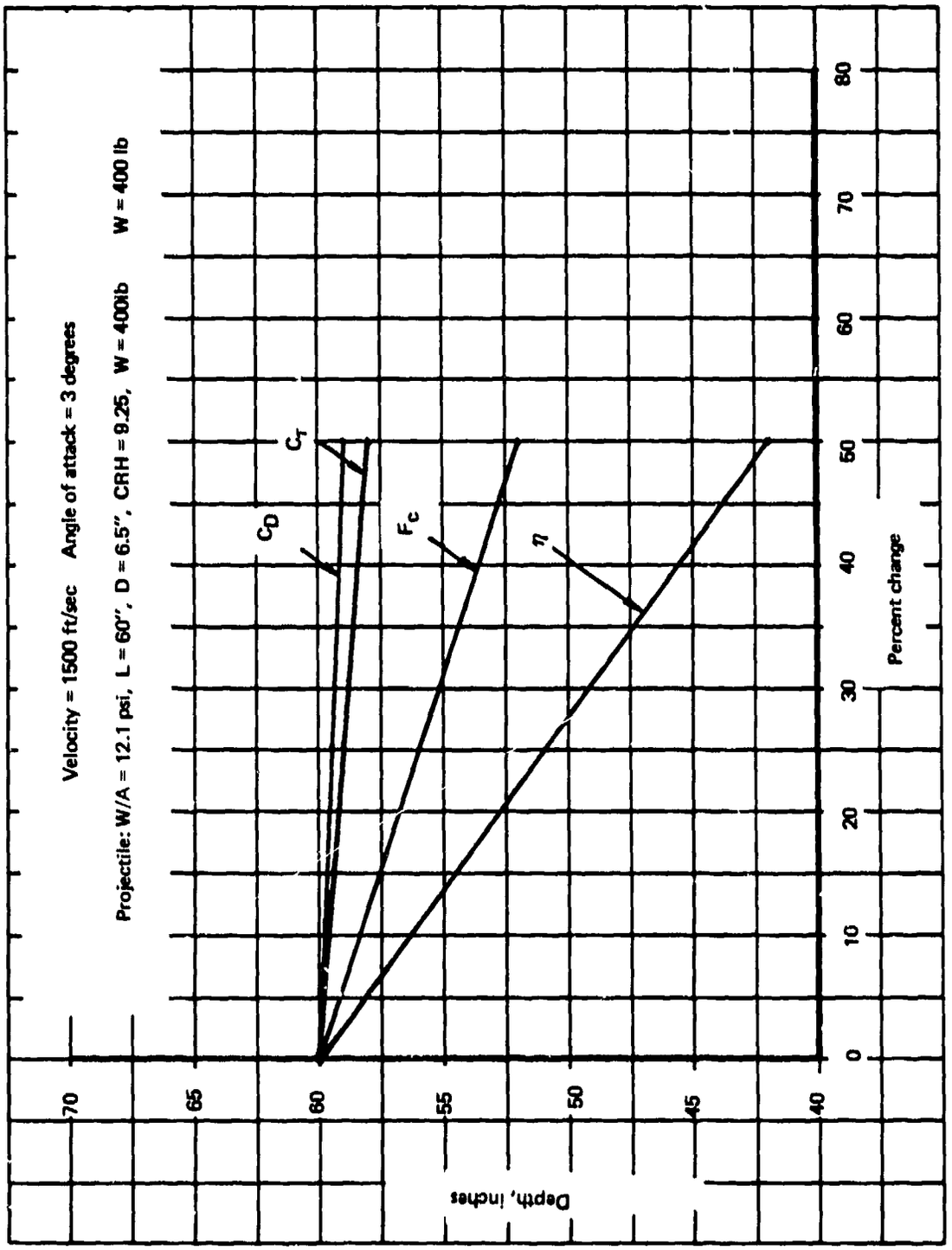

Figure 20. Performance sensitivity, $\alpha = 3°$

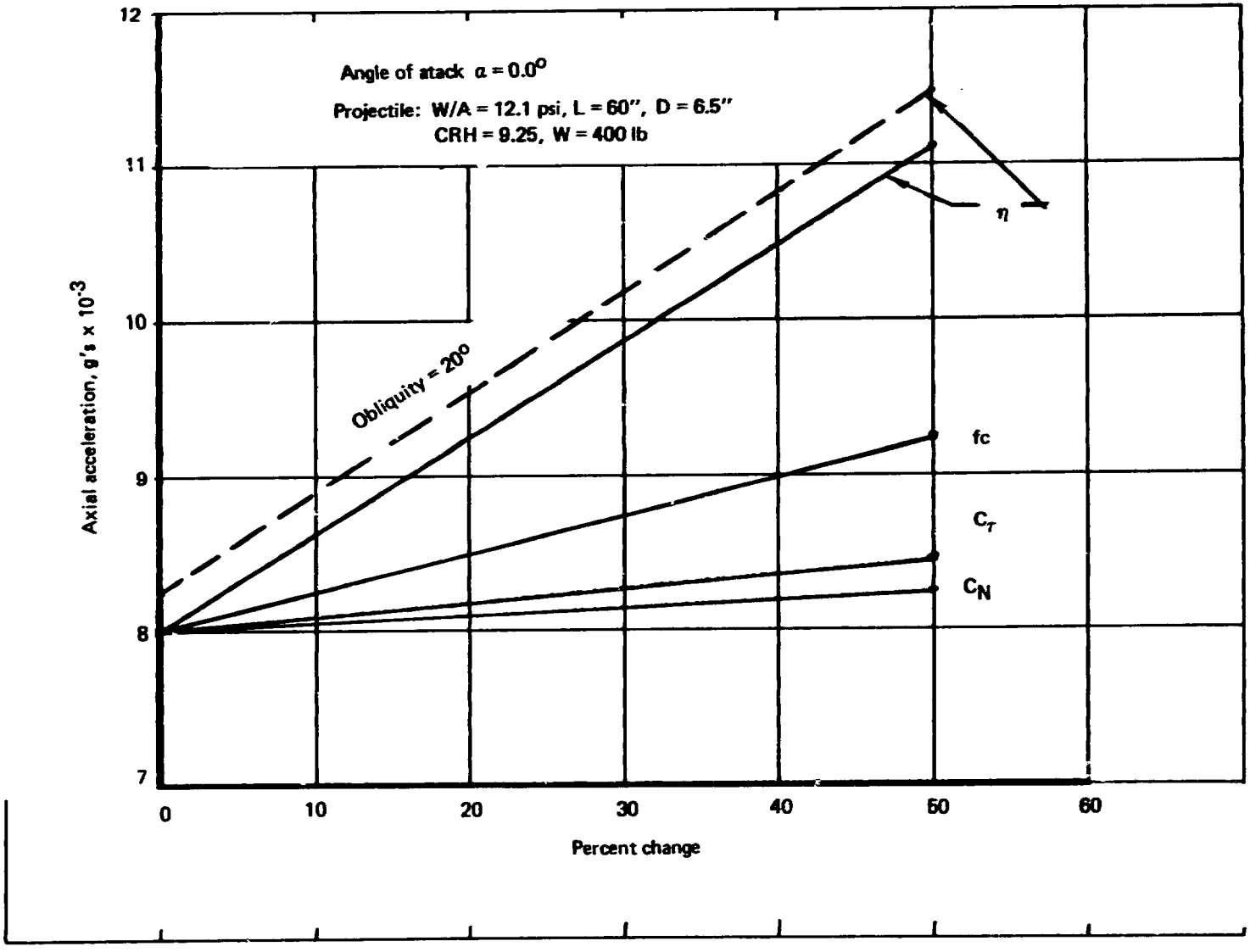

Figure 21. Axial loading environment, $\alpha = 0^{o}$

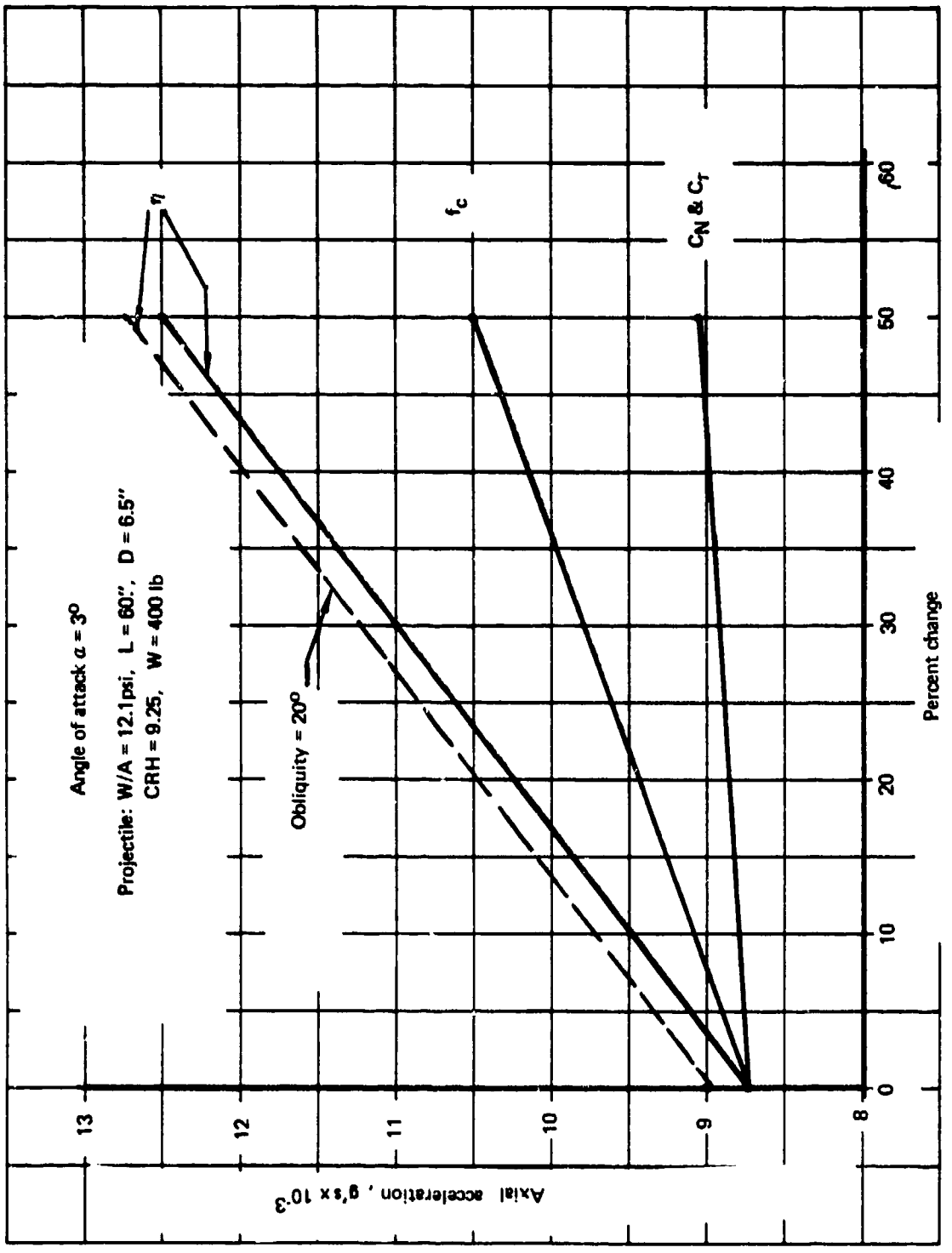

Figure 22. Axial loading environment, $\alpha = 3^{\circ}$

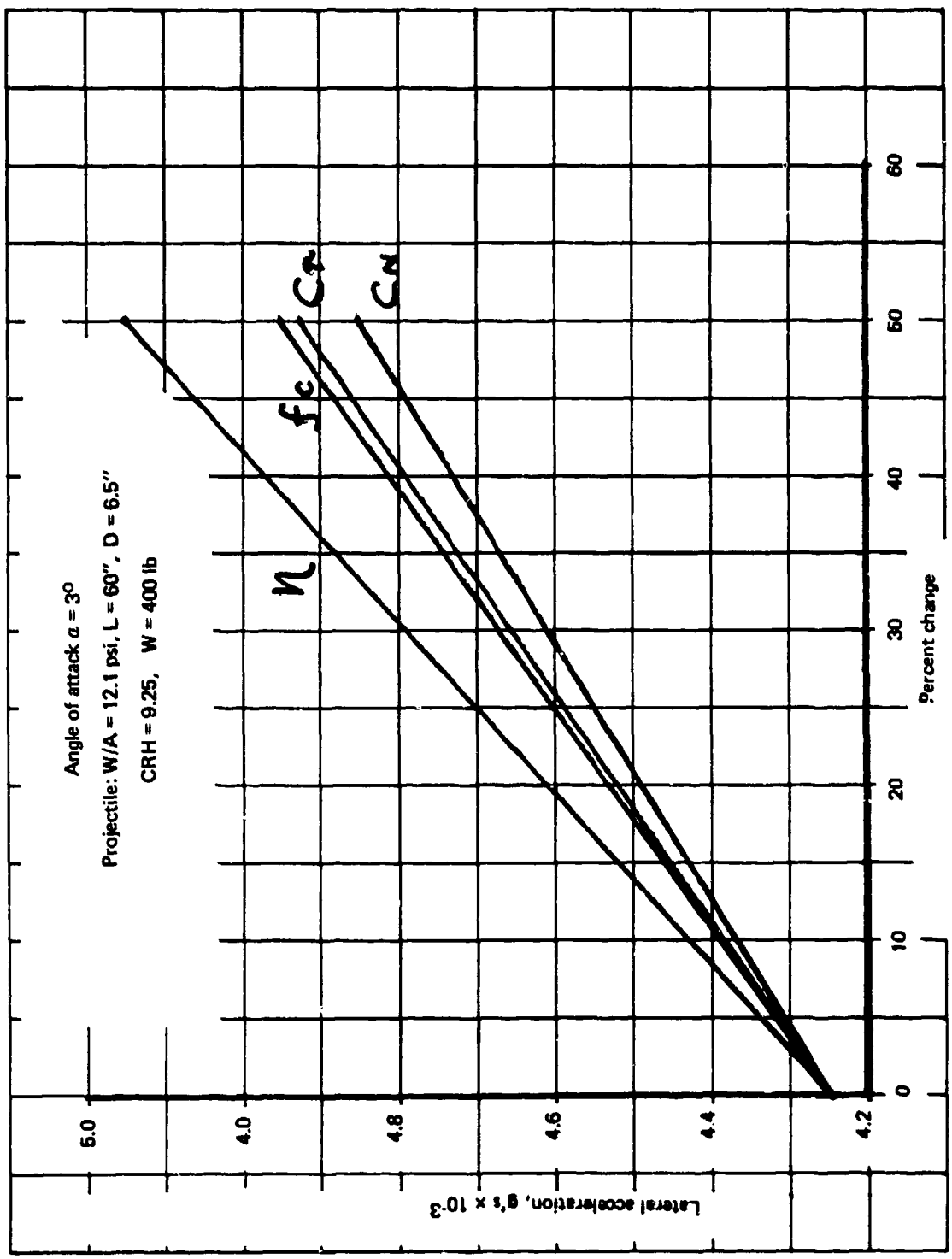

Figure 23. Lateral loading environment, $\alpha = 3^0$

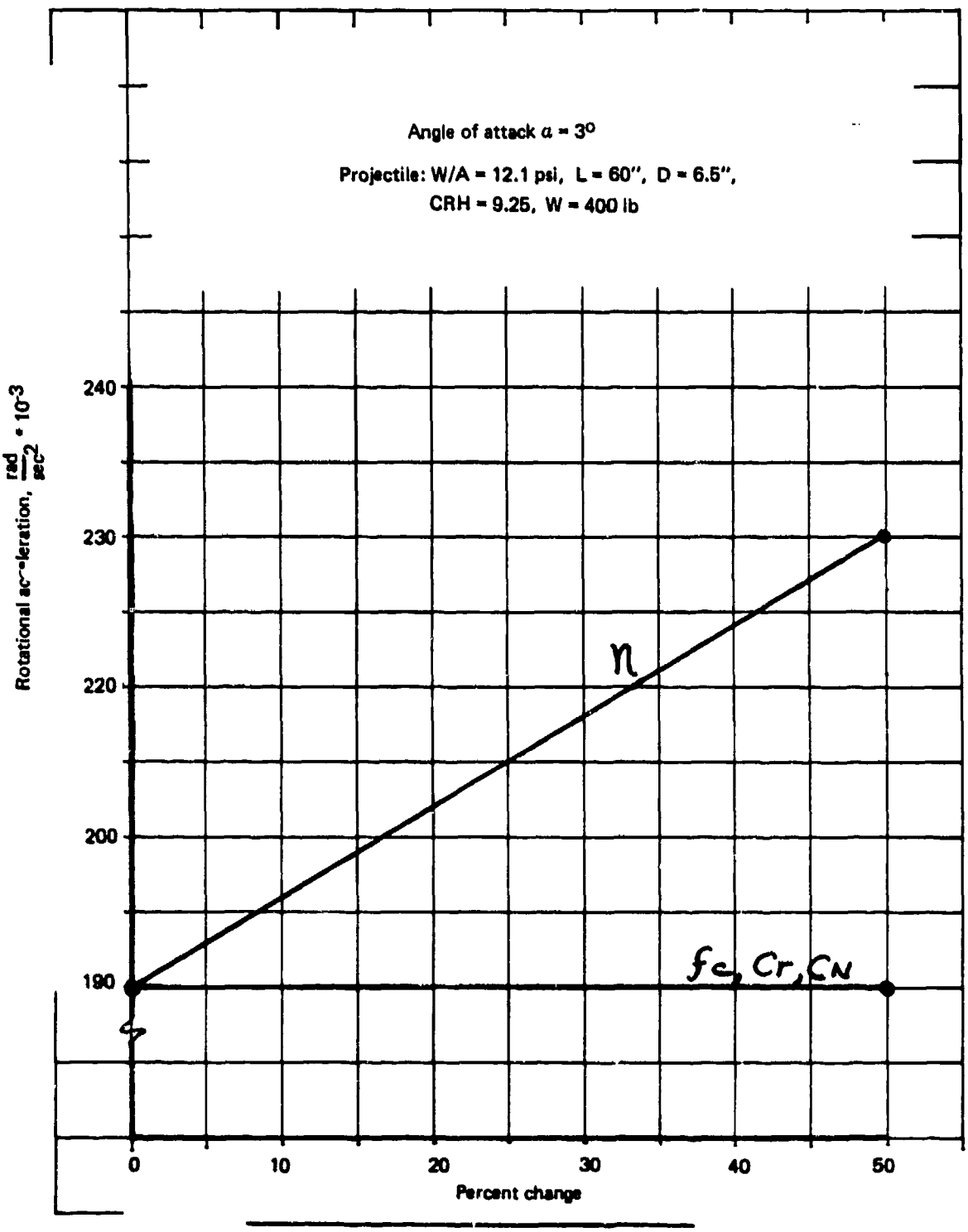

Figure 24. Moment environment, $\alpha = 3^0$

Figures 19 and 20 show penetration depth effects caused by changes in the Avco's Force Law coefficients (i.e., C_N , C_τ , f_c and η) and angle of attack where:

C_N = Normal pressure coefficient due to flow effects.

C_τ = Shear pressure coefficient due to flow effects.

η = Media structural resistance to penetration.

f_c = Media coefficient of friction (used as $f_c * \eta$).

Only two variations of these parameters were used, (i.e., 0.0 and 50% change from the nominal value), consequently only a straight line can be drawn connecting the points. It is apparent from these figures, that "η" has the most significant effect on penetration depth achieved. The change in depth caused by the 3 degree angle of attack was less than 10 percent as shown in Figure 20.

The variation in resulting rigid body g's for the normal impact situation caused by these parameter changes is presented in Figures 21 through 24. The peak axial nominal value expected for this impact situation would be on the order of 8000 g's. The maximum variation consists of an increase to 11,000 g's, again because of the "η" change.

As the angle of attack varies from zero to three degrees, the axial loads will increase because of the addition of friction and shear along the cylindrical portion of the EP. (See Figure 22.) Side loads and moments are also generated as indicated in Figures 23 and 24. The variation of axial loading environments caused by changes in obliquity is included in Figures 21 and 22. Changes in the lateral loads and moments caused by an obliquity of 20 degrees is negligible compared to the effects of angle of attack. The minor differences can be noted by referring to detailed trajectory history results presented in the data of Volume I. The most sensitive parameter for these cases is again "η". The largest variation occurs for the axial loading, again caused by "η".

Less change occurs for the lateral load and almost no change occurs for the resulting moment. The reason for this is because in the case of the axial loads, each component of the increasing load (i.e., normal and frictional component) add thereby generating a relatively large overall increase. In

the case of the lateral load and the moment, these components subtract and result in a smaller increase.

Cases 1-2, 1-17, and 1-18 were selected from Series 1 for 3-D runs to determine the surface tractions data. Peak values of pressures and shears were extracted from the basic data and are provided in Table 15. The variations in the peak levels are not significant. What is significant follows from the integration of these distributions which causes significant lateral loads and moments to be applied to the EP structure.

5.2 SERIES 2 - VARIATIONS IN W/A AND VELOCITY

The purpose of parametric simulations defined by Series 2 is to establish the effects on performance and loading environments caused by variations in "W/A" (EP weight to cross sectional area ratio, a ballistic parameter), and impact velocity. The runs selected to demonstrate these effects are presented in Table 8. Two other variables are included in the study. These are EP diameter and the parameter "CRH". "CRH" is defined as the ratio between the ogive radius and the cylinder diameter of the EP. "CRH" therefore is a measure of nose sleekness. Series 2 consisted of Runs 2.1.1 through 2.64.5 as defined in Table 8. The data summary curves for Series 2 are presented in Figures 25 through 36.

For a "CRH" of 9.25 and an EP diameter of 6.5 inches the relationship between depth of penetration and "W/A" for velocity of 1000, 2000, and 3000 ft/sec is shown in Figure 25. The peak axial rigid body "g" loads for these same variations are presented in Figure 26. The only significant trend noted for this series of runs is related to penetration performance trends as influenced by W/A as opposed to velocity. As a result of the loading theory (i.e., being relatively constant which in Avco's view is characteristic of penetration events into hard targets), increasing velocity is a much more effective way to improve penetration performance than equivalent linear increases in W/A. At the same time, the rigid body loading environments, over the velocity range of interest are not significantly altered by increases in velocity.

TABLE 15

PEAK VALUES OF PRESSURES AND SHEARS - TEST SERIES 1

Problem Number	Type 2D 3D	Projectile Data				Velocity (ft/sec)	Obliquity γ (deg)	Attack Angle α (deg)	Material Property (psi)	Surface Tractions		
				Nose Remarks						Normal Pressure SIGMAN (psi)	Shear	
		W/A (psi)	D (in)	CRH	Weight (lb)						TAUA* (psi)	TAUR* (psi)
1.2A	3D	12.1	6.5	9.25	400	1500	180	3	σ_c = 5000	55,500 (270°)	7500 (270°)	375 (180°)
1.2AI	3D	12.1	6.5	9.25	400	1500	180	3	σ_c = 5000	94,000 (270°)	12,500 (270°)	420 (180°)
1.17A	3D	12.1	6.5	9.25	400	1500	200	0	σ_c = 5000	55,000 (270°)	7250 (270°)	92.5 (180°)
1.18A	3D	12.1	6.5	9.25	400	1500	200	3	σ_c = 5000	55,500 (270°)	7400 (270°)	310 (180°)

*Note: TAUA - shear stress in the axial direction
TAUB - shear stress in the transverse direction
(See Figure 18)

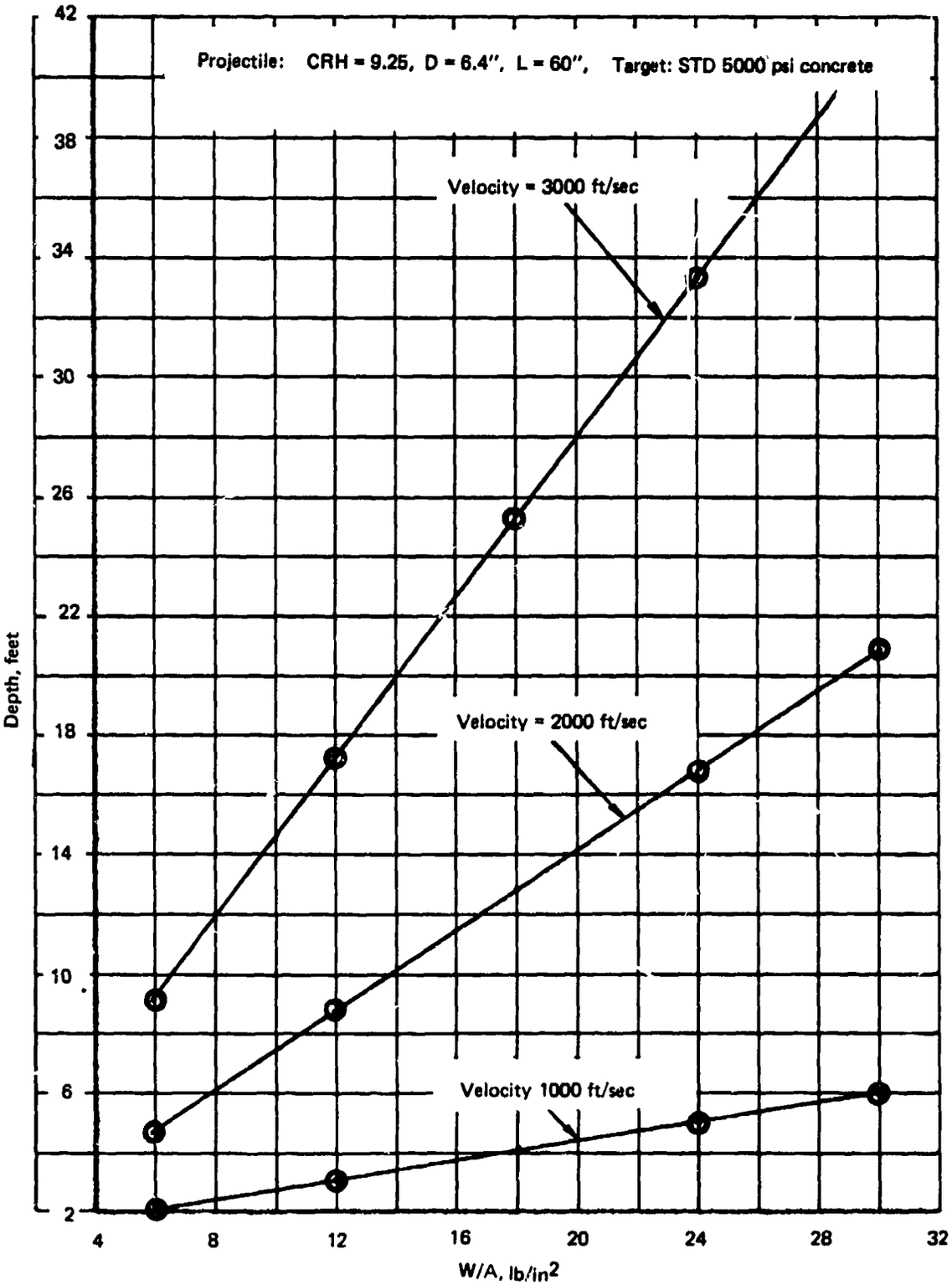

Figure 25. Penetration performance: CRH = 9.25

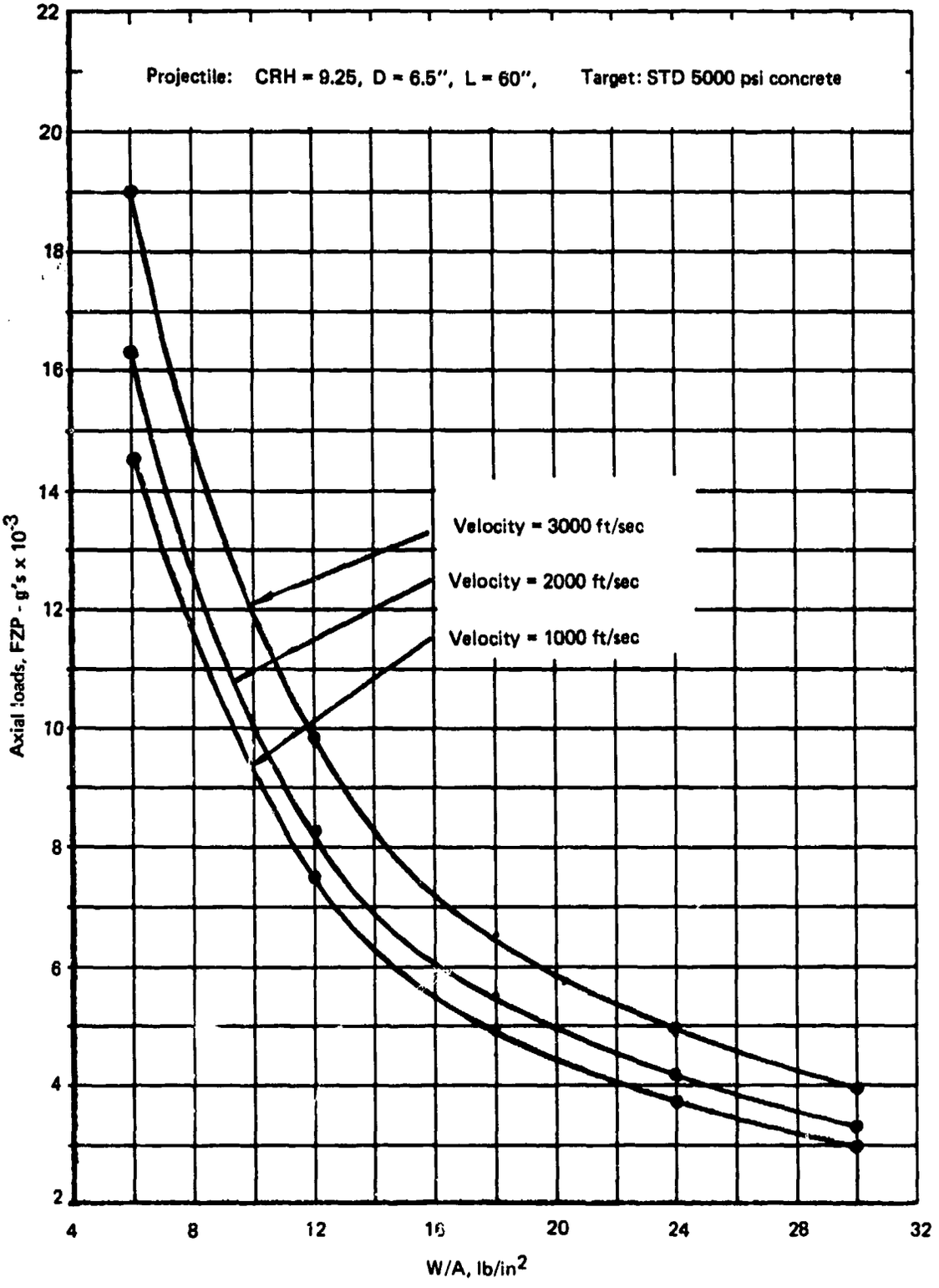

Figure 26. Axial acceleration: CRH = 0.25

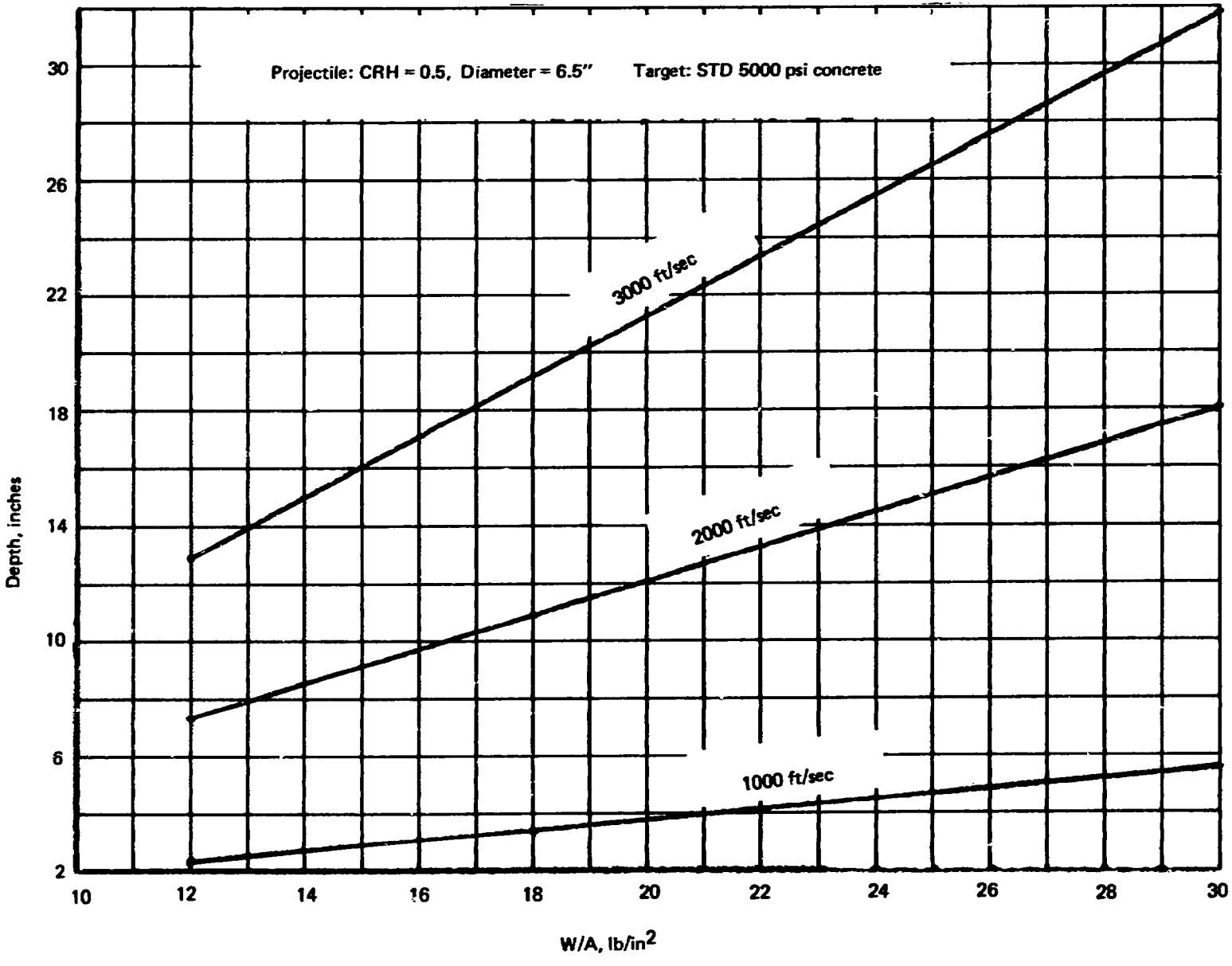

Figure 27. Penetration performance: CRH = 0.5

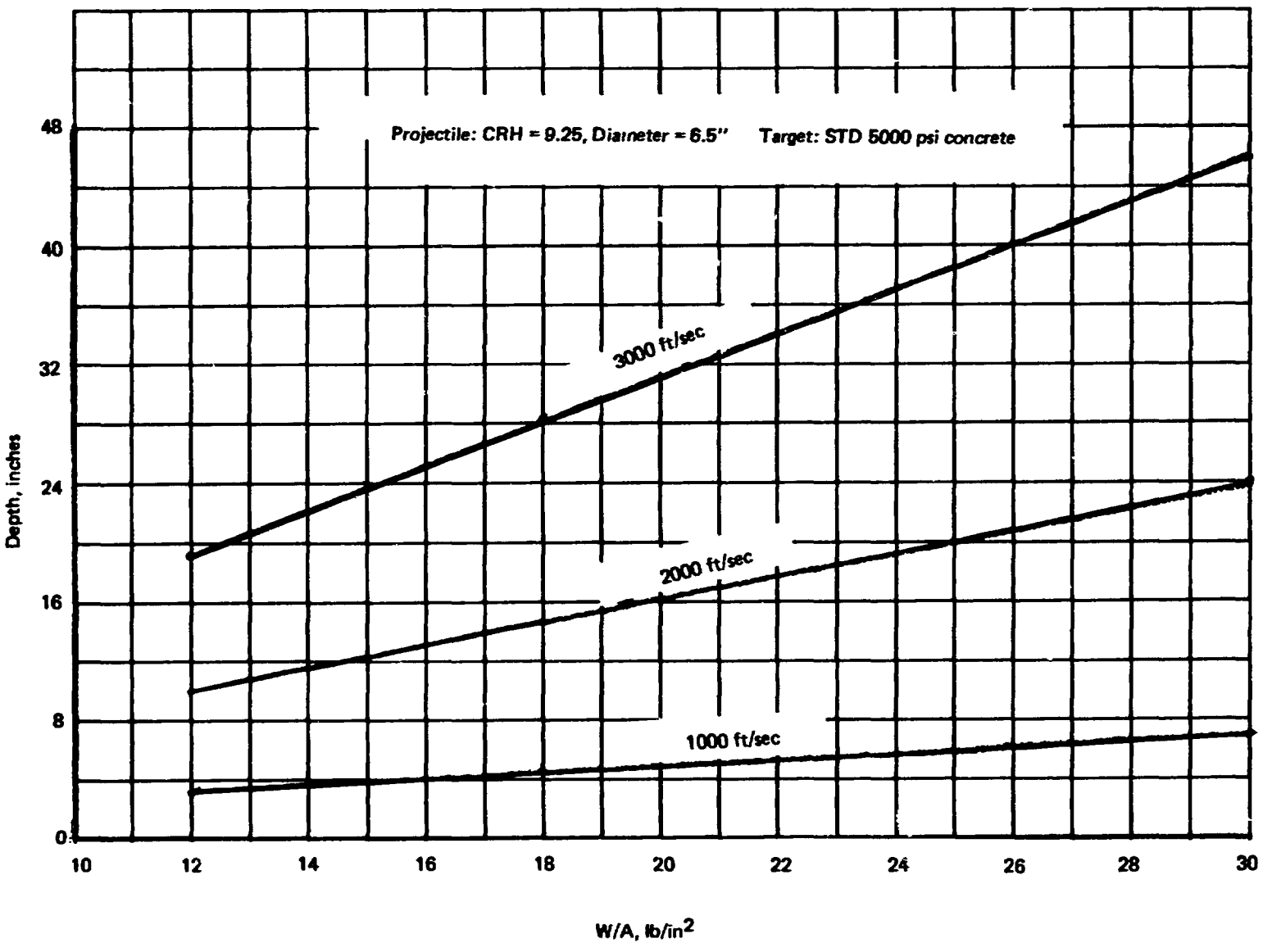

Figure 28. Penetration performance: CRH = 2.25

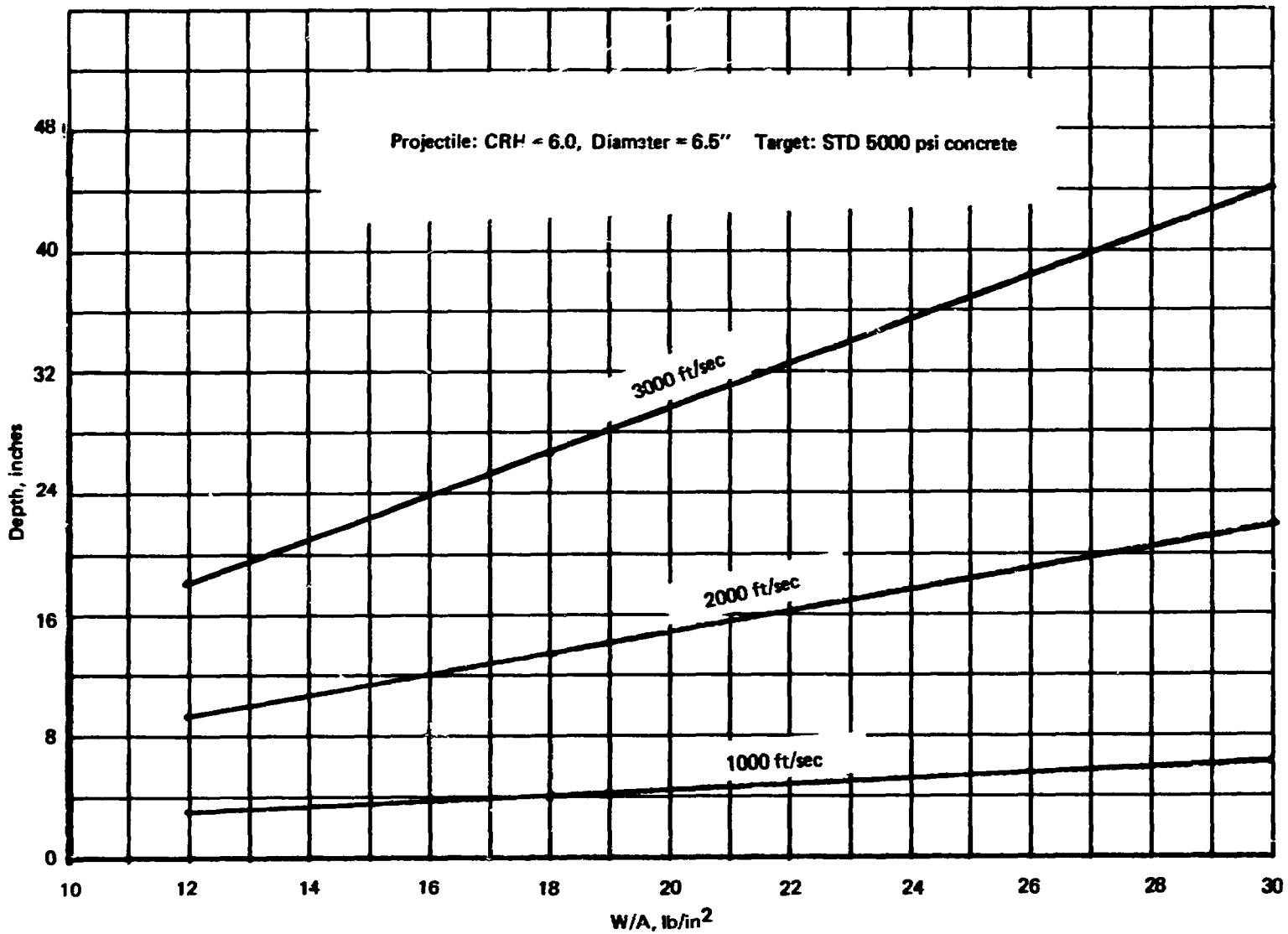

Figure 29. Penetration performance: CRH = 6.0

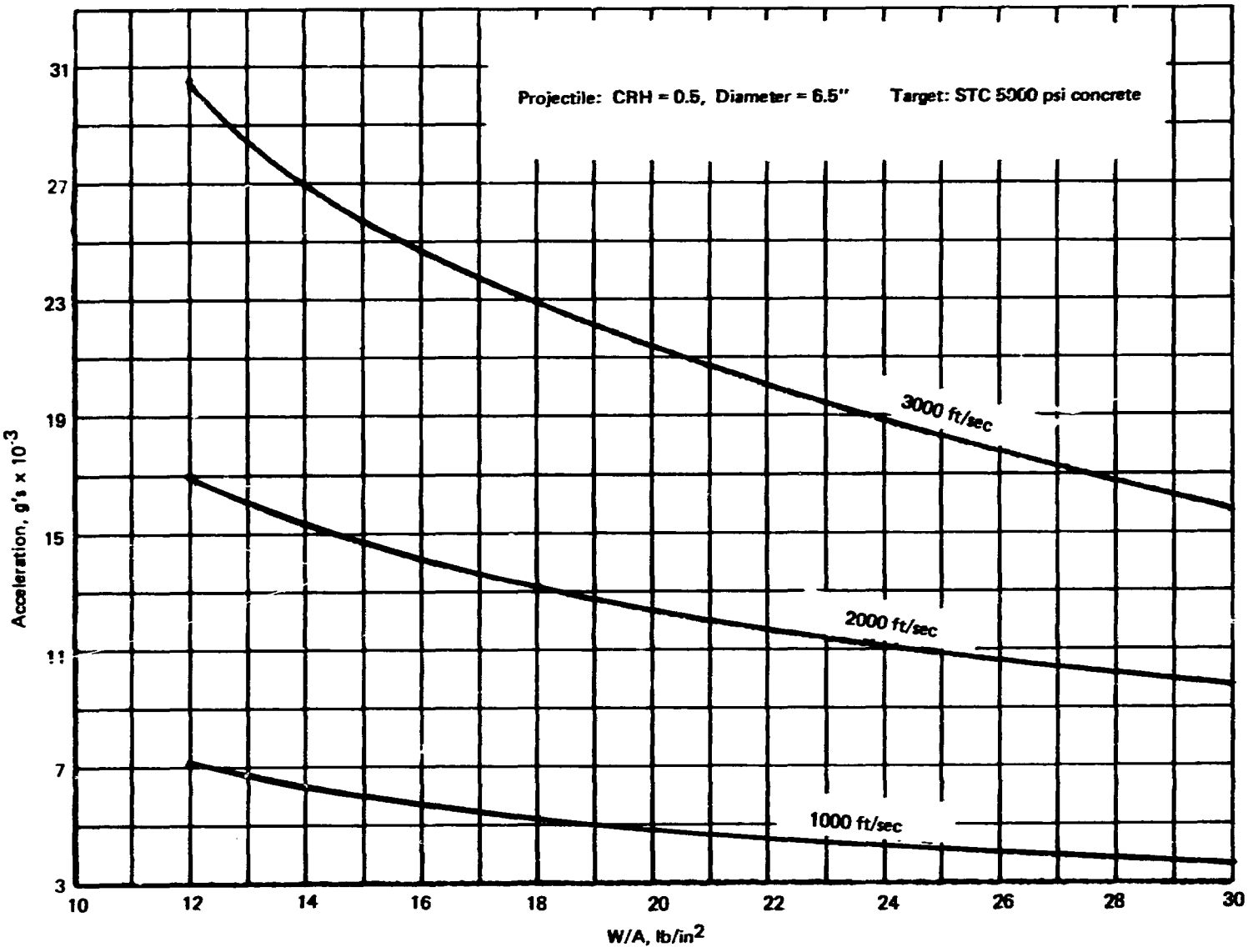

Figure 30. Axial acceleration (Shock): CRH = 0.5

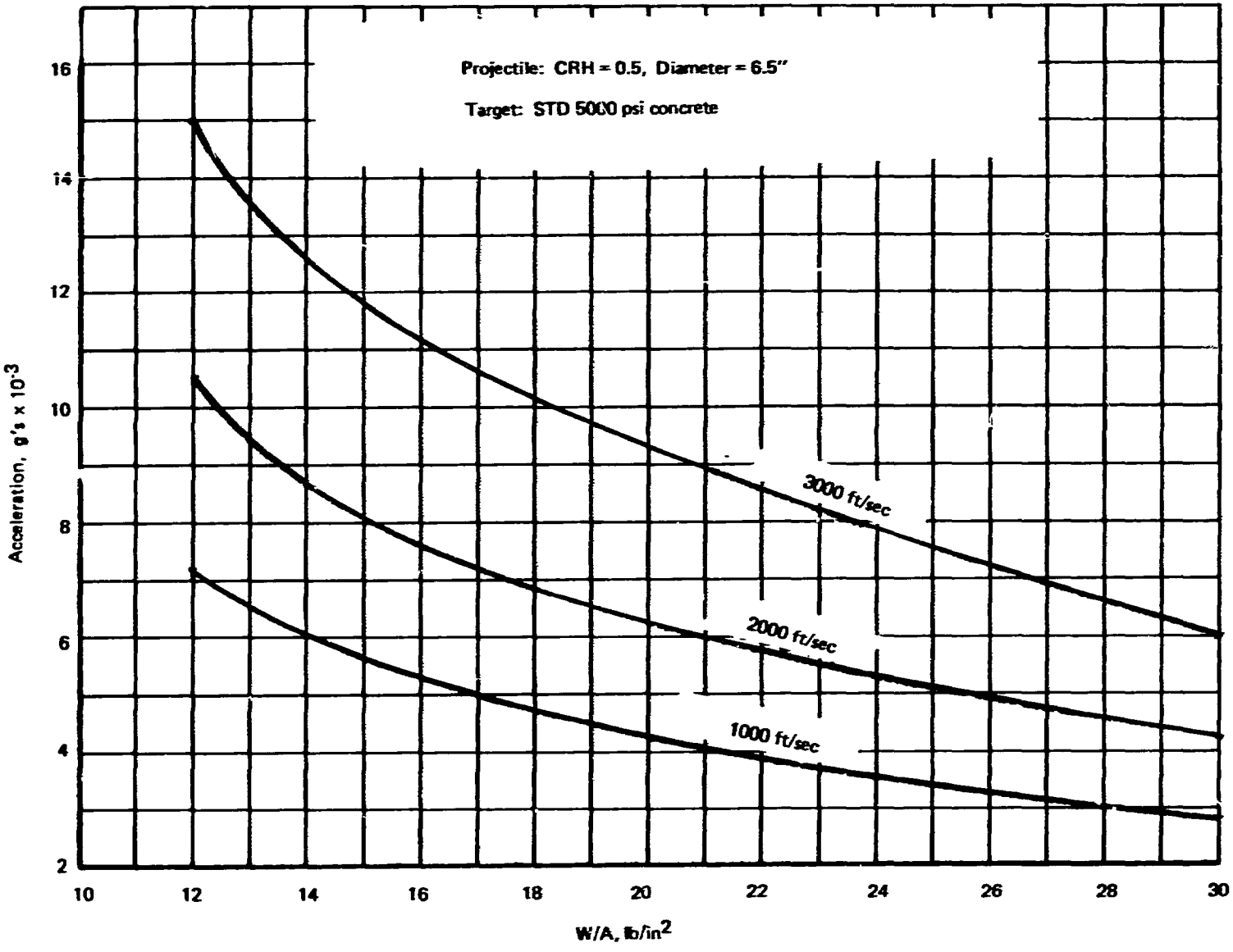

Figure 31. Axial acceleration (Rigid body): CRH = 0.5

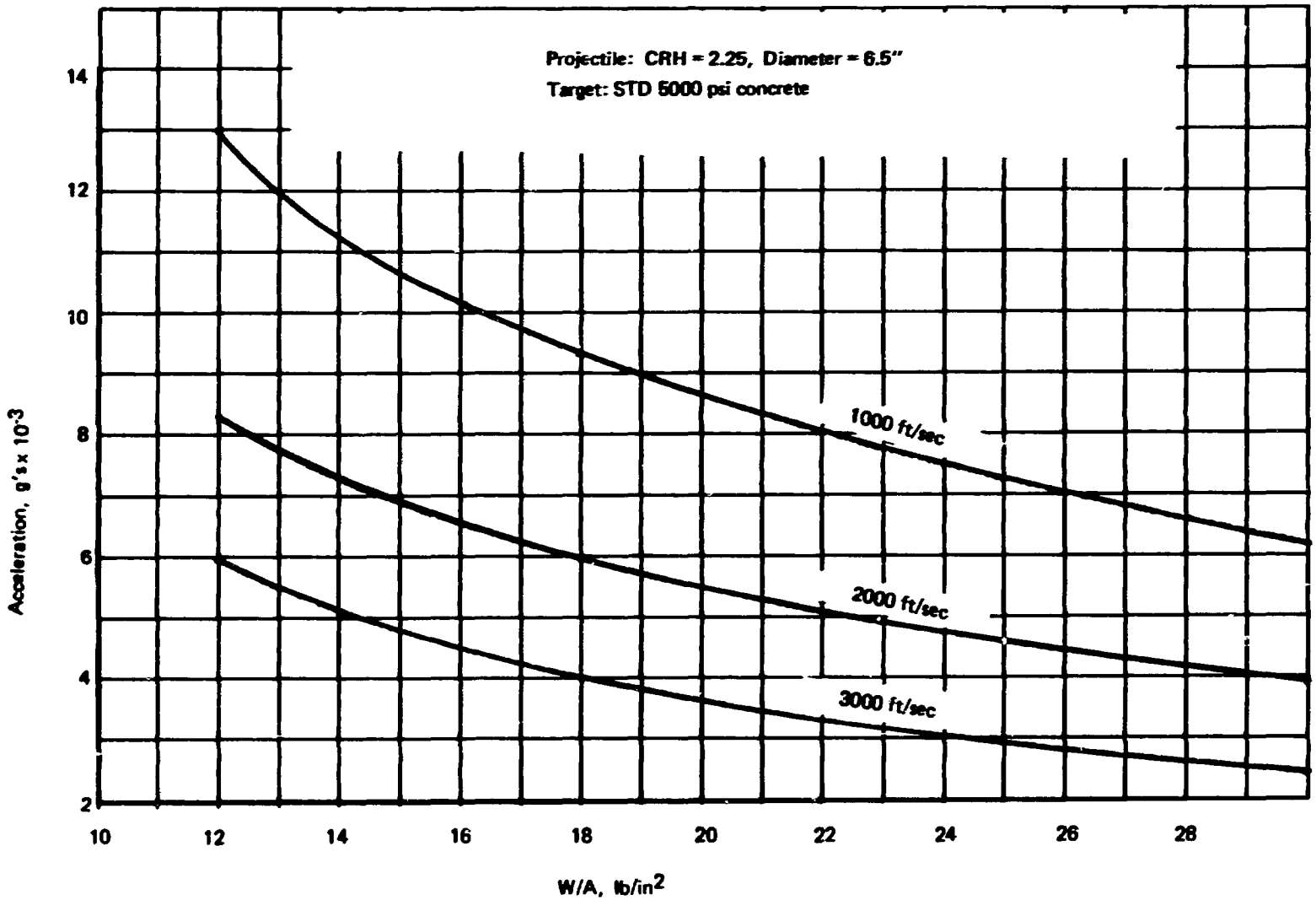

Figure 32. Axial acceleration (Shock): CRH = 2.25

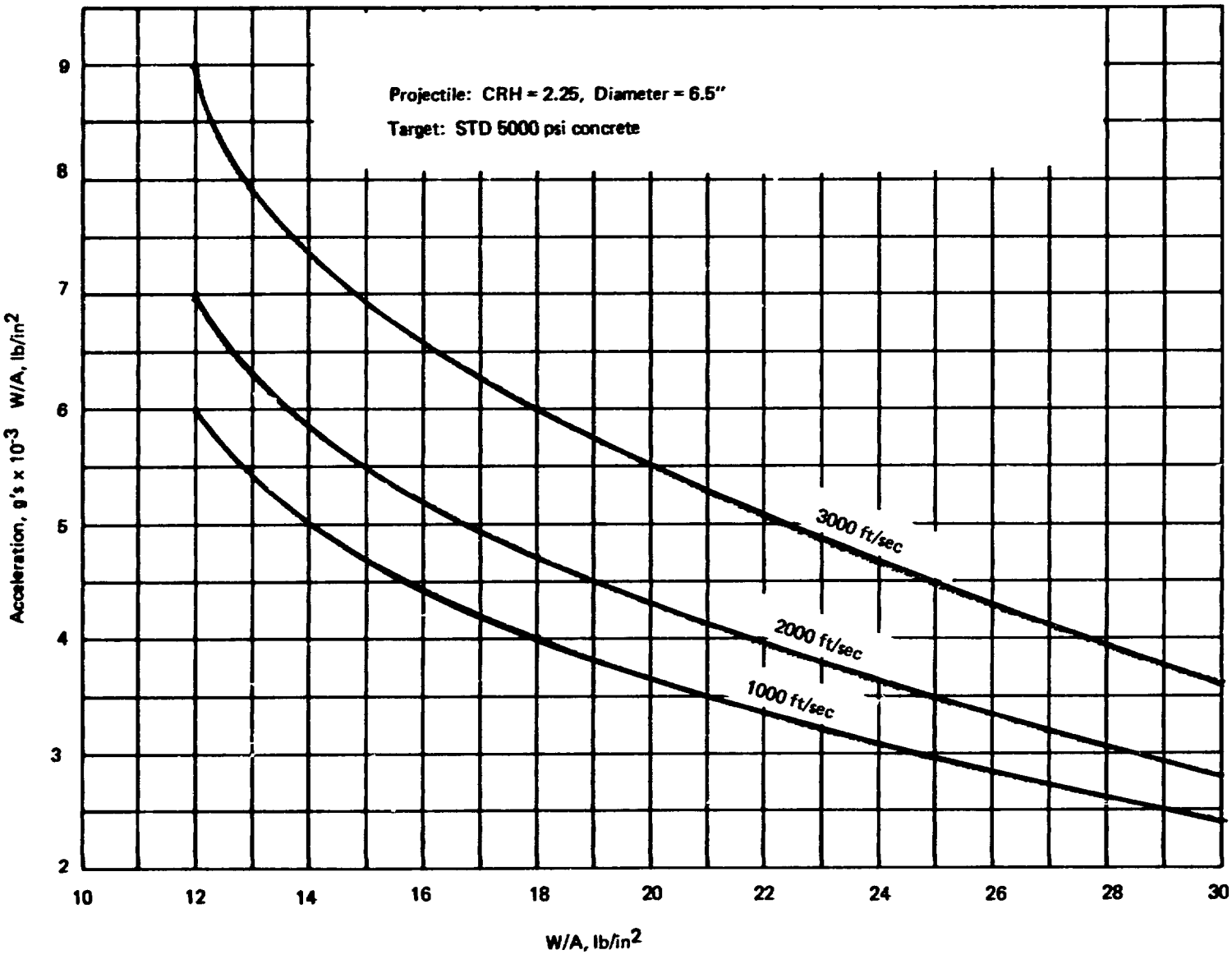

Figure 33. Axial acceleration (Rigid body): CRH = 2.25

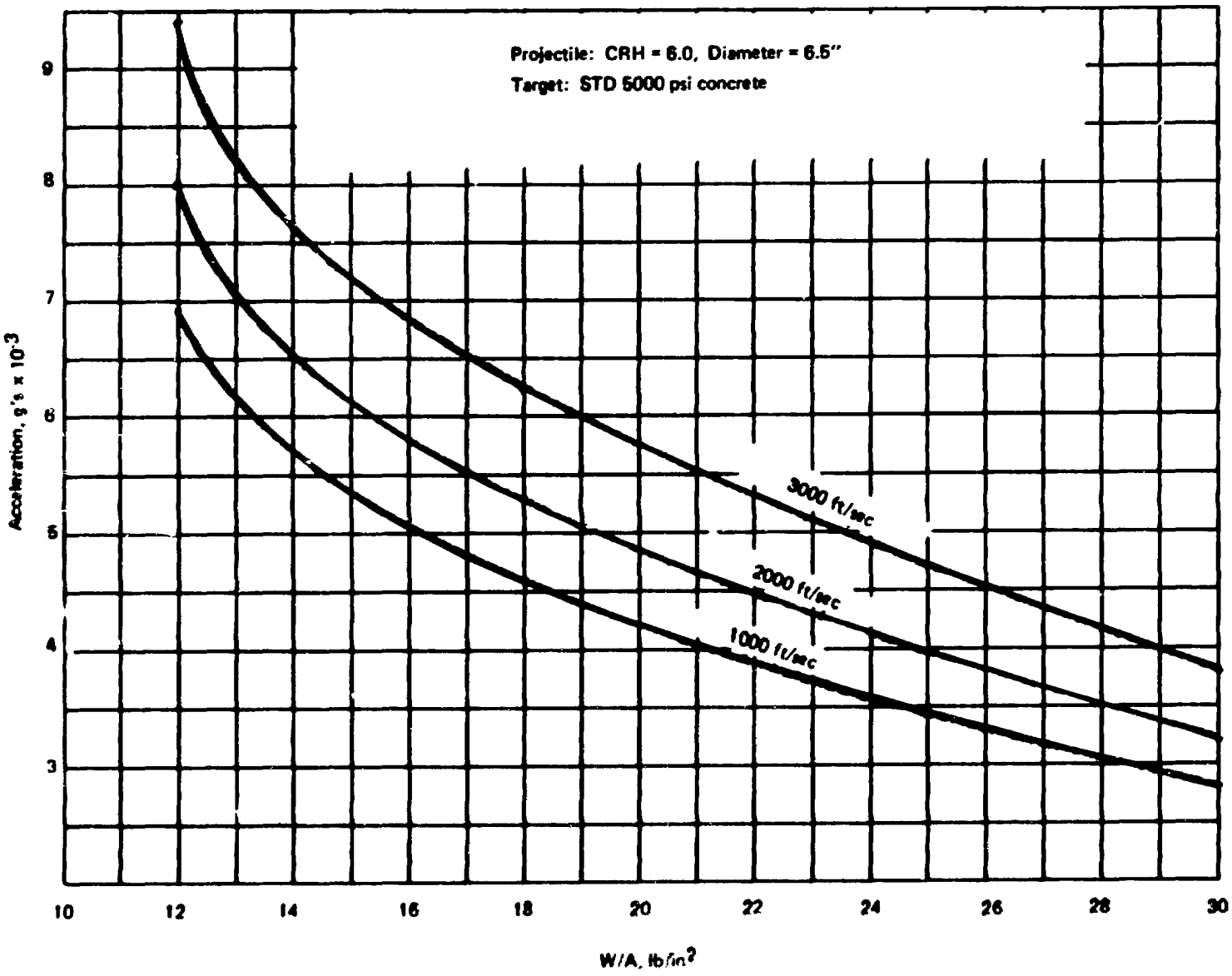

Figure 34. Axial acceleration (Rigid body) CRH = 6.0

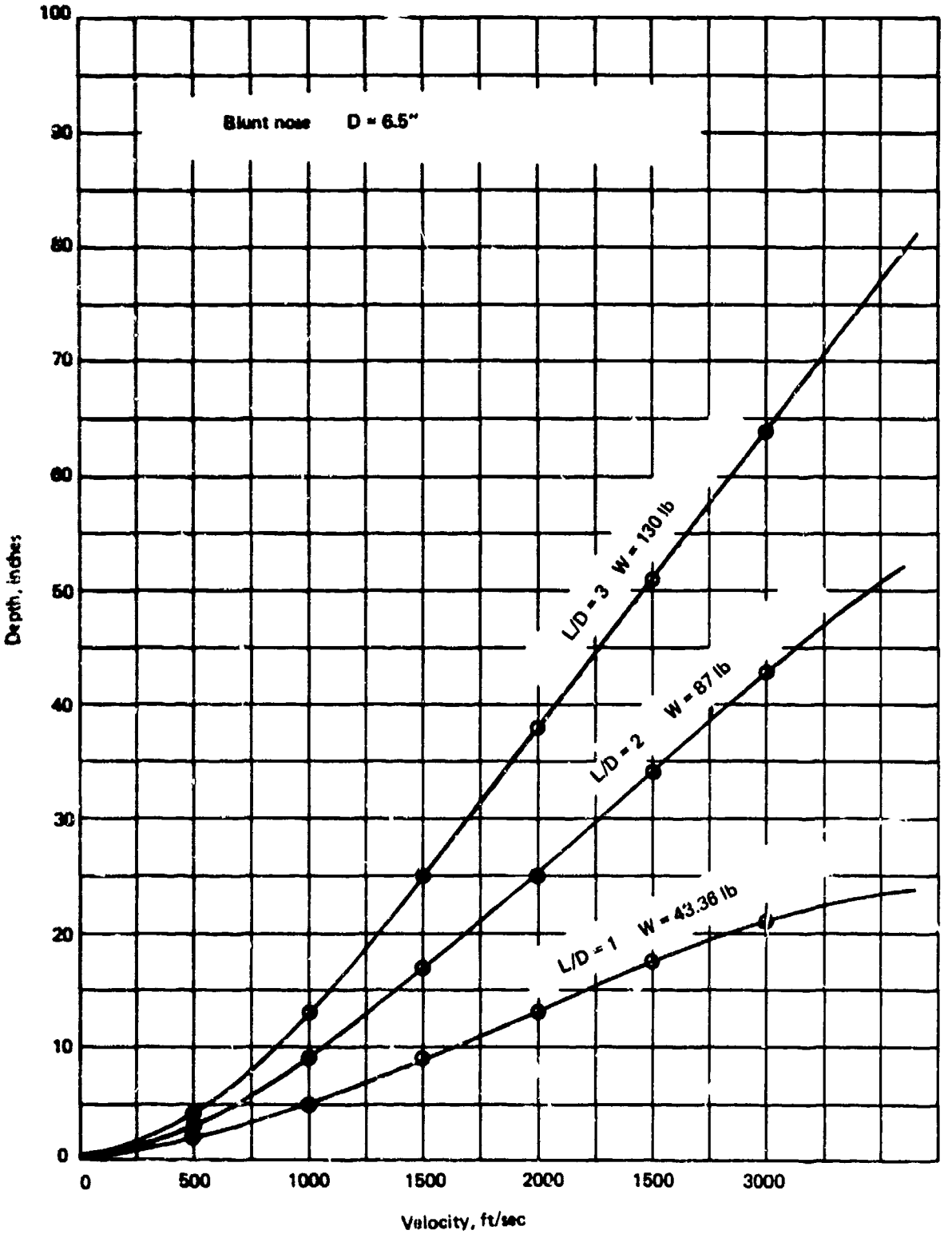

Figure 35. Penetration performance: blunt nose

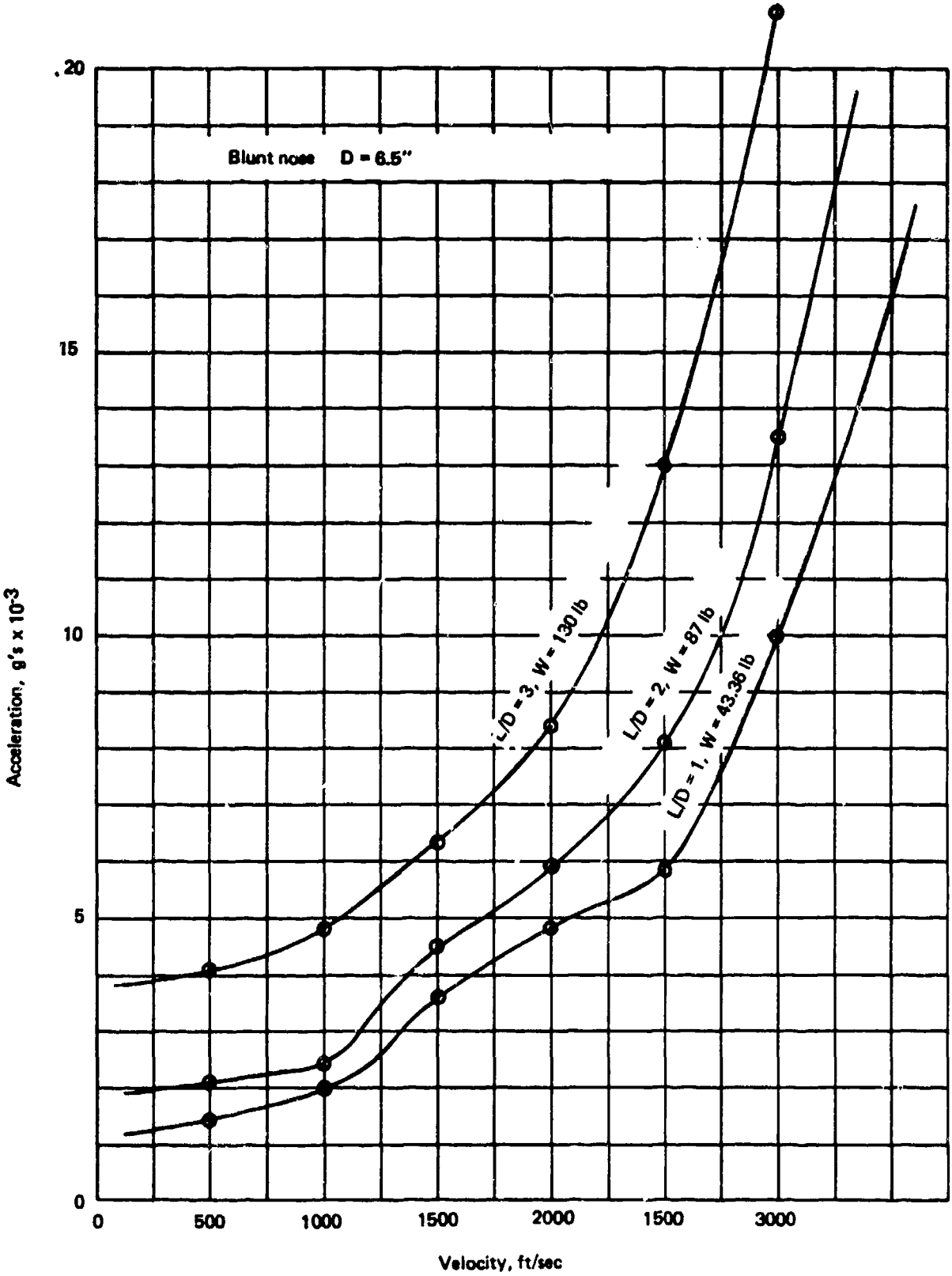

Figure 36. Axial acceleration: blunt nose

Figures 27, 28, and 29 show how performance changes as a function of "CRH" as all other parameters are held constant. There is a crossover in the effects of "CRH". This is not a very significant anomaly, but the data does imply that as "CRH" varies from 9.25 to 6.0 to 2.5 to 0.5 the penetration performance at first improves a little and then proceeds to get worse as the EP becomes fairly blunt. This effect is caused by the analytical formulation of Avco's force law and specifically by how bluntness (as controlled by "CRH") is treated in each term of the force law; i.e.:

The Impact Shock Term	= $f(\sin\theta)$, i.e., is a function of $\sin\theta$
Structural Resistance Term	
Normal Pressure	≠ $f(\theta)$
Friction Term	= $f(\sin\theta/\cos\theta)$
Equivalent Fluid Flow Term	
Normal Pressure	= $f(\sin^2\theta)$
Shear Pressure	= $f(\cos^2\theta)$

where "θ" is the local slope of the EP differential surface area.

The overall implication of this effect is that a nose shape of intermediate bluntness may be the best configuration for impacts into hard targets.

The peak loading environments for this variation in "CRH" are presented in Figures 30 through 34. For "CRH's" of 0.5 and 2.25, two peaks are given; one associated with shock (or compressibility), and one which may be related to rigid body g's. The distinction is made because the shock loading is a short duration phenomena and would be of interest to the dynamic structural design of the EP, while the rigid body loading would be of more interest to component inertial loading. The "Shock" effects are only prevalent for the low "CRH" values because of the "θ" effect previously discussed. The penetration performance and loading environments for the "blunt" nosed EP are summarized in Figures 35 and 36, respectively. The trends in penetration are as expected with respect to L/D, which basically represents a weight change only (i.e., normal impacts do not generate any side loads), and performance is somewhat below similar weight designs with sharper noses. Unlike the sharper

nose design the loading environment shows significant increases with velocity. This is because of the shock effect which is prevalent with blunt nosed projectiles. Accurate simulation of blunt nose projectiles requires the consideration of the effect of apparent mass. These phenomena appear to occur early in the impact event (i.e., during the initial phase) and consist of a wedge being entrapped on the nose of blunt projectiles. This wedge acts as an integral part of the EP and can significantly effect subsequent performances. Referring to Figures of the Series 2-2A, the nose can be seen as a conical extrusion to the basic configuration. The 3-D results for Runs 2-3, 2-6, and 2-18 were reviewed. The peak surface tractions have been obtained from this data and are summarized in Table 16. The peak stresses are the same for the 400 and 1000 pound EP (as they should be) with a fairly large increase in stress going from the 1000 to the 3000 ft/sec case.

5.3 SERIES 3 - VARIATIONS IN OBLIQUITY AND ANGLE OF ATTACK

The penetration events simulated in Series 3 were selected to establish the effects of obliquity and angle of attack on penetration performance, loads accelerations, etc. The runs selected for this series are outlined in Table 9. To avoid confusion and to separate different effects, these runs are grouped as shown in the table. Series 3 consisted of Runs 3.1.1 through 3.64.5 as defined in Table 9.

The purpose of group 3A (i.e., Runs 3-1 through 3-8) is to determine the effects of obliquity on the penetration parameters. These runs are summarized in Figures 37 through 39. The penetration depth (i.e., vertical displacement) is also a designator of ricochet performance. Although in the runs, ricochet did not actually occur, the shallow depth achieved at an obliquity of 60 degrees indicates that this type of impact condition is marginal as far as ricochet performance is concerned. The loading environments (rigid body g's) are summarized in Figure 38. It is apparent that the lateral loads increase smoothly up to 60 degrees, while only slight increases in axial loads are indicated with a sudden drop off at 50 degrees. This is because of surface effects which is shown in the detailed stress histories. Peak surface stresses remain pretty much the same over this obliquity range and are presented in

TABLE 16

PEAK SURFACE TRACTIONS - TEST SERIES 2

Problem Number	Type 2D 3D	Projectile Data				Velocity (ft/sec)	Obliquity γ (deg)	Attack Angle α (deg)	Material Property (psi)	Surface Tractions*		
		W/A (psi)	D (in)	Nose Remarks						Normal Pressure SIGMAN (psi)	Shear	
				CRH	Weight (lb)						TAUA (psi)	TAUB (psi)
2.3	3D	12.1	6.5	9.25	400	1500	0	0	5000	55,000 (270°)	7250 (270°)	0 (180°)
2.6	3D	12.1	6.5	9.25	400	3000	0	0	5000	72,500 (270°)	1400 (270°)	0 (180°)
2.18	3D	12.1	6.5	9.25	1000	3000	0	0	5000	97,000 (270°)	17,500 (270°)	0 (180°)

*See Figure 18.

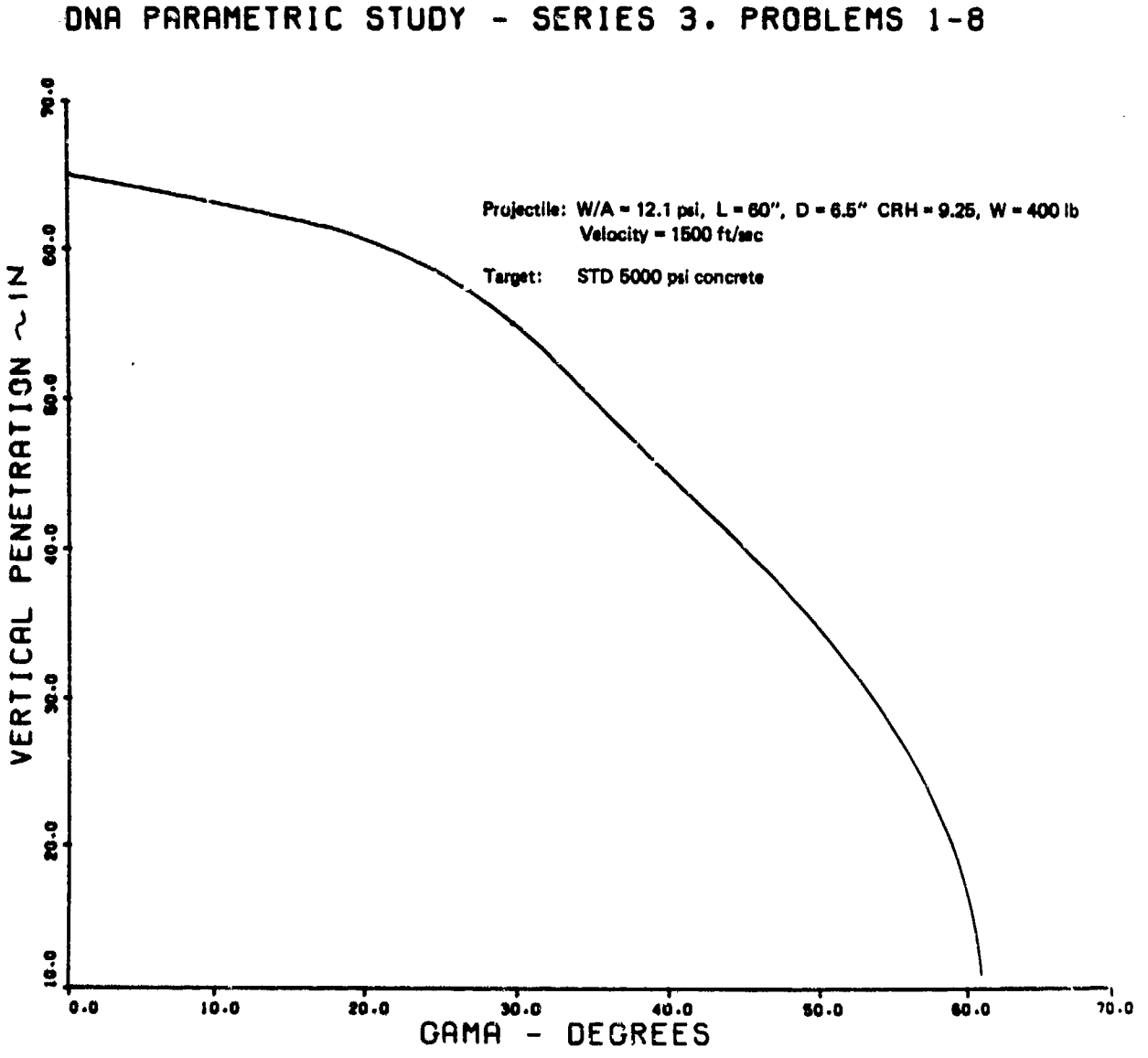

Figure 37. Penetration performance: obliquity

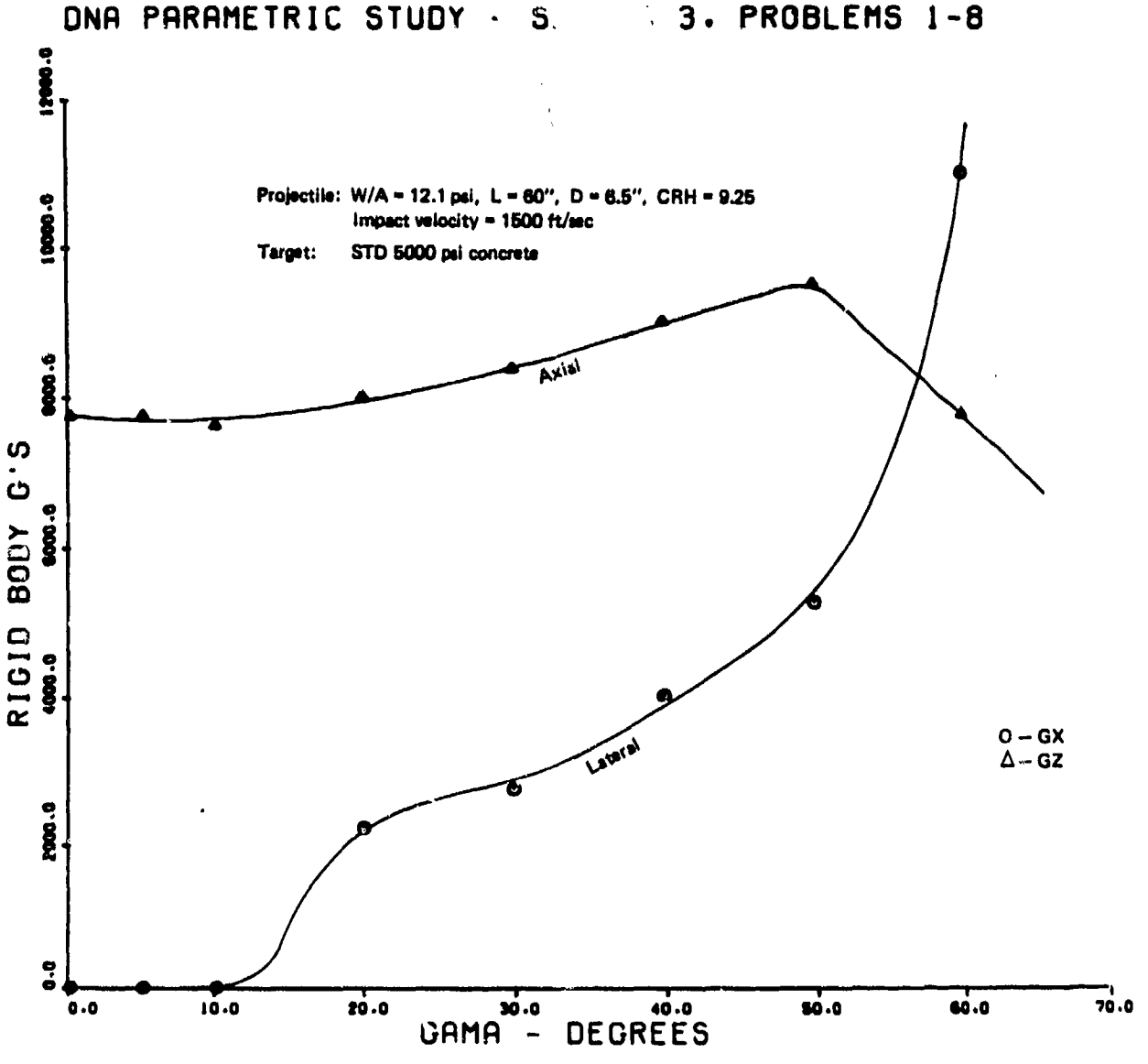

Figure 38. Loading environments (Rigid body g's)

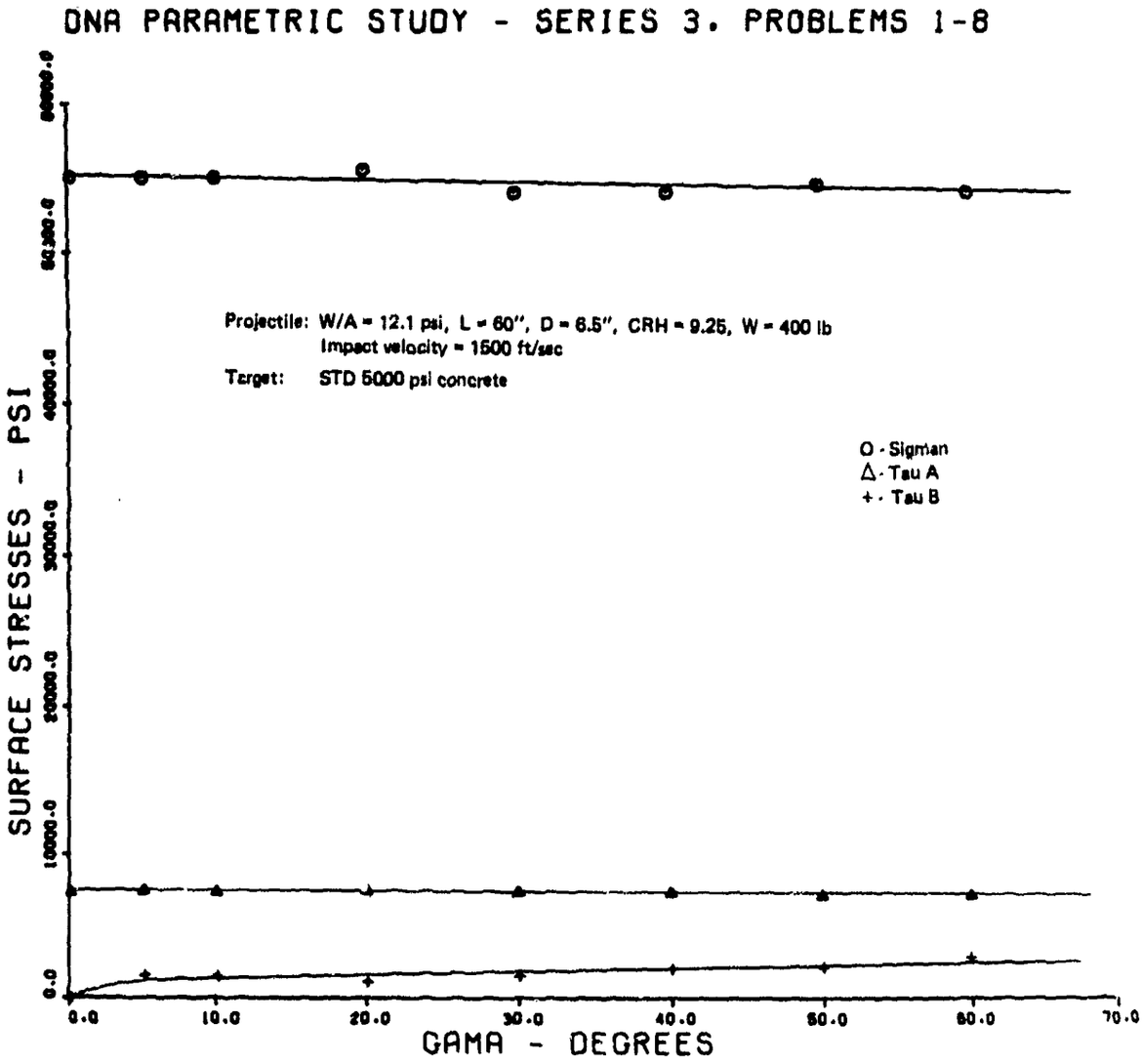

Figure 39. Variation of surface tractions

Figure 39. The integral of the stress distributions is the parameter of importance.

Group 3B (i.e., Runs 3.17 through 3.24) represents an angle of attack effect investigation with some changes in velocity and CRH. This data is summarized in Figures 40 through 44. The effect of angle of attack on penetration performance, axial and lateral rigid body accelerations, and surface stress is shown in Figures 40 through 44 for both positive and negative values of angle of attack, respectively.

It is apparent that penetration performance (i.e., trajectory depth) is not significantly affected by angle of attack as is not the axial loading environment. The lateral load however is significantly affected by angle of attack (Figure 42) and this (as was verified by angle of attack impact tests) has structural integrity implications relative to EP impact survival. A steep gradient occurs between $\alpha = 0^{o}$ and 1^{o} because the angle of attack must first overcome the effects of obliquity, which produce a lateral load opposite to that of positive angles of attack.

Cases 17, 19, and 20 were rerun with an increase in velocity to 2500 ft/sec. These runs are designated 17A, 19A, and 20A and, referring to Figures 40, 41 and 42 as expected, a significant increase in penetration depth was achieved. These same cases were again run with a velocity of 1500 ft/sec and 2500 ft/sec with a CRH of 2.25. Little change in terradynamic performance occurs because of this change. Figures 43 and 44 represent what changes occur when the angle of attack switches from a nose down to nose up situation. For this low obliquity situation, little change in penetration performance occurs. The shape of the lateral accelerator curve however is somewhat smoother than for the nose down angle of attack situation.

Cases 3.31 through 3.38 involved a slight modification in the configuration and a change in impact velocity (i.e., 1500 to 2500 ft/sec) as baseline conditions for determining the effects of obliquity. The configuration change consisted of a small 45 degree angle tip over a length of 0.25 inch on the nose of the EP instead of a pure ogive shape all the way to the point. Runs 3.31.1 through 3.38.5 are summarized in Figures 45 and 46. The overall

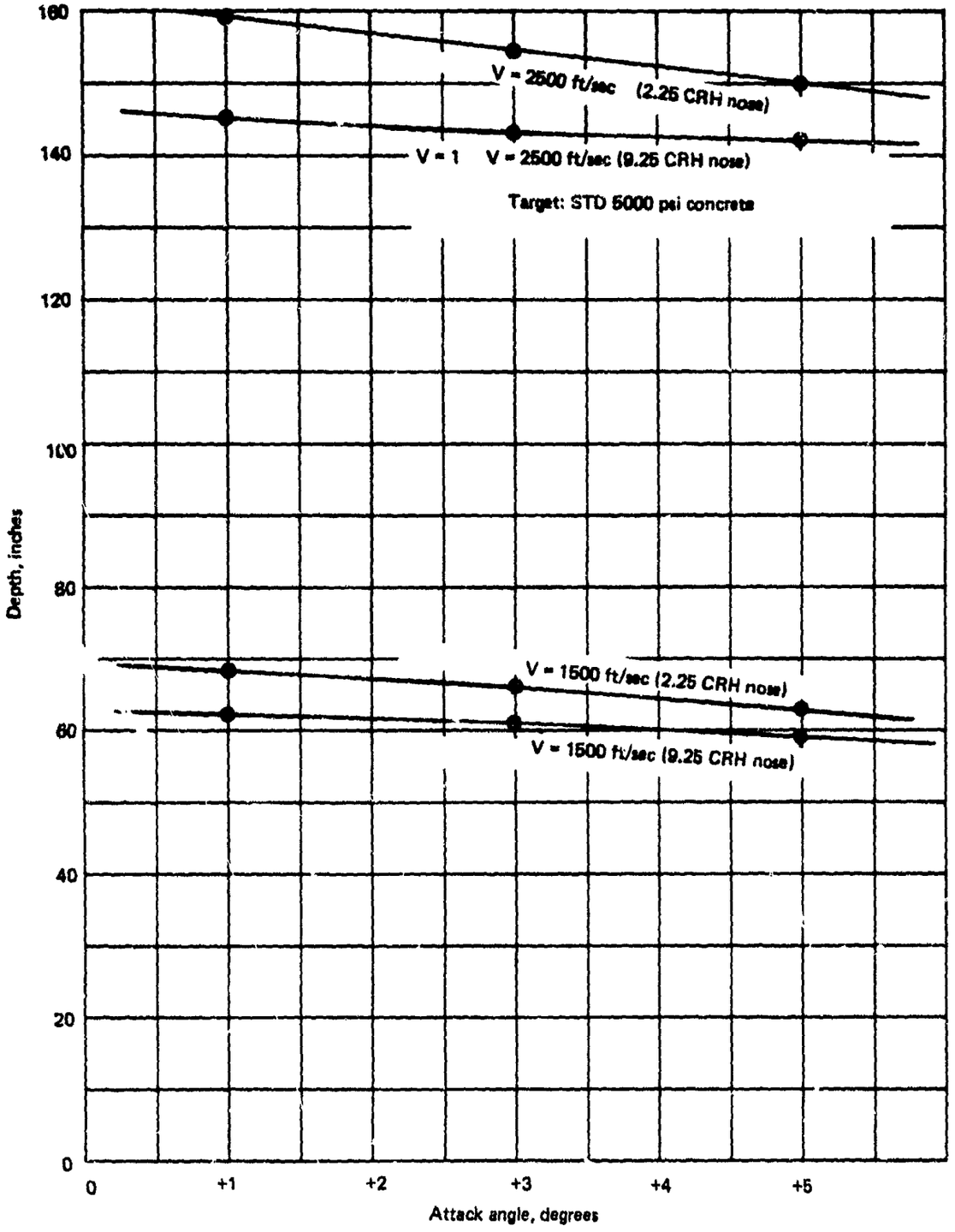

Figure 40. Penetration performance: positive attack angle

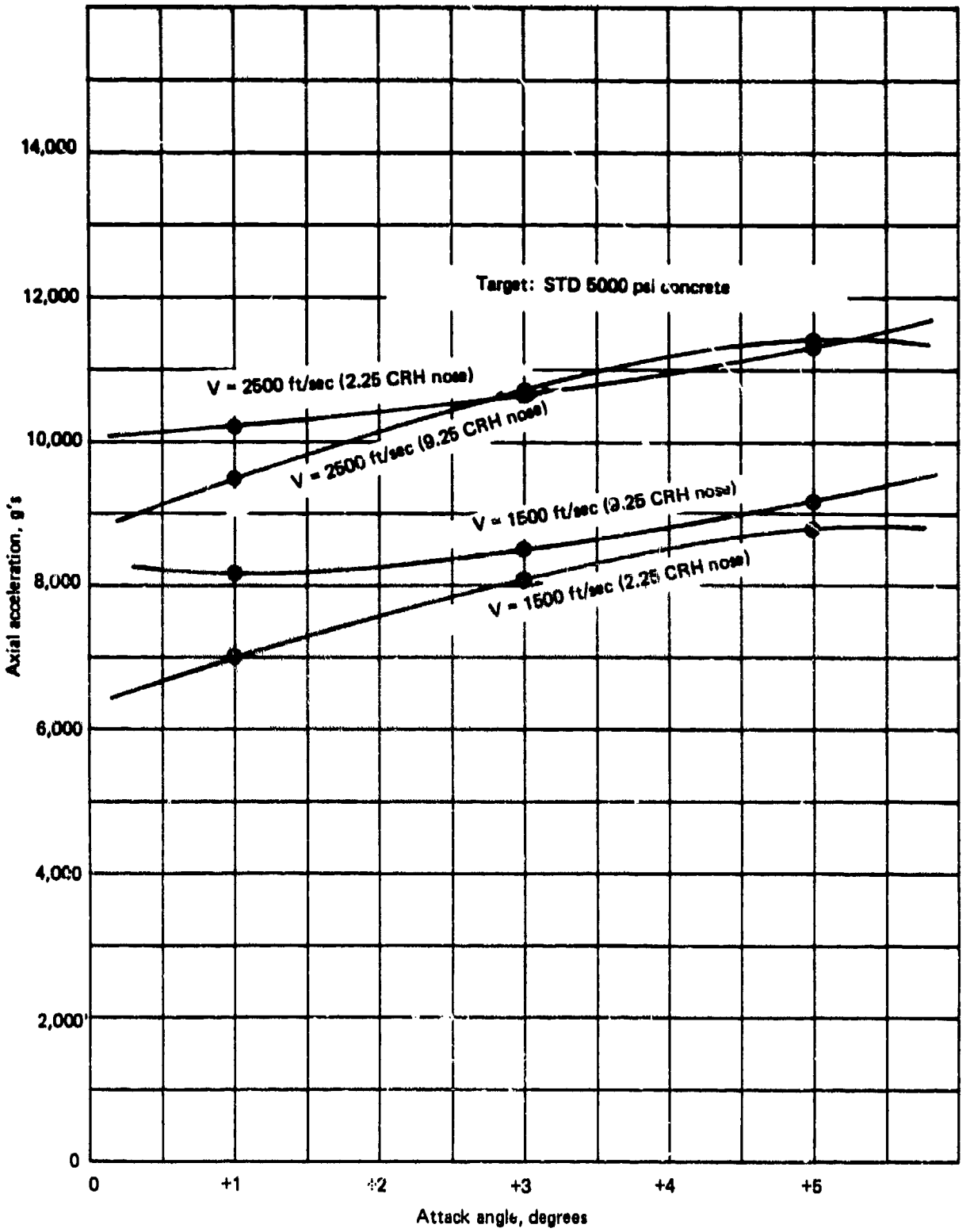

Figure 41. Axial acceleration: positive attack angle

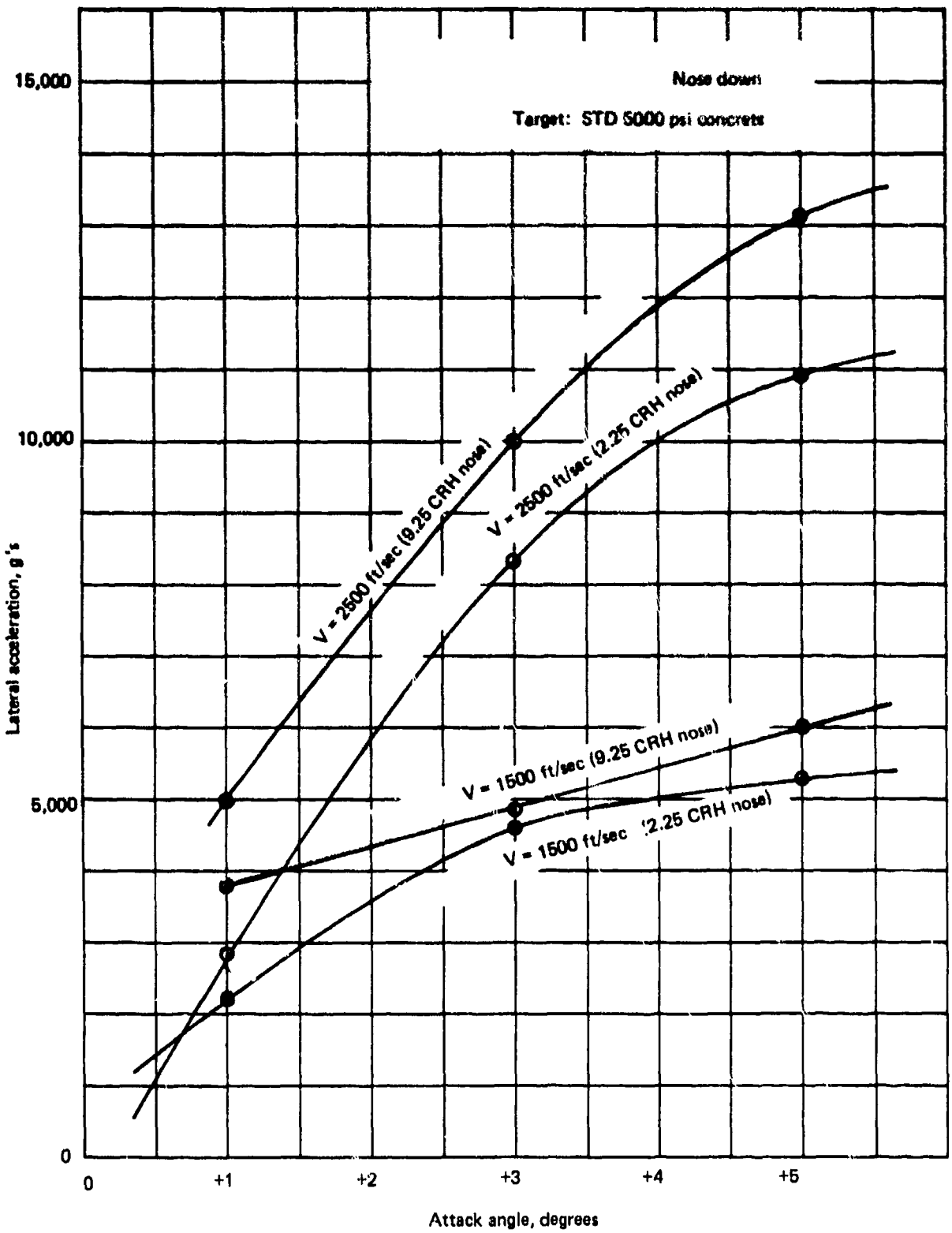

Figure 42. Lateral acceleration: positive attack angle

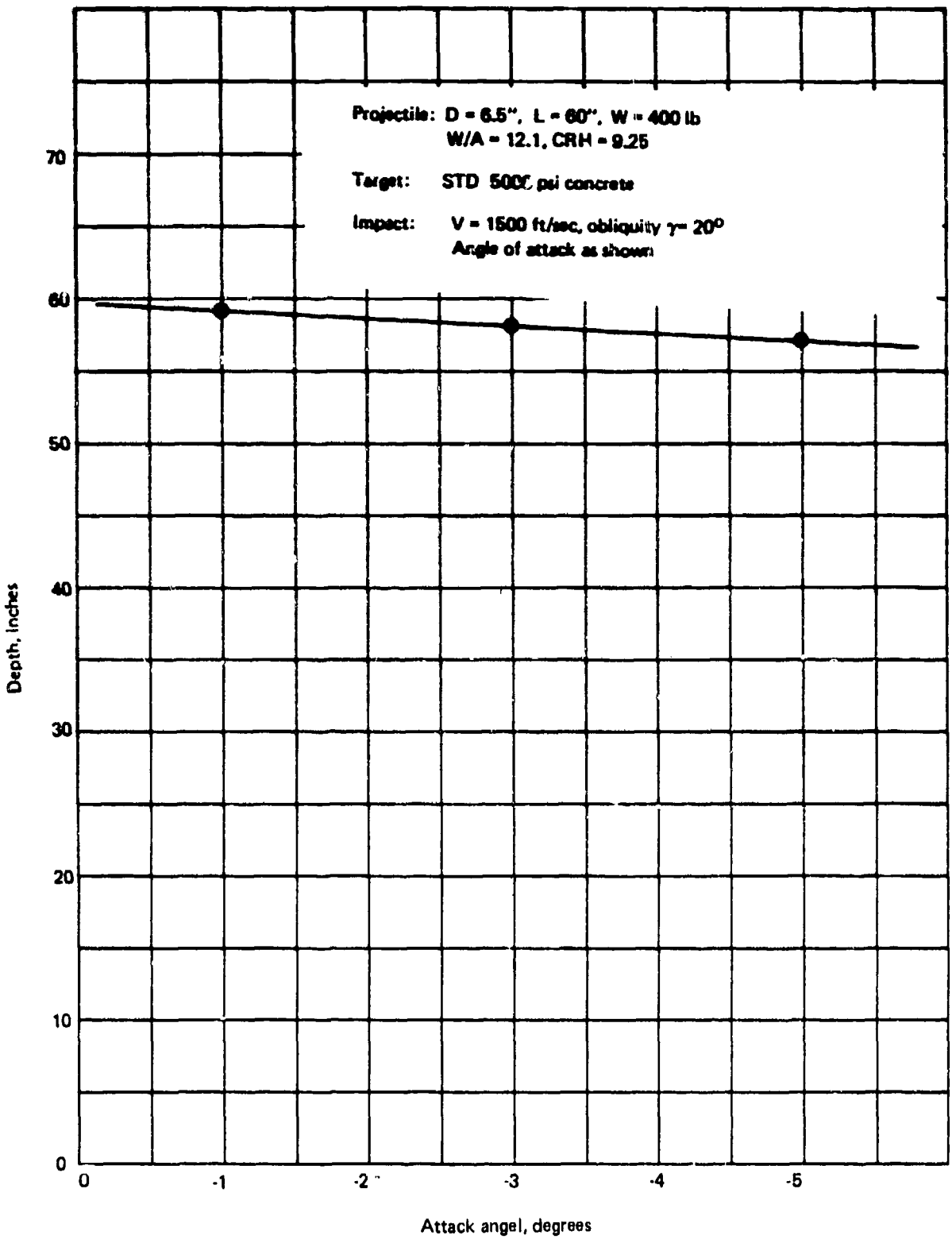

Figure 43. Penetration performance: negative attack angle

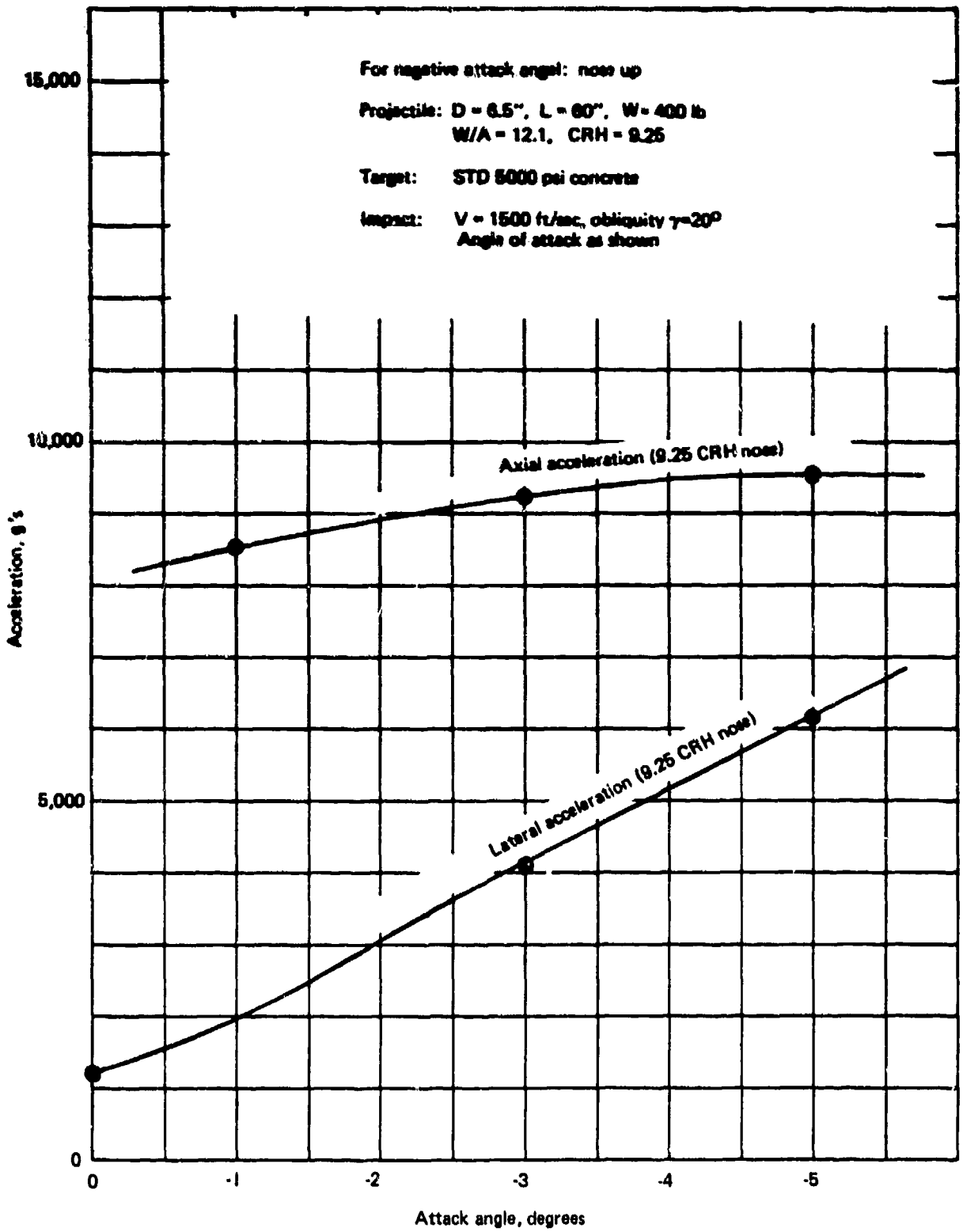

Figure 44. Axial and lateral acceleration: negative attack angle

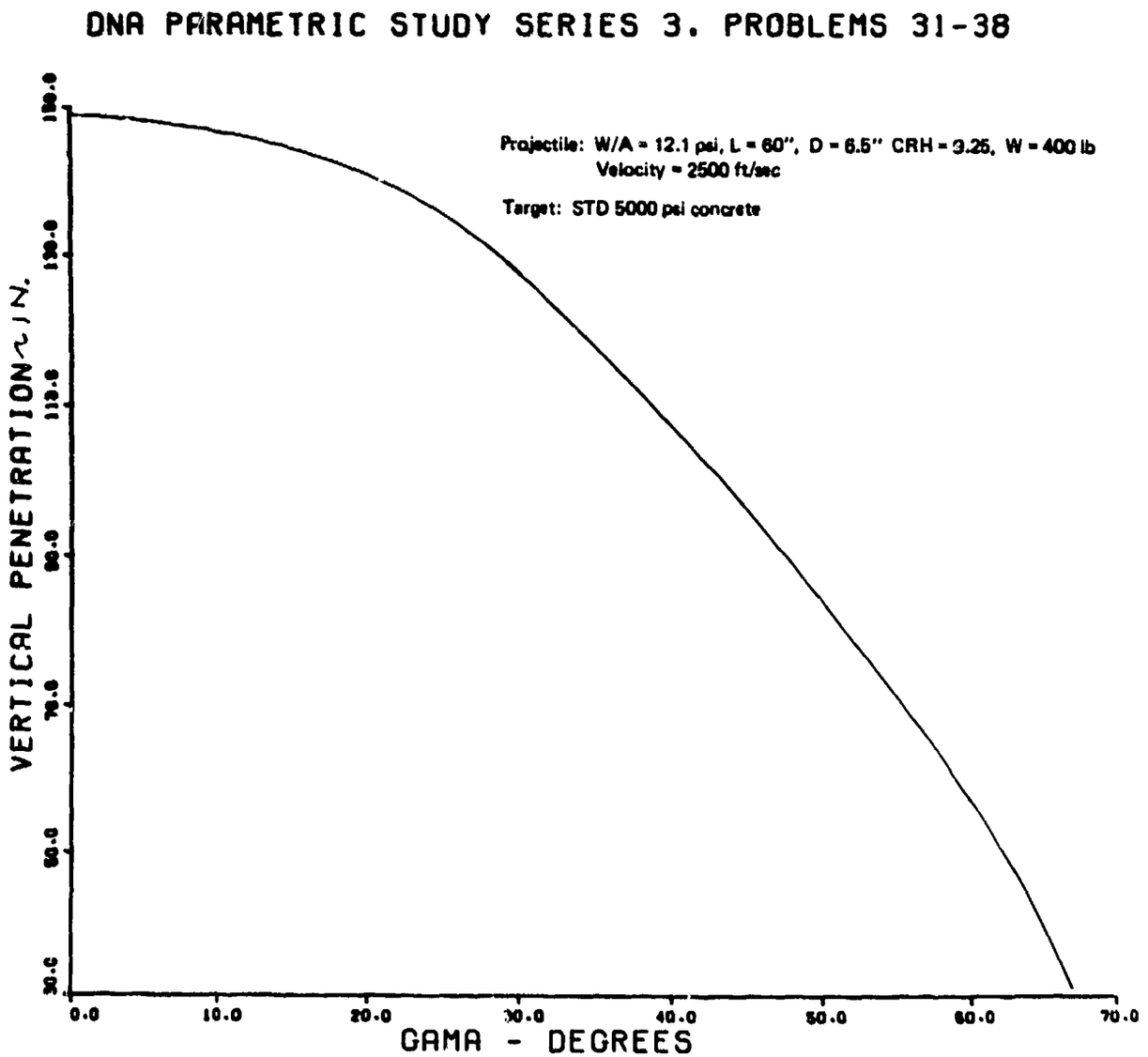

Figure 45. Penetration performance: (With nose tip of 45°)

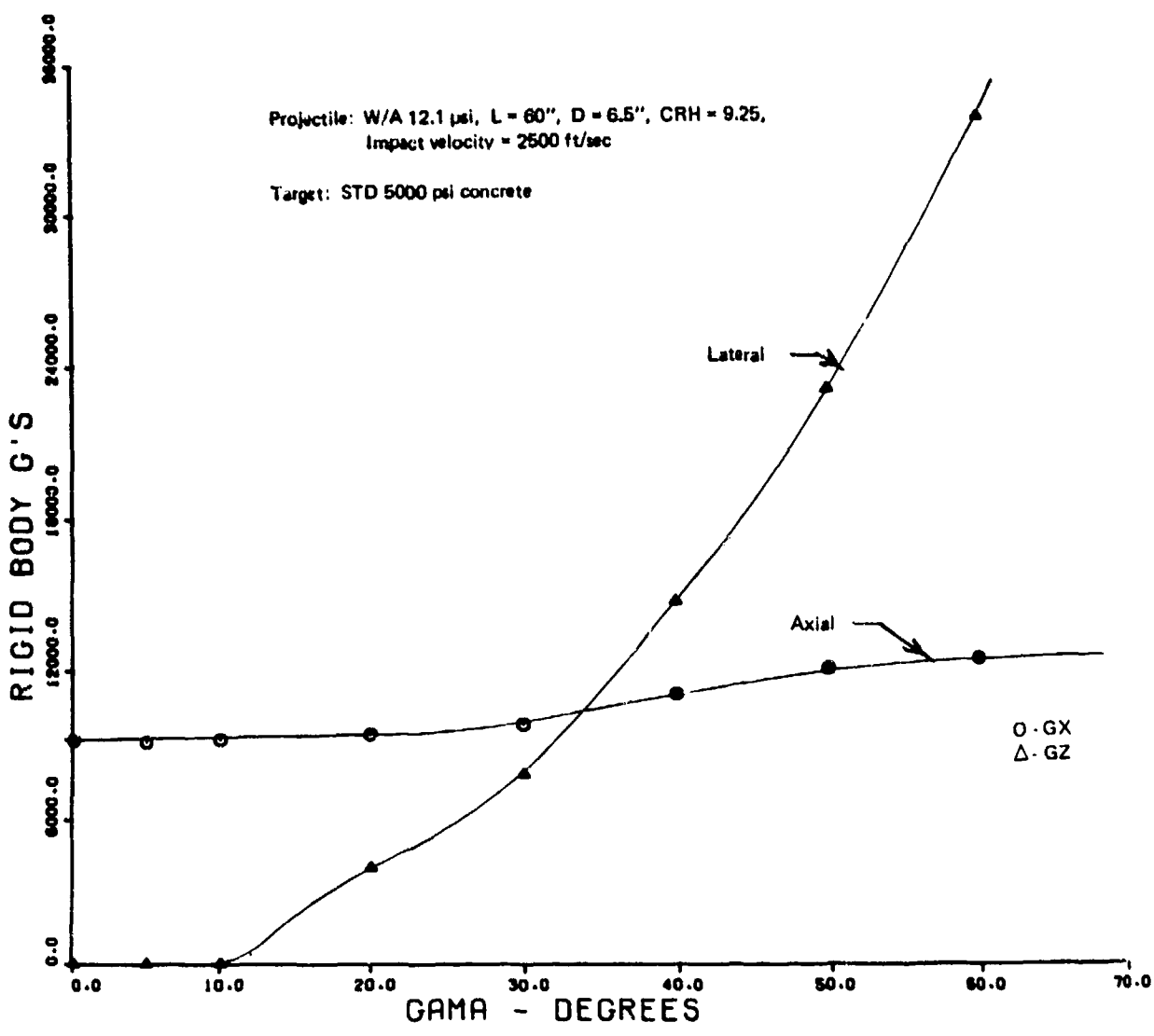

Figure 46. Loading environments: (With nose tip of 45°)

effect of the tip by itself is difficult to ascertain because of the significant change in velocity, however its overall effect is expected to be small. The effect of this increase in velocity is to delay the onset of ricochet by approximately five degrees.

Cases 3.39 through 3.47 were deleted from the original matrix.

Cases 3.48 through 3.53 involve investigation into the performance of a biconic EP configuration. This design is shown in Figure 47. The biconic design represents a departure from the ogive nose type EP in that resulting flow fields are induced to separate at the shoulder of the forward cone for a period of time during the penetration event. There are two pertinent questions to be asked and resolved relative to the performance of this type design:

- For how long a period during the event is separation induced?
- How much of the after flare remains in the void generated by the wake?

As a demonstration of the importance of these phenomena, consider an approximate loads comparison between the biconic design in question and a design which allows the forward cone to continue out to the full diameter of the flare. Assuming that flow separation is induced at the shoulder of both designs so that the entire aft flare and/or cylinder is in the wake, the load on the cylinder cone configuration is approximately proportional to:

$$F_{AC} \simeq P\pi R_o^2$$

and on the biconic,

$$F_{AB} \simeq P\pi R_{BC}^2$$

where

F_{AC} = resulting axial load on the cone cylinder design
F_{AB} = resulting axial load on the biconic
P = average normal pressure
R_o = cylindrical radius
R_{BC} = forward cone radius

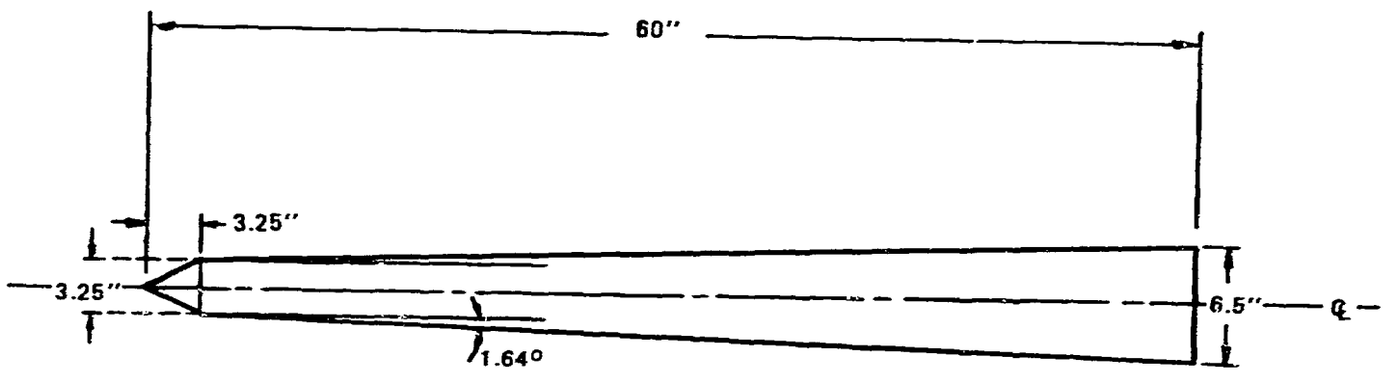

Figure 47. Biconic EP configuration

The ratio of resulting loads is therefore approximately R_o^2/R_{BC}^2 or in this case, 4. It is apparent that: if separation did occur at the shoulder; and if the entire flare were within the wake; and if the flare remained so during the entire penetration event, then the penetration performance would improve by a factor of 4. Actual performance is somewhat below this optimistic figure. At the present time, there is not sufficient data to define exactly the extent of these possible effects. A limited number of scale model test shots were conducted into a hard target in which an ogive nosed EP was compared to a biconic configuration where the ratio $R_o^2/R_{BC}^2 = 2.4$ The increase in penetration performance of the biconic was only 15 percent which was a reduction of 2.1 less than the area ratio factor. Assuming that this reduction factor remained constant (a big assumption) then the biconic design would have a performance increase on the order of 4/2.1 = 1.9 times better than the straight cone EP design. It is Avco's opinion that the performance improvements indicated by the above manner of deduction is very optimistic for impact situations into hard targets. The trend, however, is real and in conducting Runs 3.48 through 3.53, a conservative assumption of the degree of wake effects was made. The summary curves for these cases are presented in Figures 48 through 50. The improved performance factor of this biconic design over the standard ogive EP computes to be 1.08; i.e., Run 1.01 achieved a penetration depth of 66 inches while the biconic configuration went 71 inches.

The detailed trajectory data for Runs 3.60 through 3.64 is summarized in Figures 51 and 52. These runs were conducted to provide more detailed data on the effects of velocity and weight increases. As before, the most significant trend is the real improvement in penetration depth with velocity accompanied by not too great an increase in rigid body loads.

5.4 SERIES 4 - EFFECT OF L/D ON STABILITY

Runs 3.17, 18, 20 and 22 were rerun in the 3-D format to provide surface traction information. These data are presenced in Figures 3.17.1 through 3.22.10. The peak pressures are summarized in Table 17.

The purpose of the Series 4 parametric study is to determine the effects of EP L/D (length to diameter ratio) on projectile stability. The target

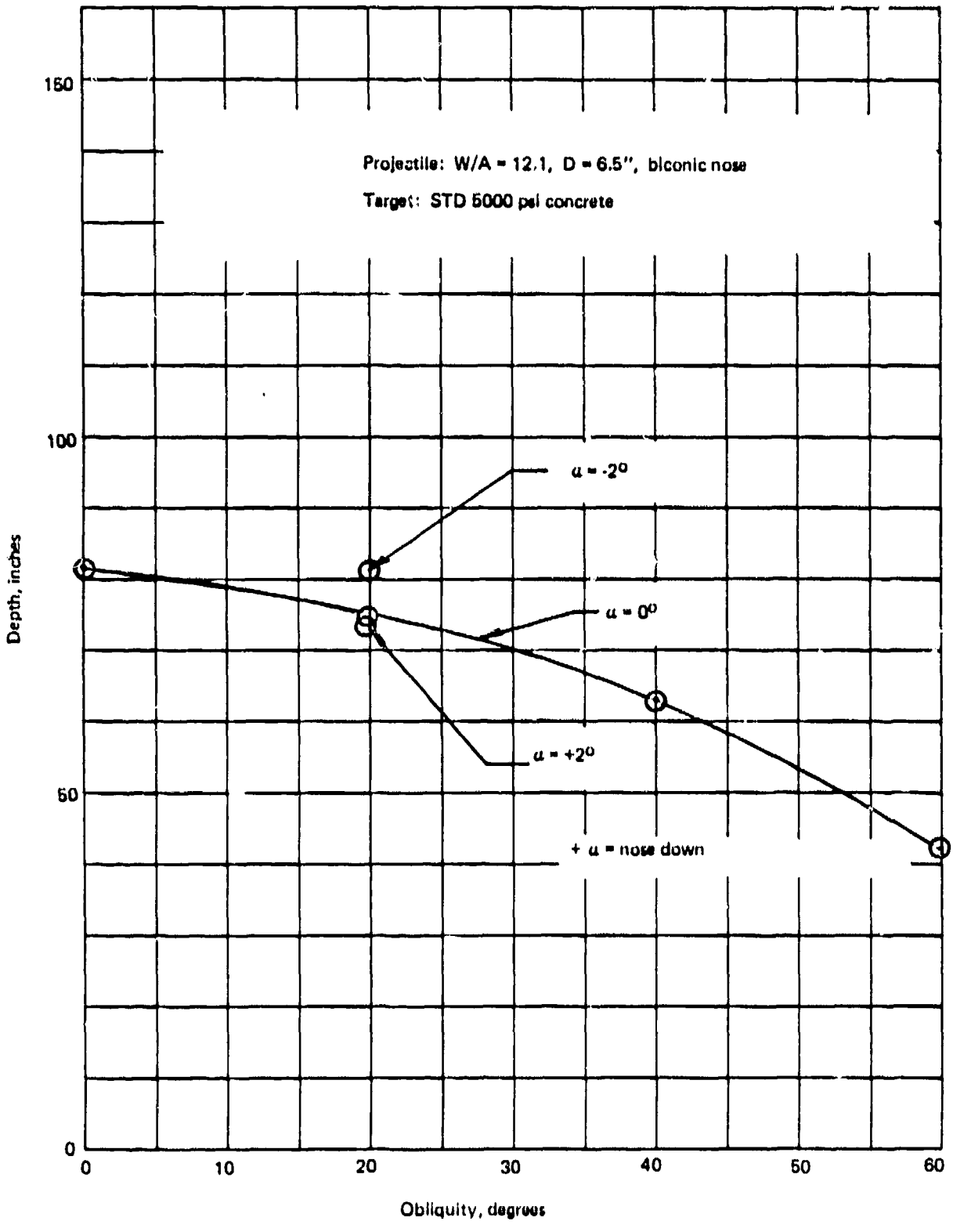

Figure 48. Penetration performance: biconic nose

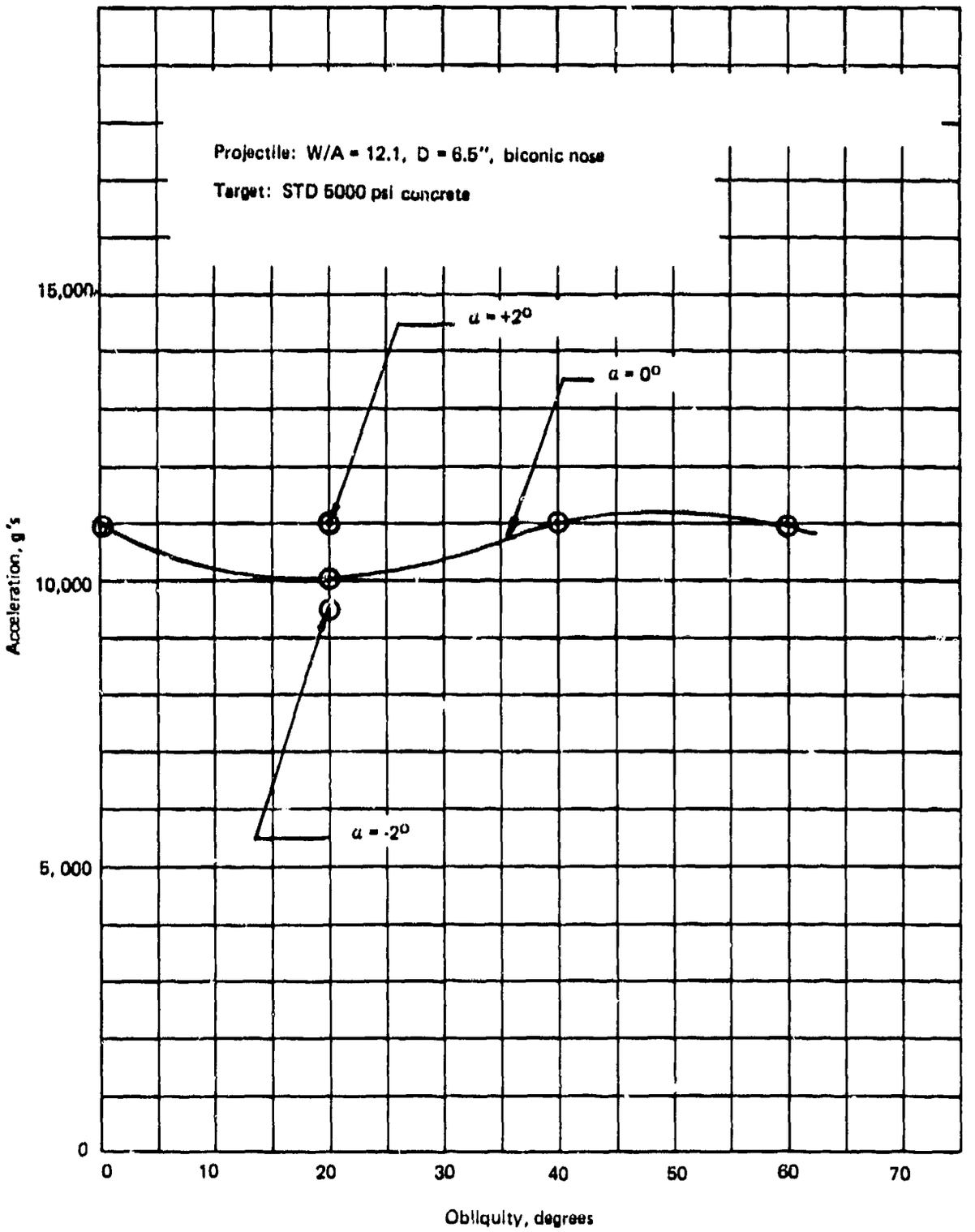

Figure 49. Axial acceleration: biconic nose

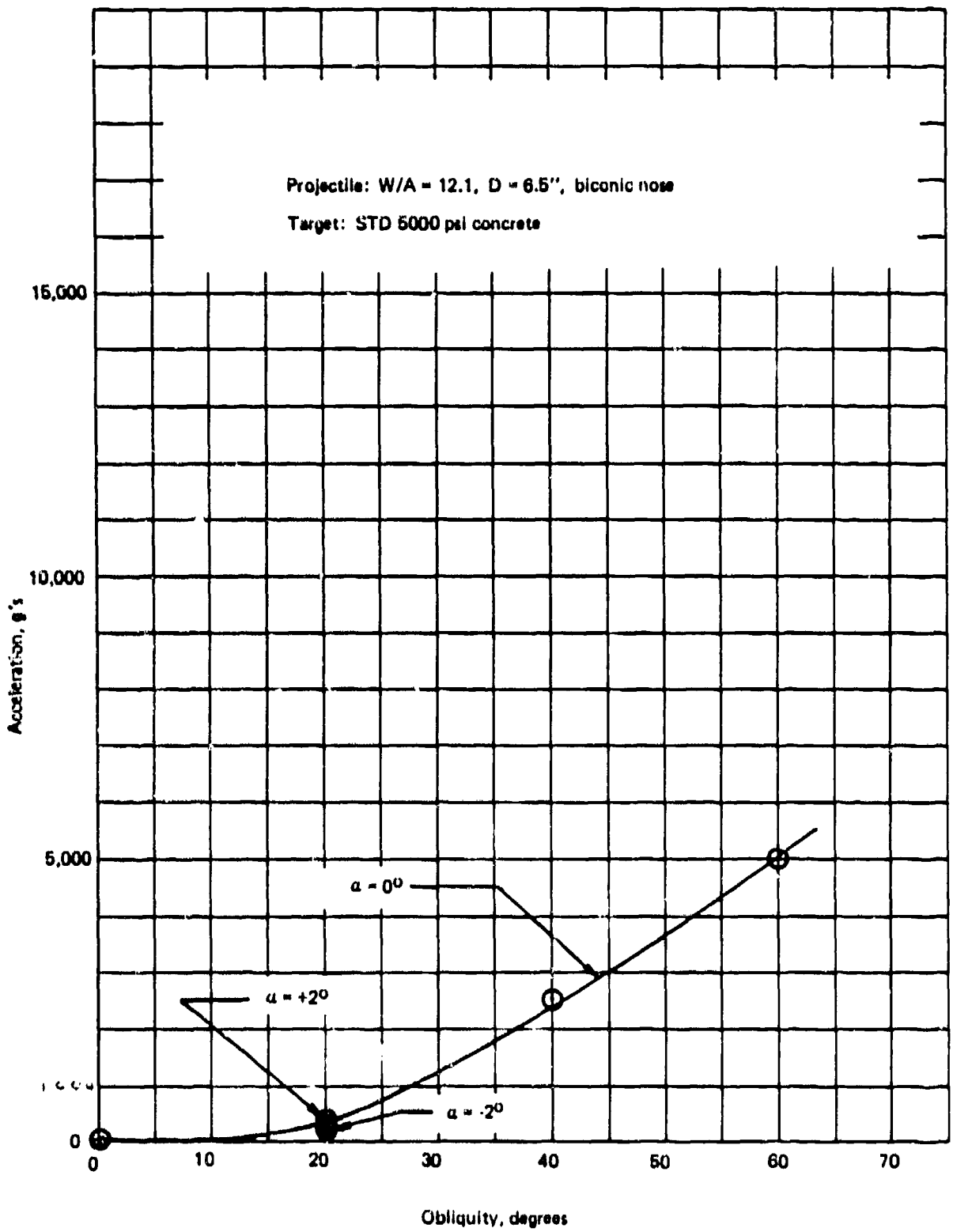

Figure 50. Lateral acceleration: biconic nose

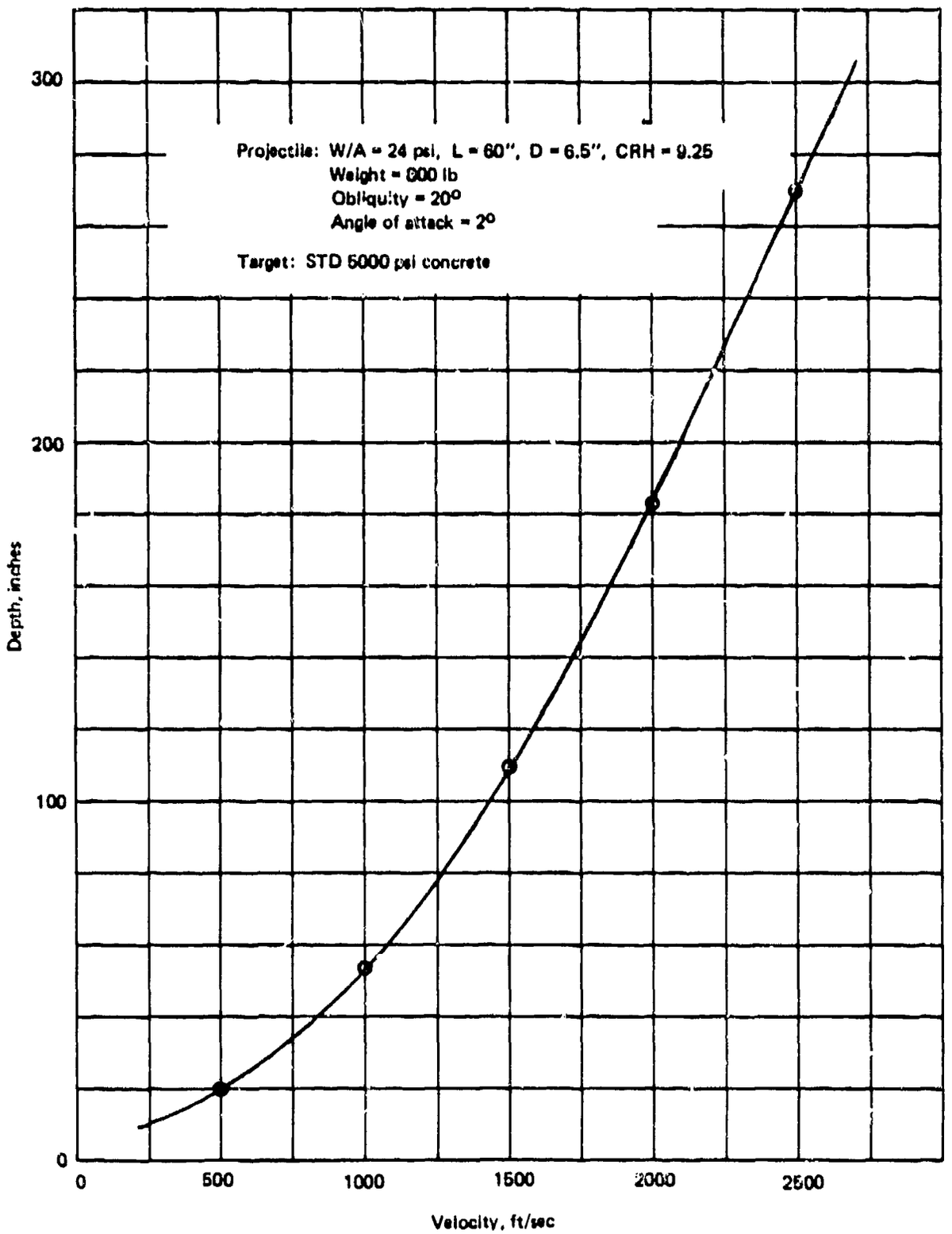

Figure 51. Penetration performance: velocity effects

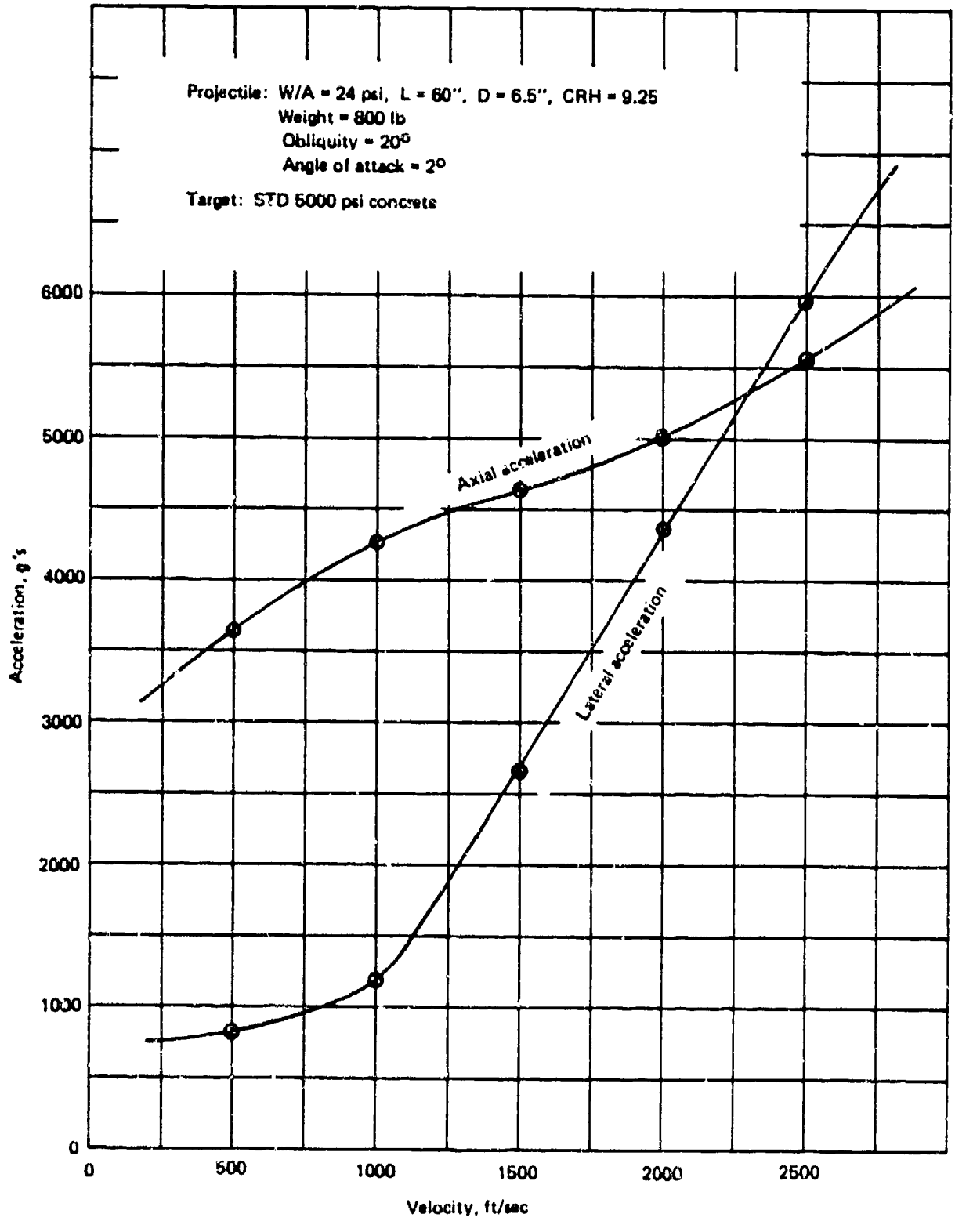

Figure 52. Axial and lateral acceleration: velocity effects

TABLE 17

OBLIQUITY AND ANGLE OF ATTACK EFFECTS ON SURFACE TRACTIONS

Problem Number	Type 2D 3D	Projectile Data				Velocity (ft/sec)	Obliquity γ (deg)	Attack Angle α (deg)	Material Property (psi)	Surface Tractions		
		W/A (psi)	D (in)	Nose Remarks CRH	Nose Remarks Weight (lb)					SIGMAN (psi)	TAUA (psi)	TAUB (psi)
3.17	3D	12.1	6.5	9.25	400	1500	200	+1	5000	55,000 (270°)	7250 (270°)	25 (180°)
3.20	3D	12.1	6.5	9.25	400	1500	200	+5	5000	56,000 (90°)	7600 (90°)	560 (180°)
3.18	3D	12.1	6.5	9.25	400	1500	200	+2	5000	55,000 (90°)	7350 (90°)	150 (180°)
3.18B	3D	12.1	6.5	2.25	400	1500	200	+2	5000	62,000 (270°)	8100 (90°)	0 (180°)
3.22	3D	12.1	6.5	9.25	400	1500	200	-2	5000	55,000 (270°)	7400 (270°)	370 (0°)

media in this case is a relatively standard clay sand mix (glacial till). This media has been tested extensively at Avco for resistance-to-penetration characteristics. Consequently, the results of this study can be considered quite accurate and relatable to the real world.

The L/D range considered varied from 4 to 10 where the 10 value was associated with the standard ogive 400 pound EP. The EP weight for the other EP's was decreased proportionally by the L/D ratio. The exterior configurations of these EP's are shown in Figure 53. Blunt nosed EP's were also considered in this study and are shown in Figure 54. The detail trajectory for the ogive and blunt nose EP configurations is detailed in runs 4.01.1 through 4.08.5 and 4.09.1 through 4.12.5 respectively and are summarized in Figures 55 through 59. It is apparent that the most significant result of this study is that the low L/D EP's are not that much less stable than the higher L/D EP's. There are basically two reasons which explain this result. They are:

- the center of gravity location;
- the penetrated media is till.

For EP's, as it is for all things that fly, the location of the center of gravity (cg) with respect to the effective center of applied forces is of prime importance to its stability. An aft located cg will cause the projectile to be unstable while a forward cg will enhance its stability. During this study, the center of gravity was assumed to remain at 53.5 percent of the EP's overall length. This is slightly aft of the mid point. When dealing with actual EP designs, maintaining this cg location becomes more difficult as the EP becomes shorter. This is particularly true for ogive shaped EP's because the ogive shape itself does not provide as much volume up forward for ballast. For this study therefore, placement of the cg was somewhat optimistic.

The fact that the penetrated media was till, aided in stabilizing the EP's because of particular characteristics relative to its resistance-to-penetration. Till exhibits relatively high shear strength and friction. This characteristic results in relatively high shear stress applied along the length of EP when the EP develops angle of attack. This shear stress is stabilizing and contributes to a large degree to the stable flight patterns

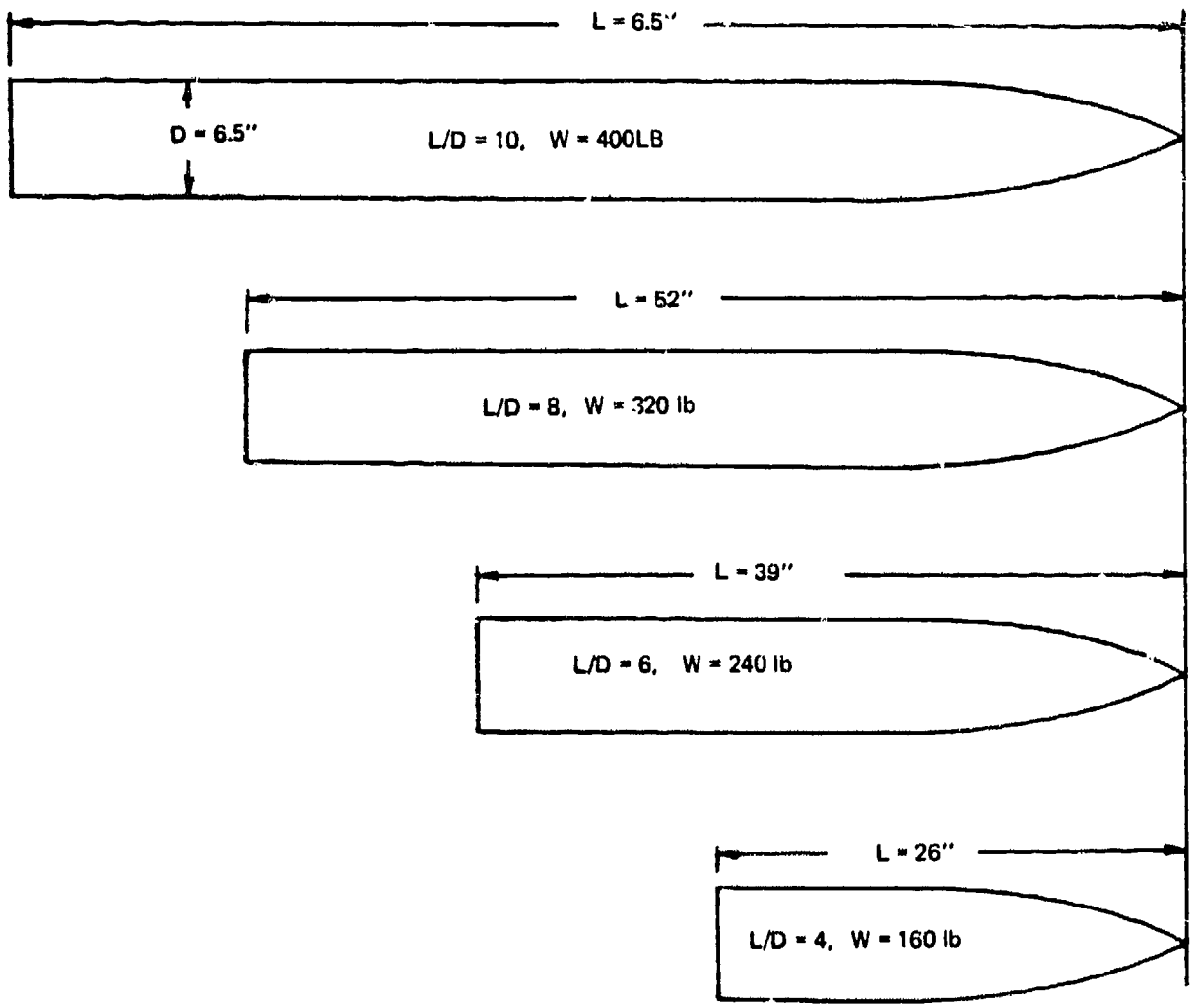

Scale 1/10

Figure 53. Exterior configuration of EP

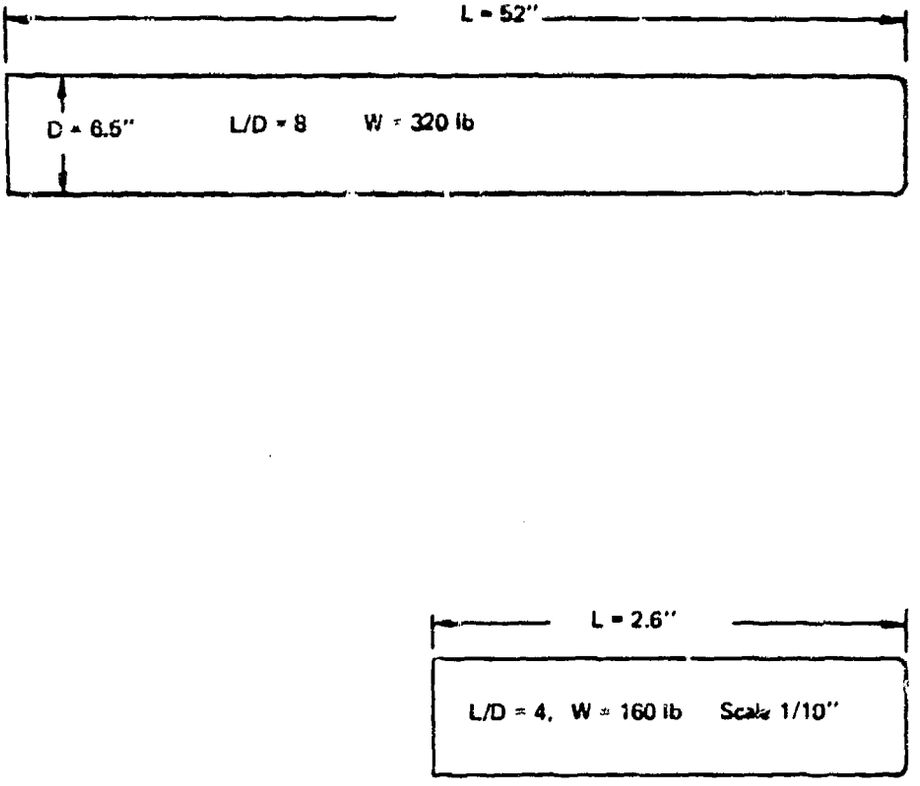

Figure 54. Blunt nose configuration of EP

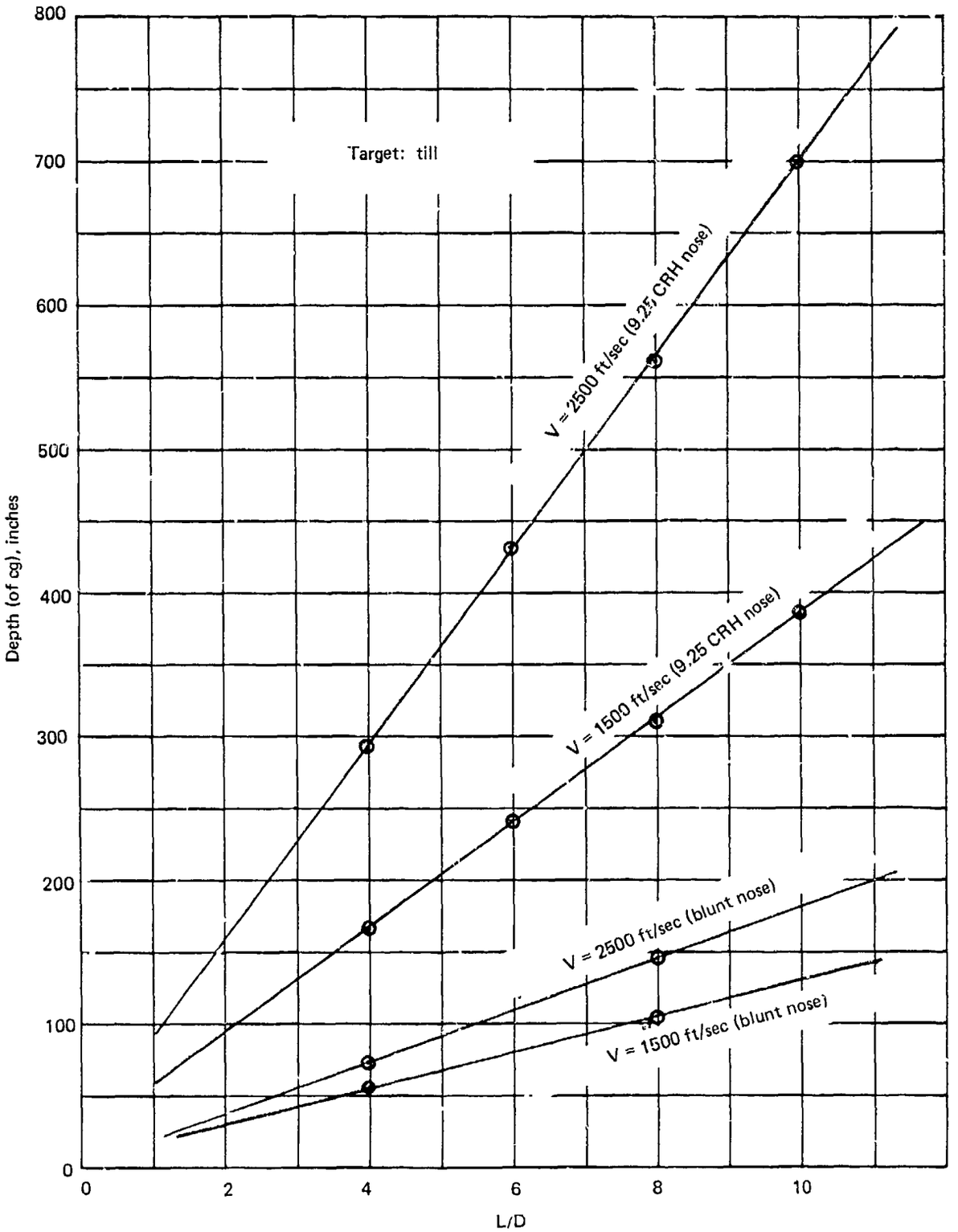

Figure 55. Penetration performance: CRH = 9.25 and blunt nose

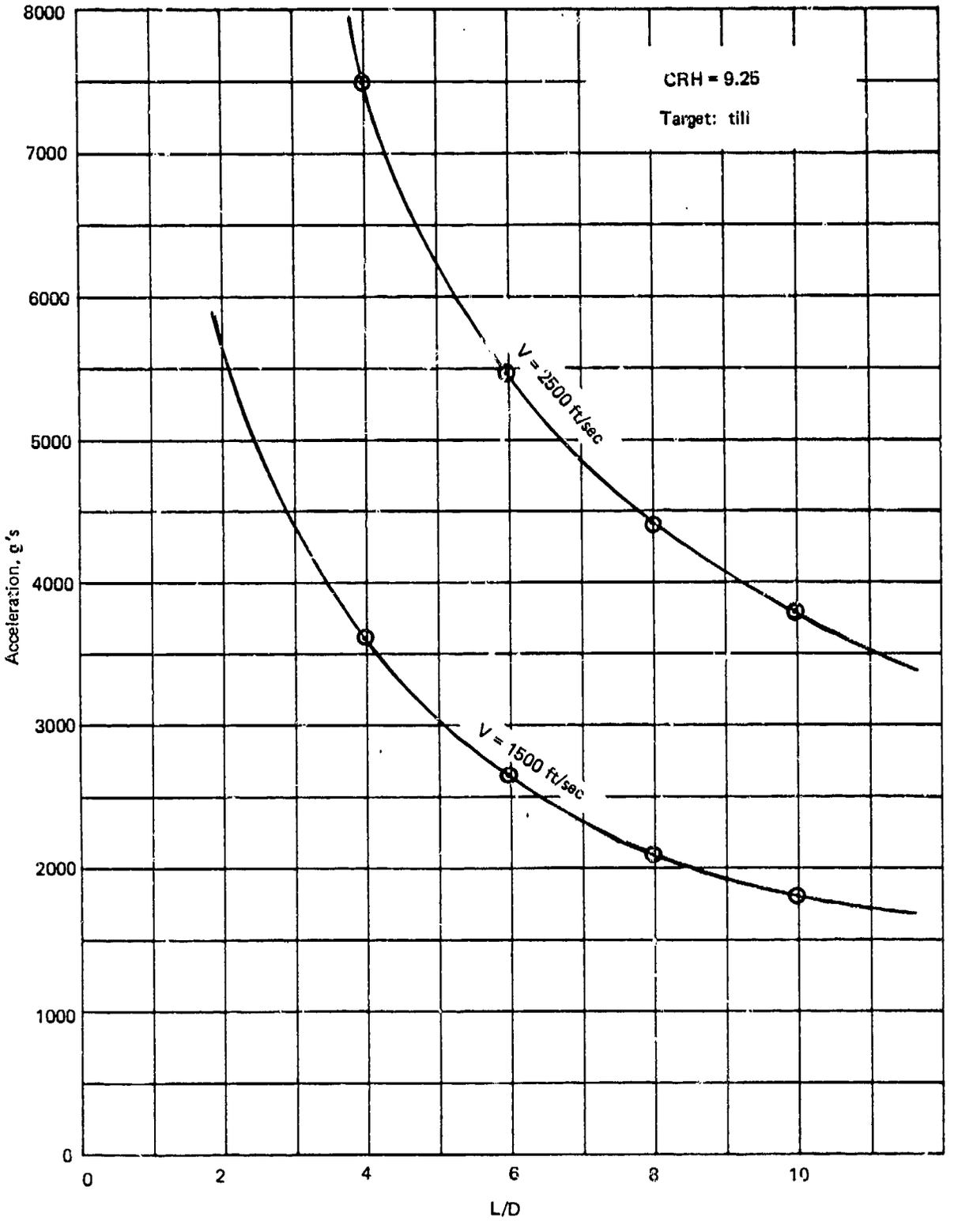

Figure 56. Axial acceleration: CRH = 9.25

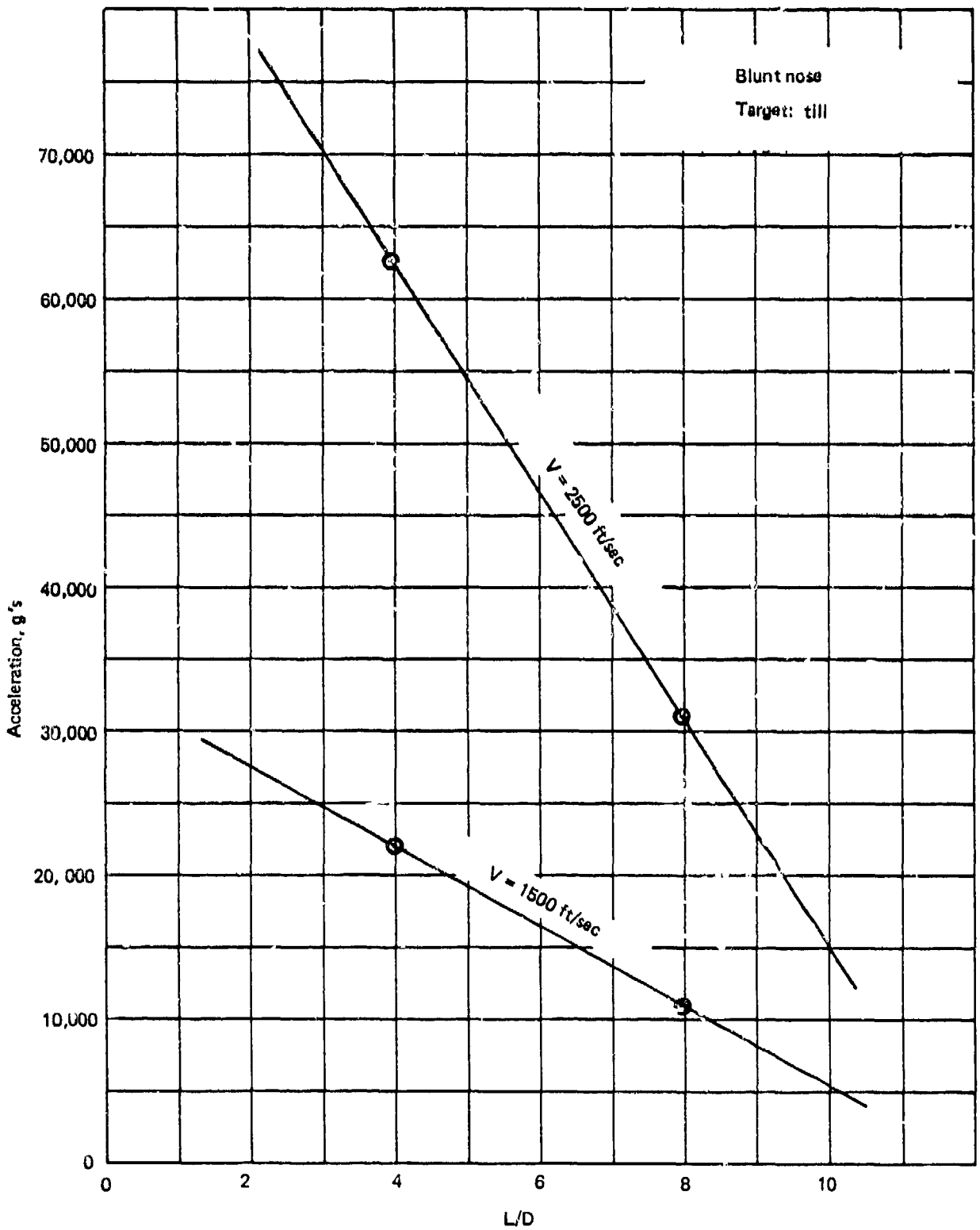

Figure 57. Axial acceleration: blunt nose

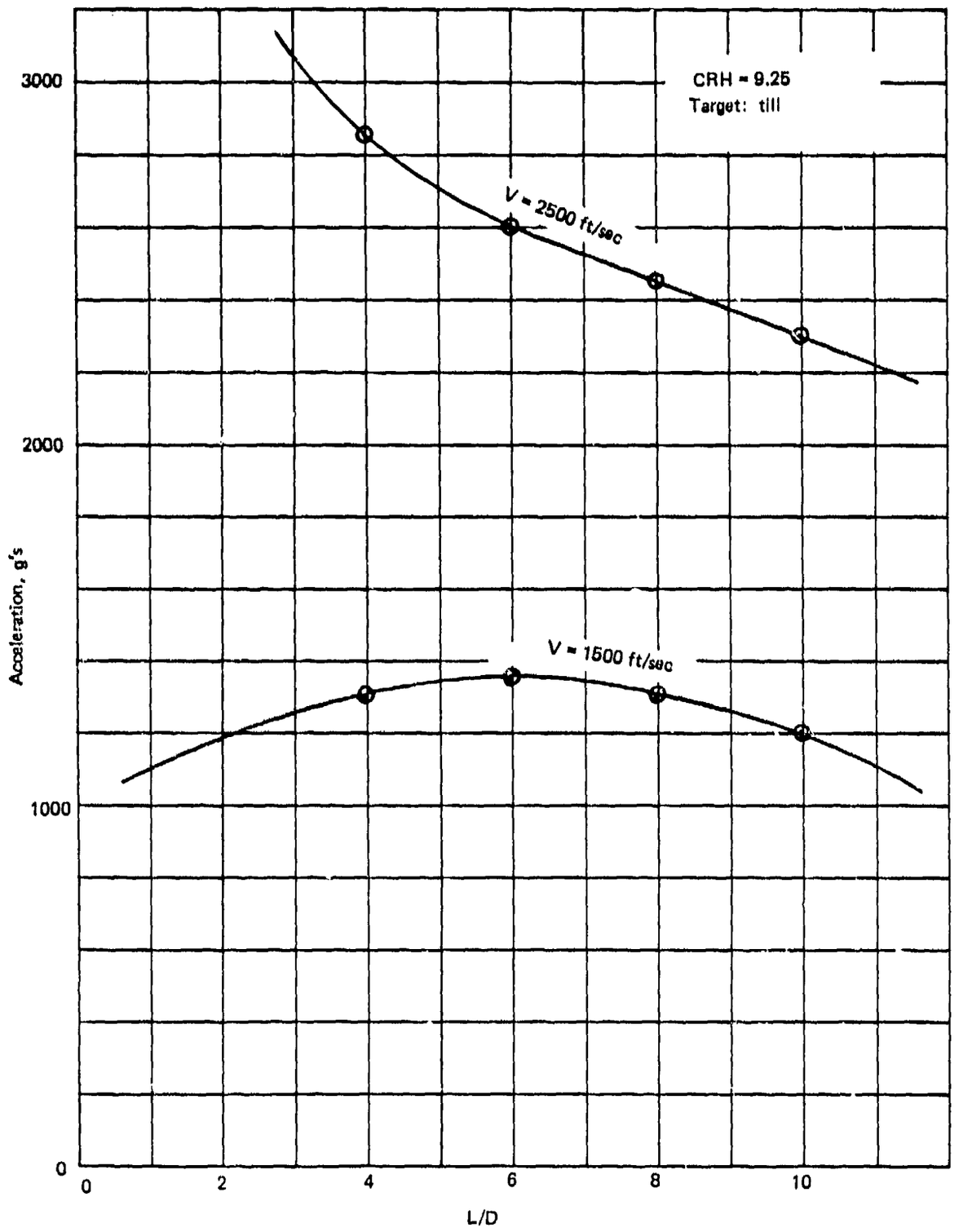

Figure 58. Lateral acceleration: CRH = 9.25

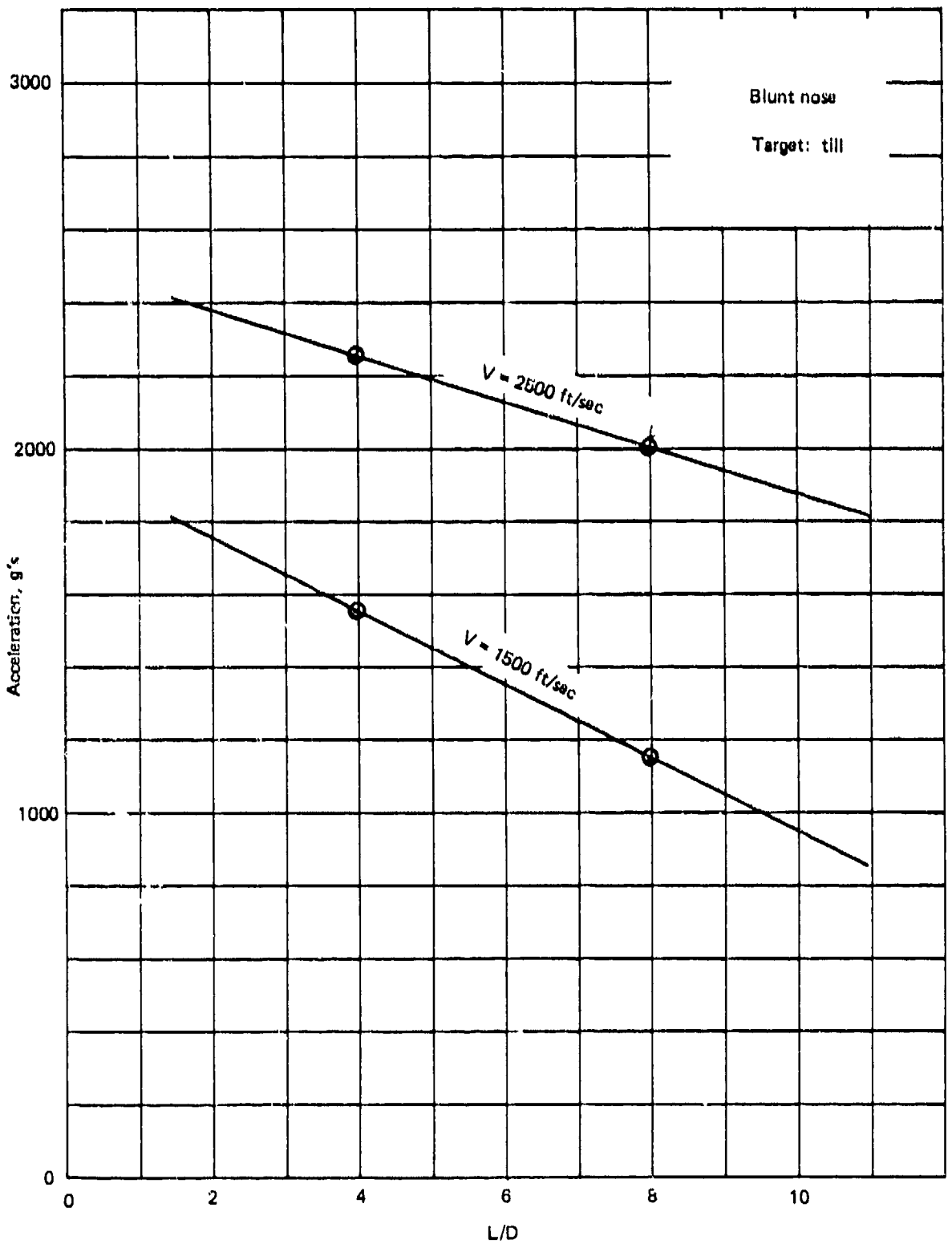

Figure 69. Lateral acceleration: blunt nose

of these EP's. This would not be the case in a media such as air, water, or dry sand. In such media, these short EP's would probably be quite unstable.

5.5 SERIES 5 - MEDIA VARIATIONS

Series 5 was reduced in scope from the original matrix to include three simulations into a reduced strength concrete and three simulations into till (i.e., the same media used in Series 4) and a prediction into welded tuff. The matrix of runs selected for this study is given in Table 11. The data are summarized in Figures 60 and 61. No significant conclusions were drawn from this study except that, in the case of the concrete runs, this performance is more typical of what would be expected in the field. As discussed before, the baseline concrete resistance-to-penetration parameters used in this study was selected conservatively high. The value of the trajectory data and the performance trends provided during this study is dependent on the credibility of the tools used to generate the information. As an indication of accuracy of the results a prediction was to be made of an impact event into a welded tuff target at the Tonapa test site and was to be made prior to an actual test. This type of check was done once before into a soft target (i.e., the Watching Hill Test Site in Canada) with remarkable success.*

The conditions of the proposed test shot included the use of the standard ogive nose EP, 400 pounds, 65 inches long and 6.5 inches in diameter to be fired normally at 1500 ft/sec into a welded tuff target media. The media properties data were provided by WES (Waterways Experiment Station) and are summarized in Figure 62. Avco fitted the bilinear curve through the data provided and executed the conversion procedure described in Section 2.0 to establish the force law coefficients with which to make the required predictions. The variation in target strength was used in the simulations.

Two predictions were initially made, one at 1500 and one at 2000 ft/sec with the 1500 ft/sec prediction submitted to DNA prior to the test. (This was done in memo form and is included in Appendix A, dated June 9, 1975.) The impact velocity however was 1640 ft/sec instead of 1500 ft/sec and the nose of the EP achieved a depth of 11.0 feet.

*Impact and Penetration Study, Contract DNA 001-75-C-0181, Final Report 1974.

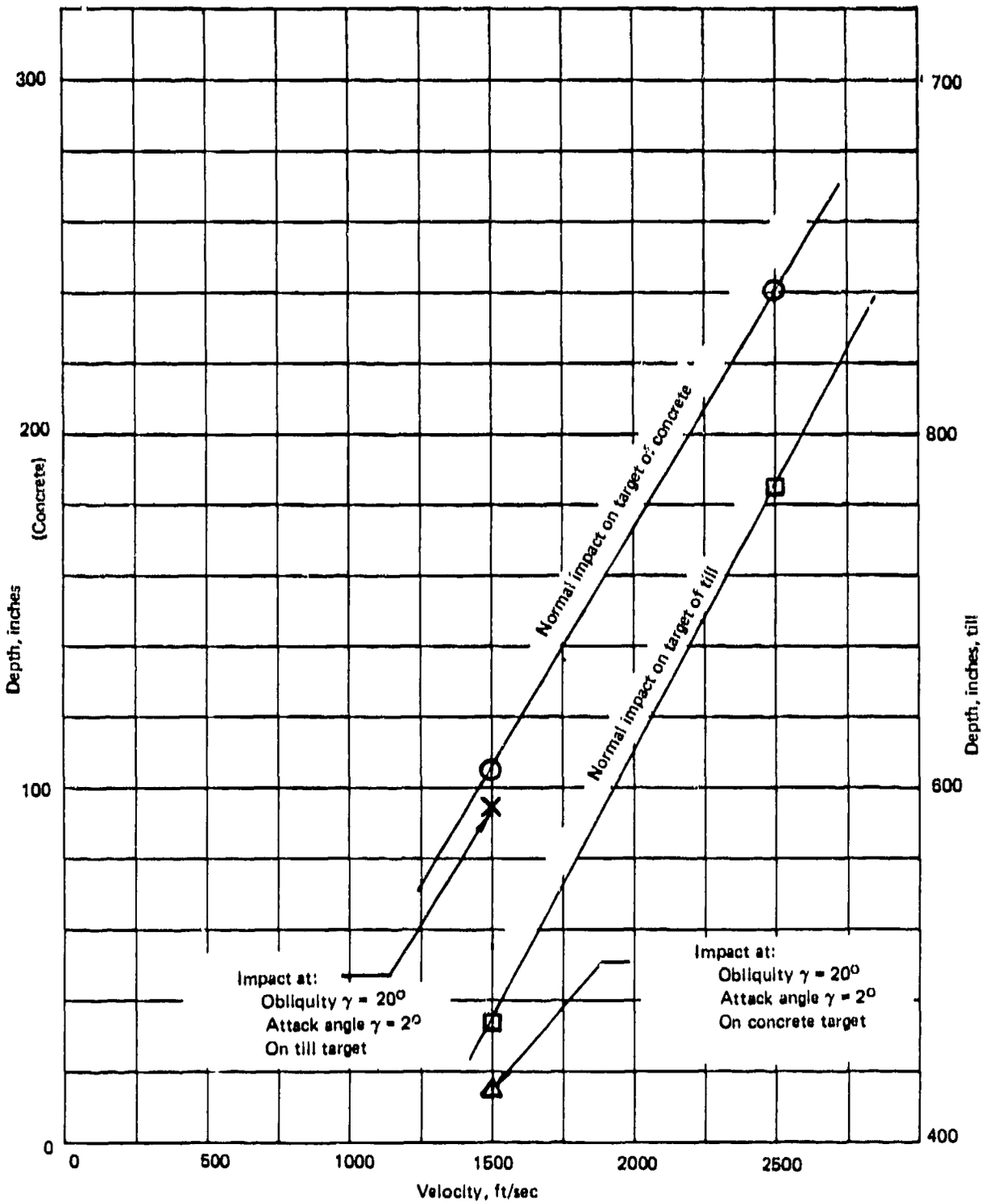

Figure 60. Penetration performance: concrete and till

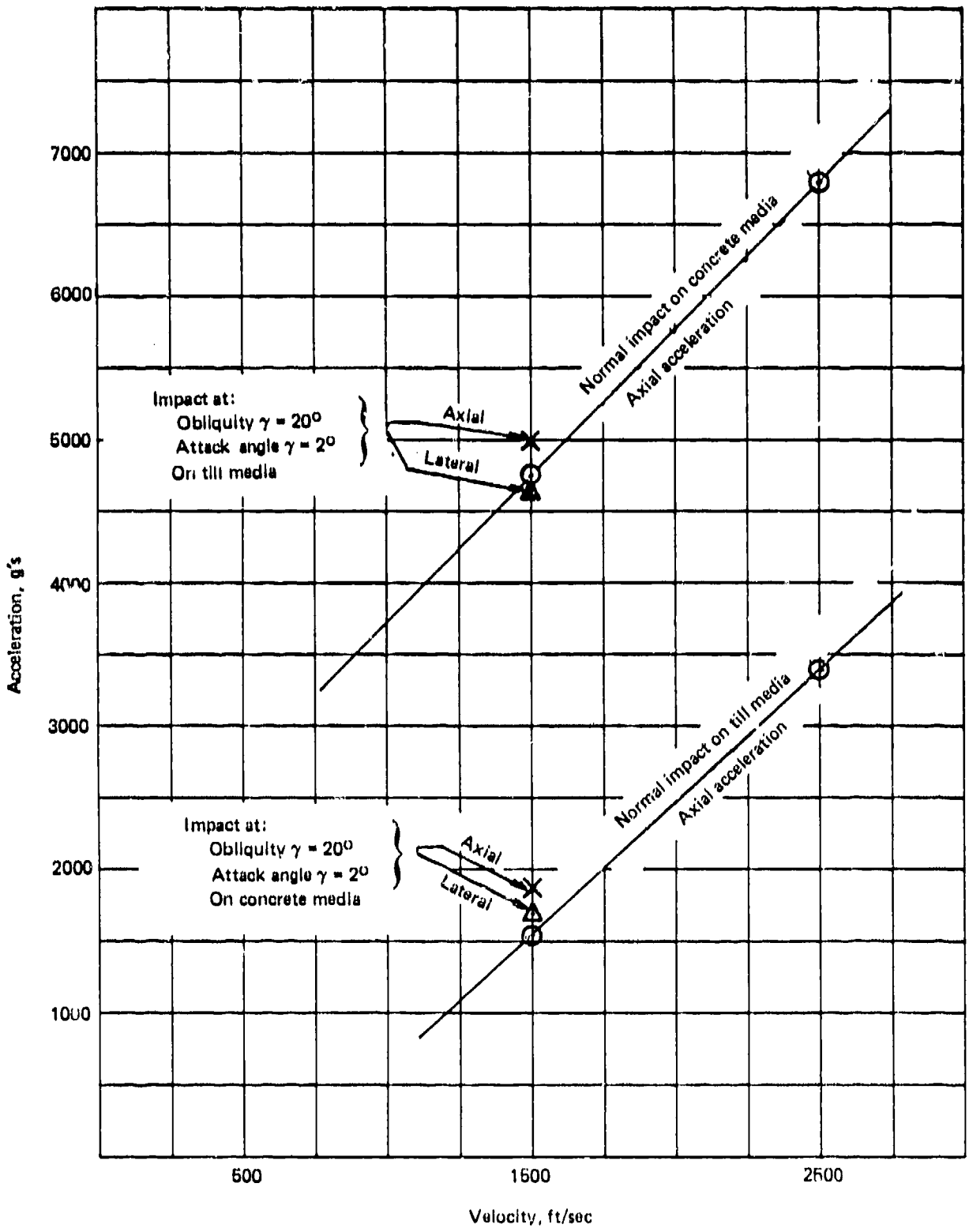

Figure 61. Axial and lateral acceleration: concrete and till

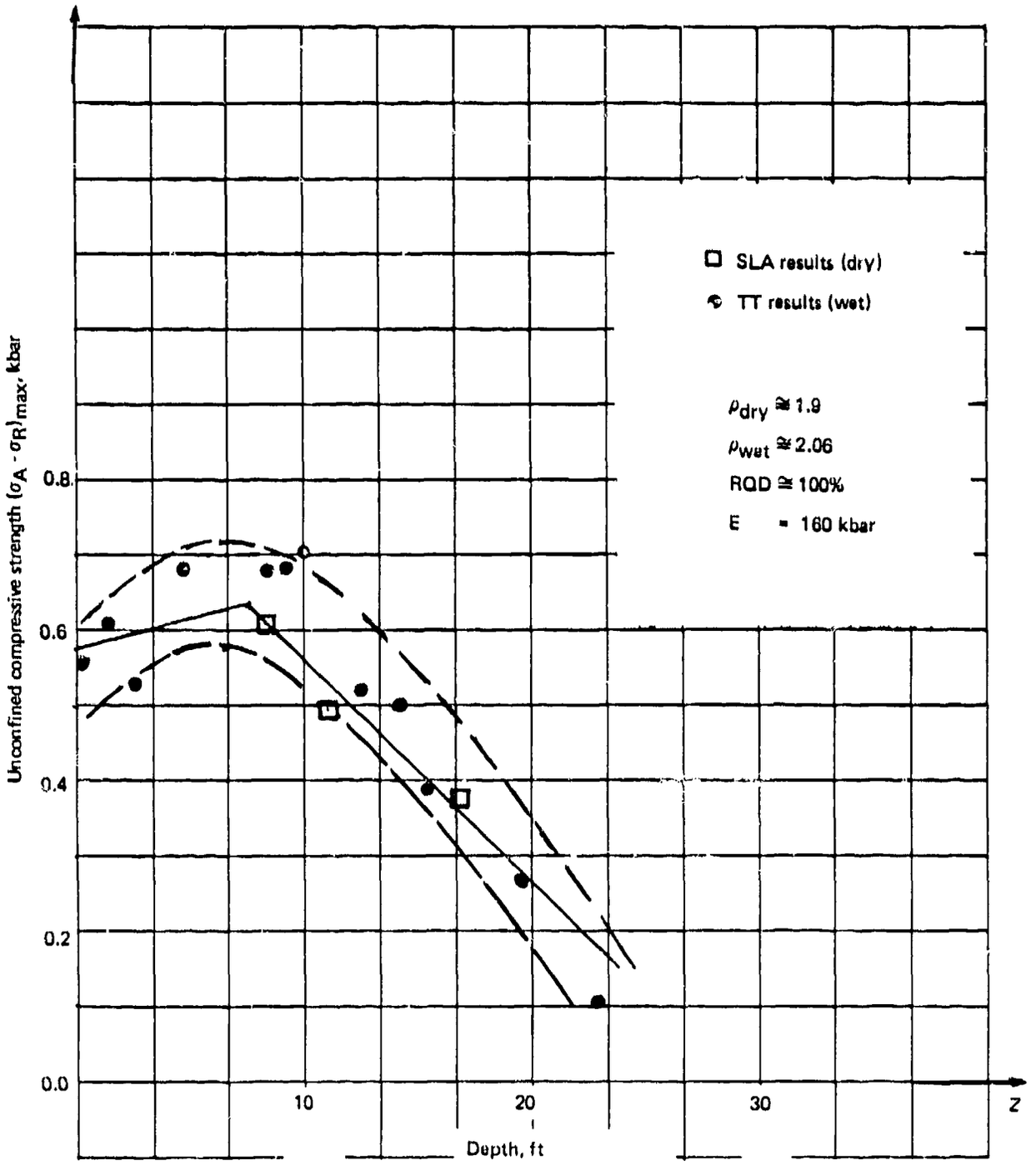

Figure 62. Media properties data (Provided by WES)

These impact conditions were resubmitted for a new estimate of predicted depth with the result being 11.3 feet. The final prediction is based on Runs 5.1A.1 through 5.3A.5 summarized in Figures 63 through 65. It should be pointed out, referring to Figure 65, that the sudden increase in axial g's is caused by the separation of a 157 pound sabot used to accelerate the EP. Figures 66 and 67 summarize the trend of penetration depths achieved within the range of 1500 to 2000 ft/sec. It is evident that the accuracy of the simulator and the conversion techniques to establish the appropriate force law coefficients is quite good.

5.6 SERIES 6 - RICOCHET PREDICTIONS

The purpose of Series 6 was to establish the ricochet performance of two operational bombs, the Mk 82 and Mk 84, in a representative hard target. The physical characteristics of these two warheads and their configurations are shown in Figures 68 and 69.

The hard target is made up of four layers shown in Figure 70 along with their engineering properties. Using the Cavity Expansion Theory conversion procedure, the structural resistance term computes to be 35,545 psi, 2,536 psi, 747 psi and 431 psi, for the four layers, respectively. The matrix of runs selected for this study is summarized in Table 12. The impact velocity of 700 ft/sec was specified by expected delivery conditions, with the obliquities chosen to establish the ricochet angle to an accuracy of 5 degrees.

The detailed trajectory data was generated in Runs 6.1A.1 through 6.14C.3 and are defined in Table 12. The simulations which depicted ricochet are provided in Figures 71 through 76. Summary curves for the ricochet performance are provided in Figure 71 for the Mk 82 and Figure 72 for the Mk 84. It is apparent from these curves that for the 0 degree angle of attack case the Mk 82 experiences ricochet at 55 degrees and the Mk 84 at 60 degrees. The difference is attributed to the increased size of the Mk 84 over the Mk 82. Referring to the summary curves (Figures 71 and 72) a ±5 degree angle of attack causes a change of approximately 10 degrees in the ricochet angle. A reasonably smooth curve can be estimated and drawn between the apparent ricochet points for the angle of attack cases.

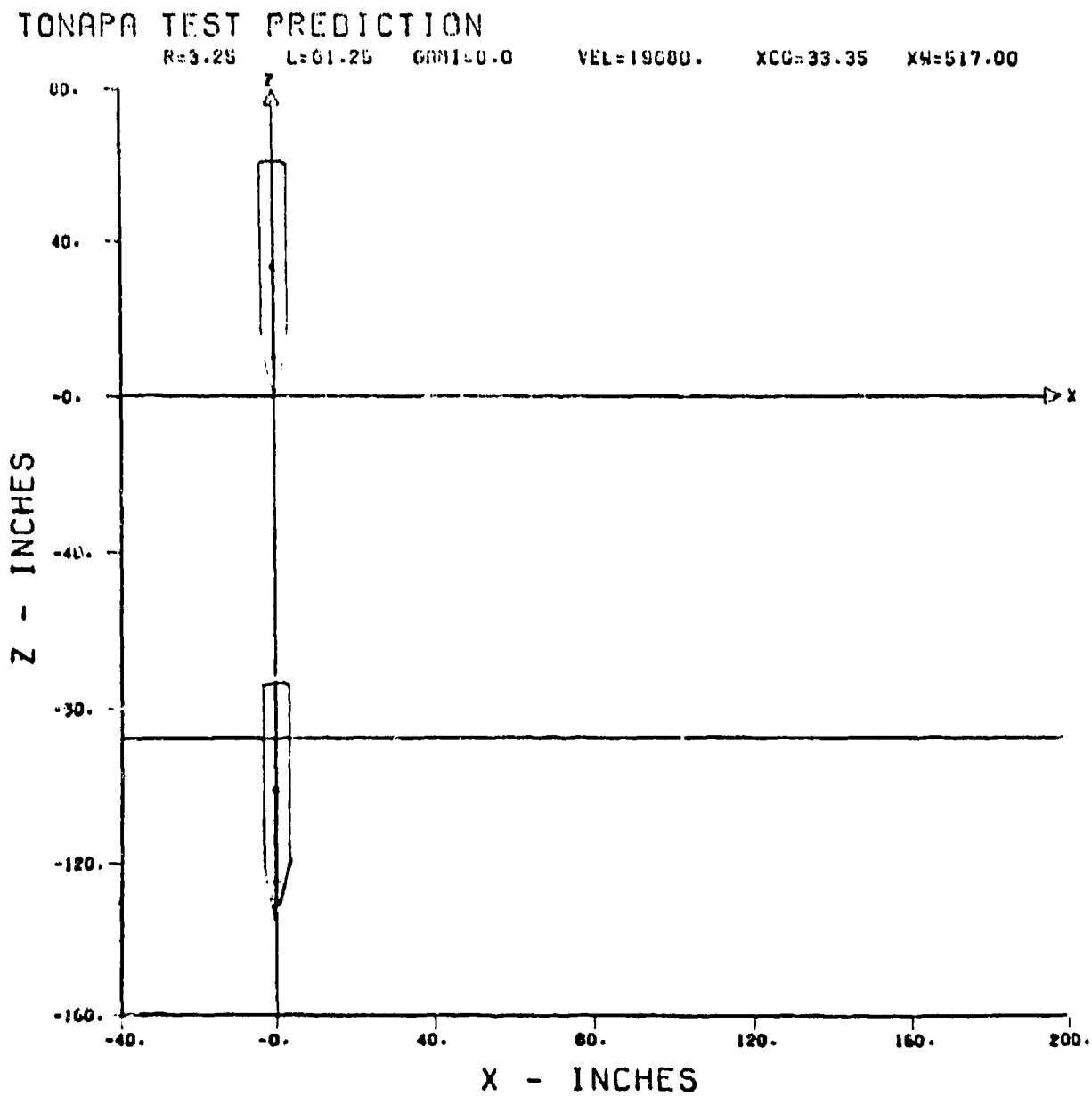

Figure 63. Tonapa test prediction: trajectory

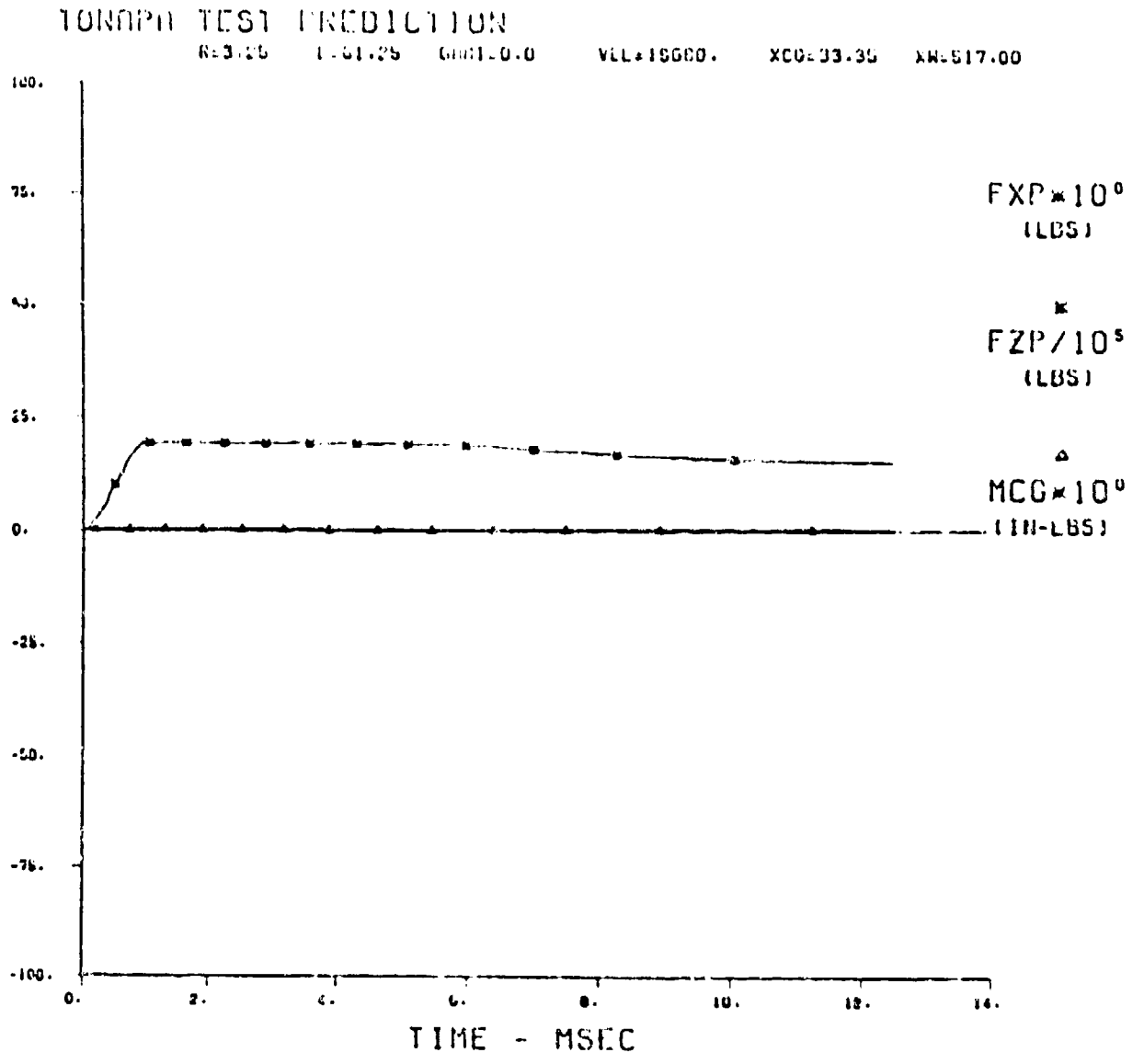

Figure 64. Tonapa test prediction: loads

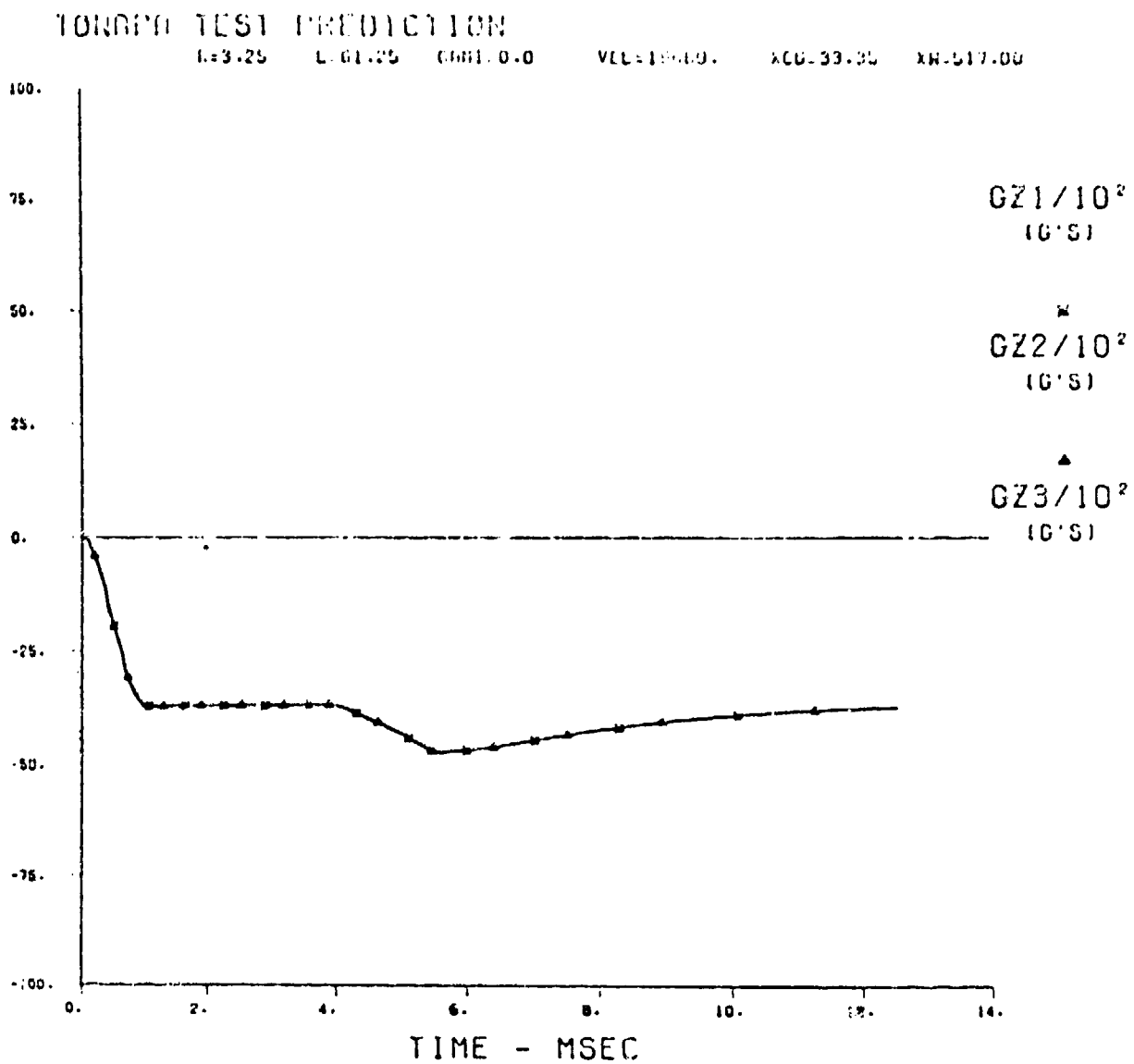

Figure 65. Tonapa test prediction, axial acceleration

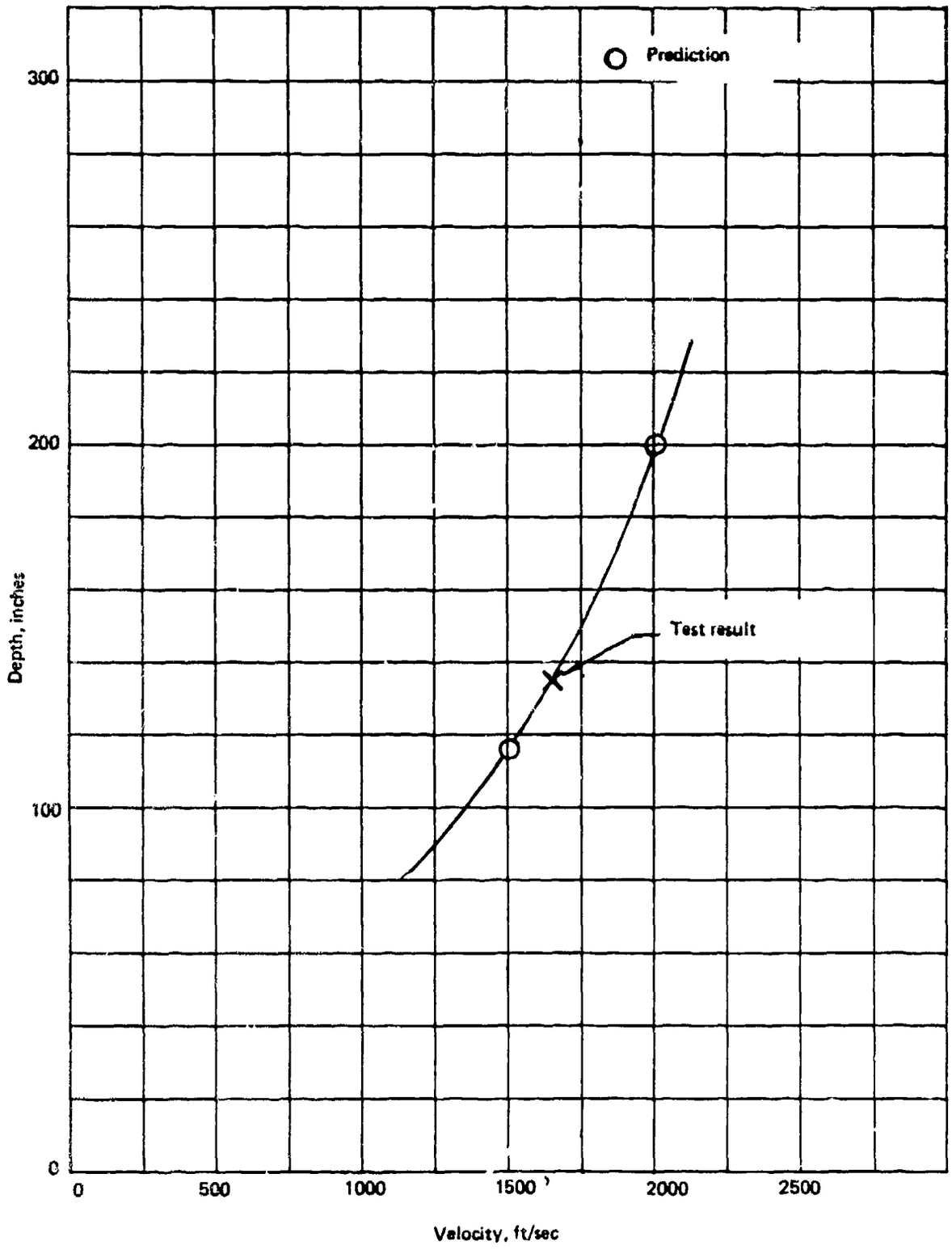

Figure 66. Penetration performance: prediction and test result

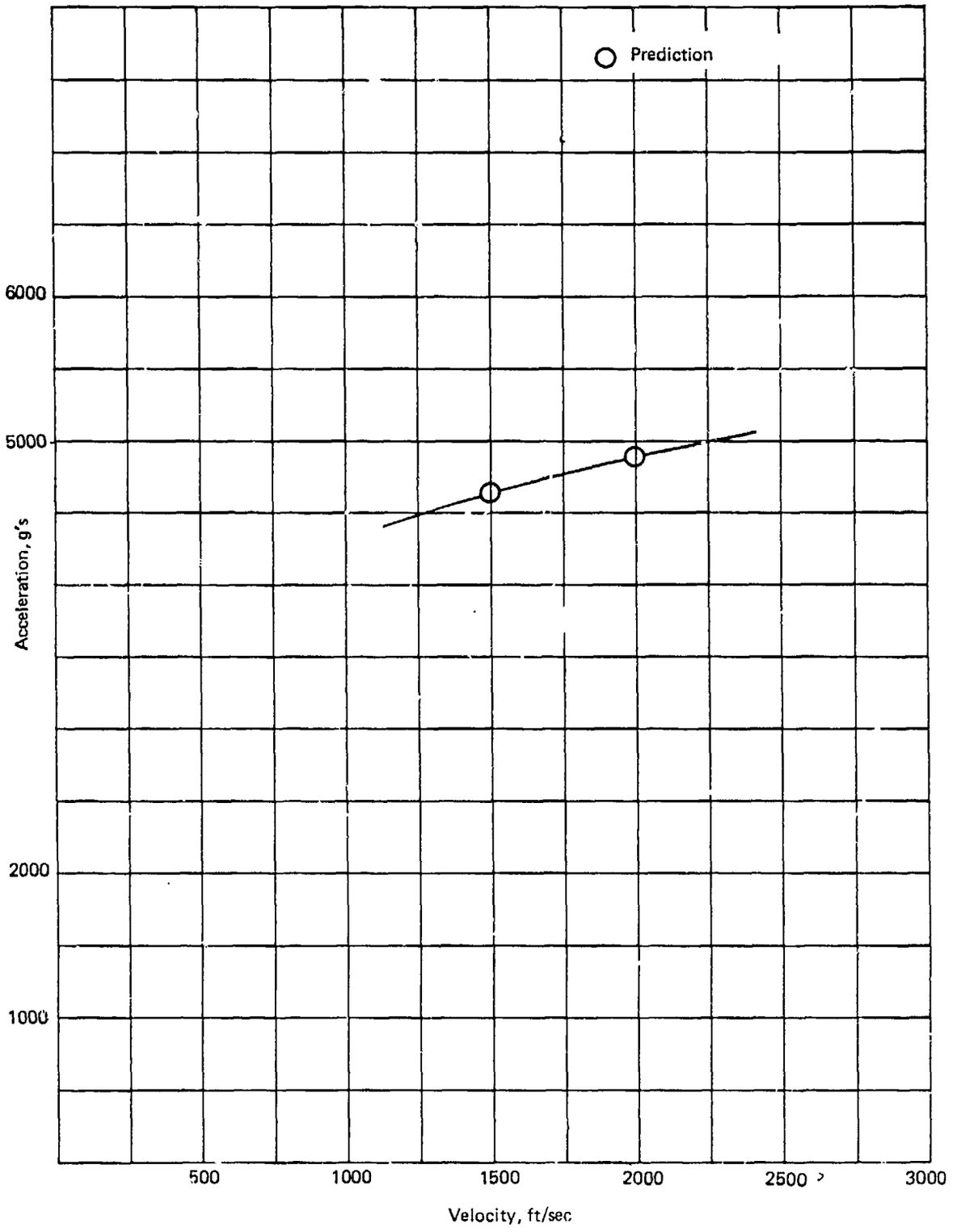

Figure 67. Axial acceleration: prediction and test result

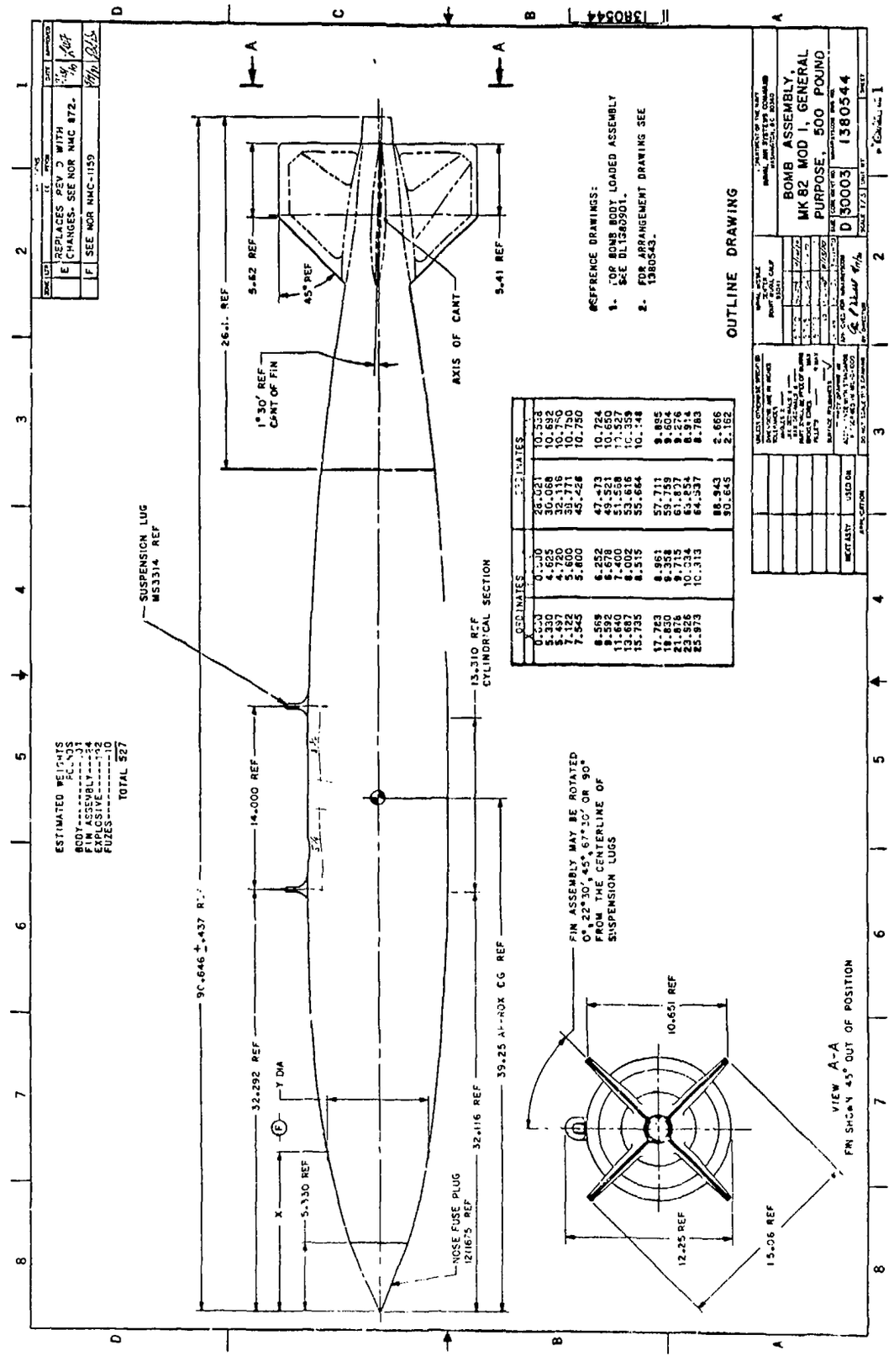

Figure 68. Mark 82 design

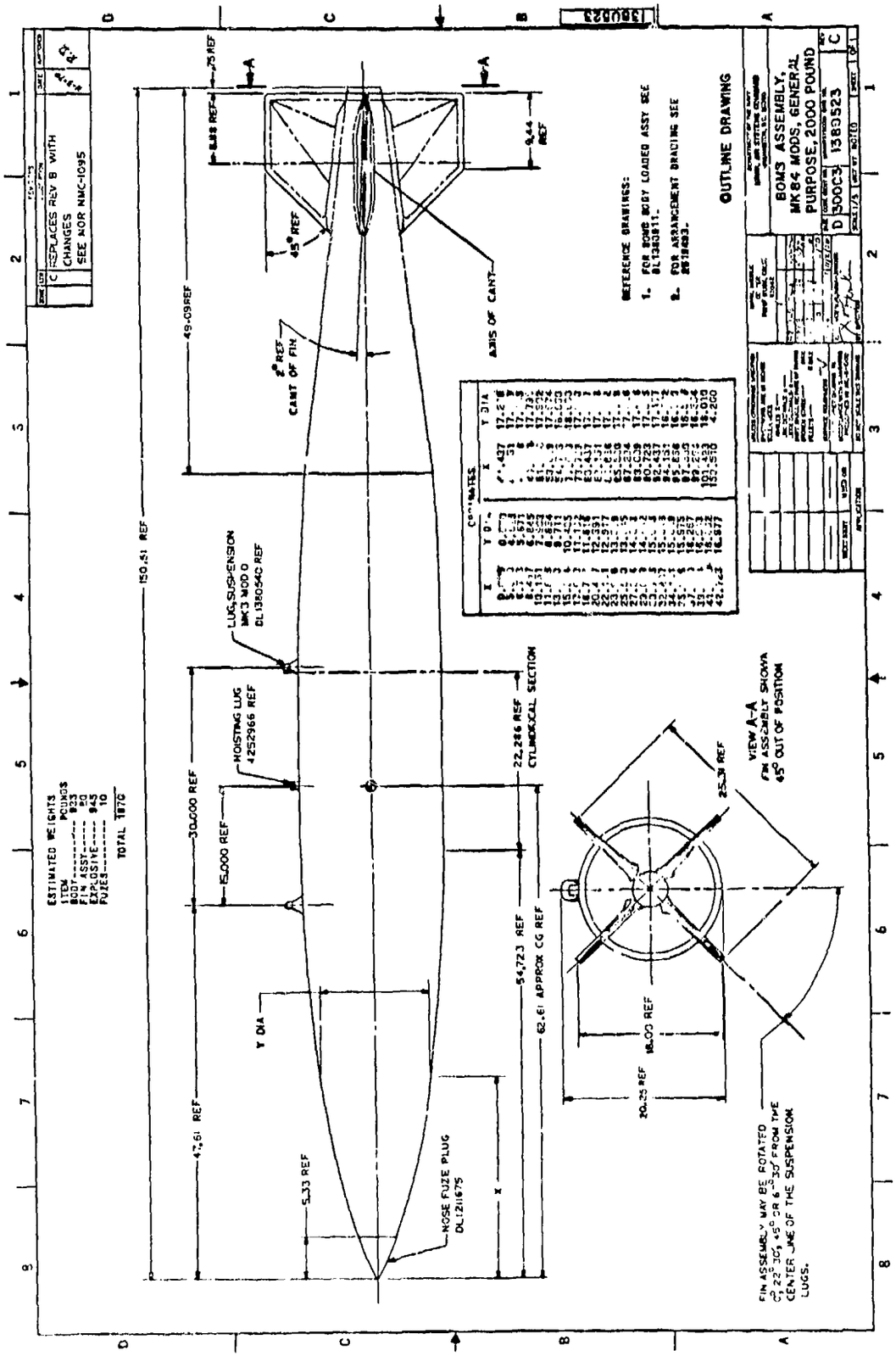

Figure 69. Mark 84 design

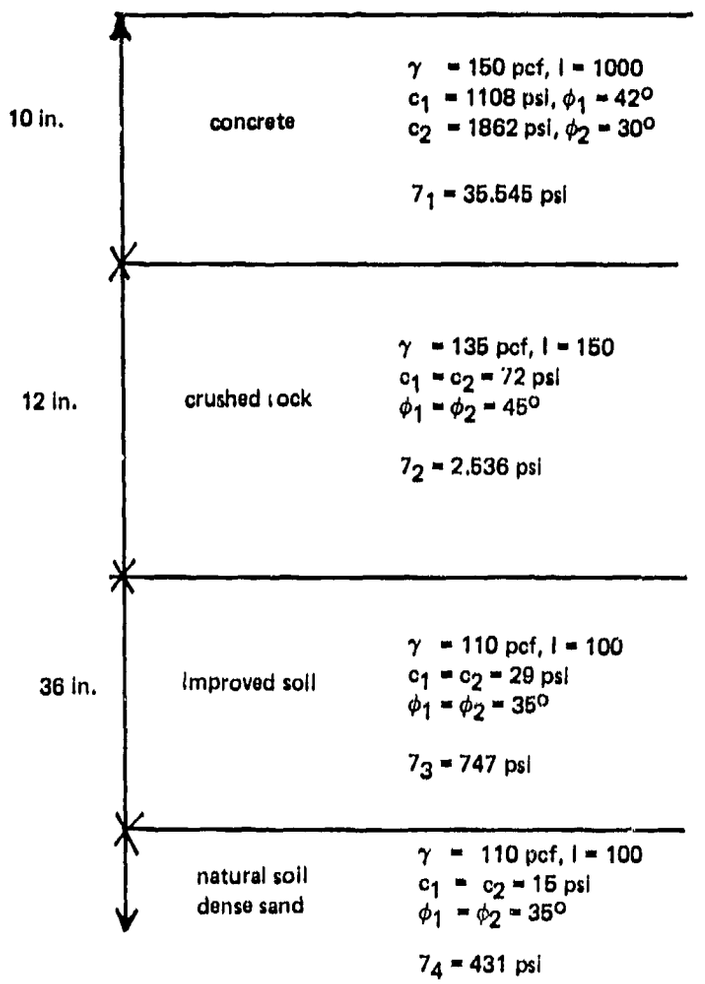

The material constants are defined as follows:

γ = density

ϕ = friction angle

c = cohesion

$I = \frac{\text{shear modulus}}{\text{shear strength}}$

where the Mohr-Coulomb failure surface is approximated by:

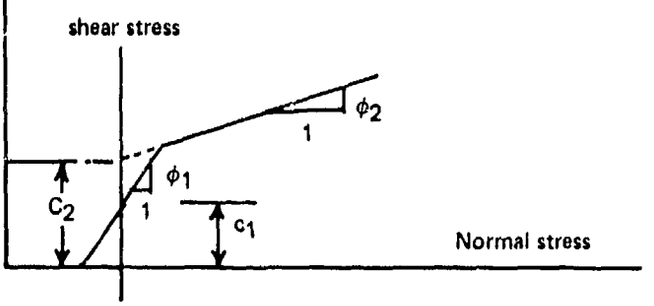

Figure 70. Mark 82 and 84 target description

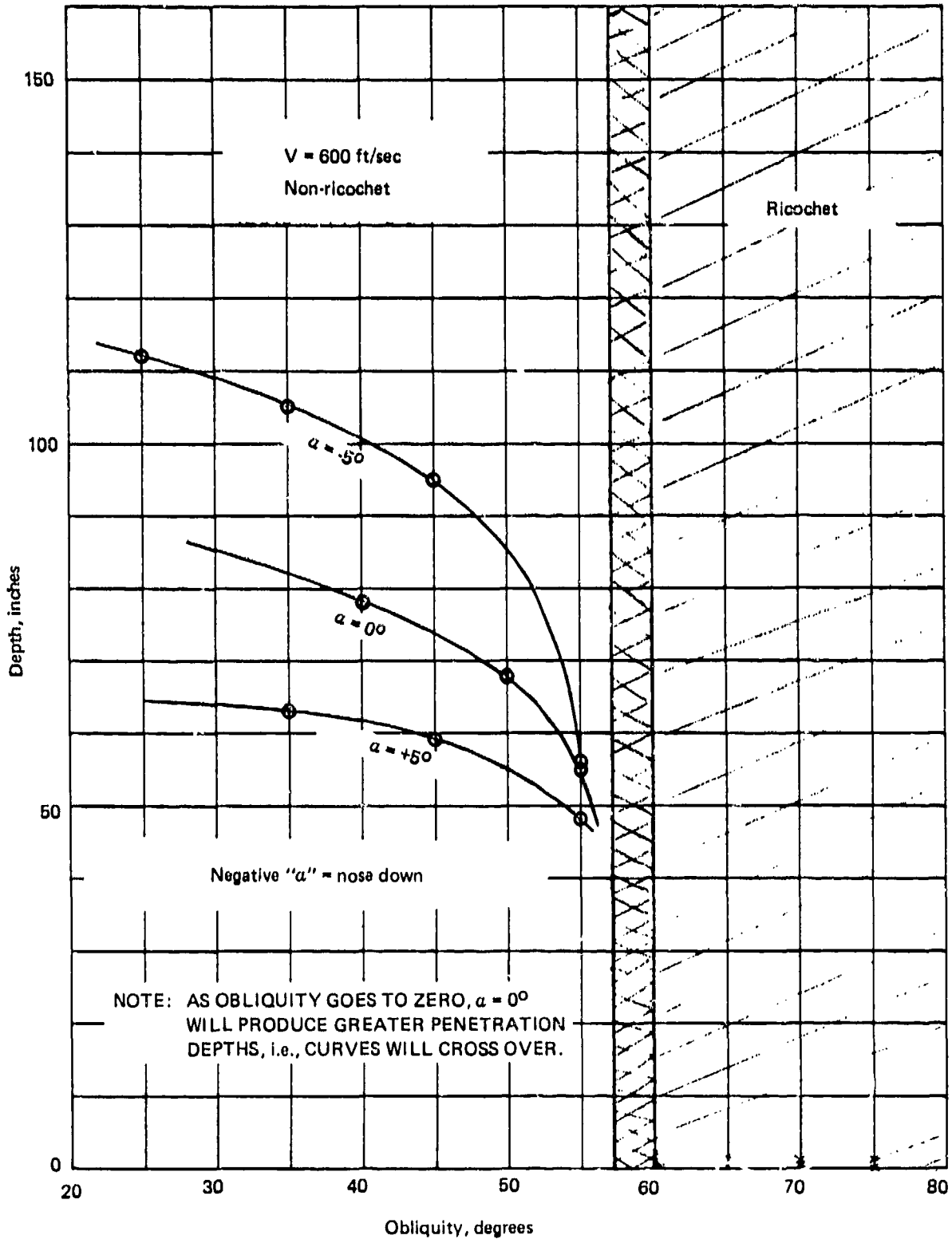

Figure 71. Penetration performance: Mark 82

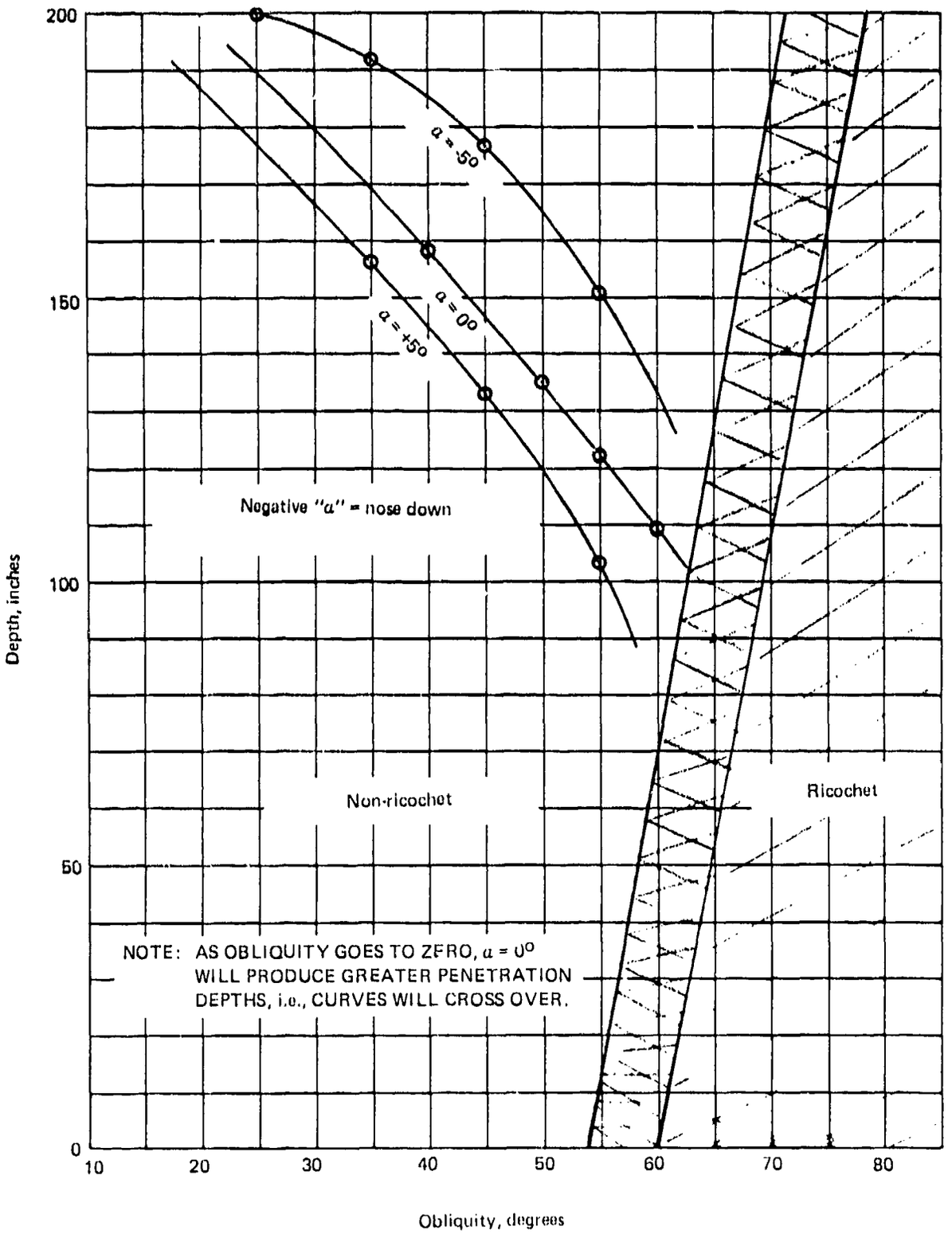

Figure 72. Penetration performance: Mark 84

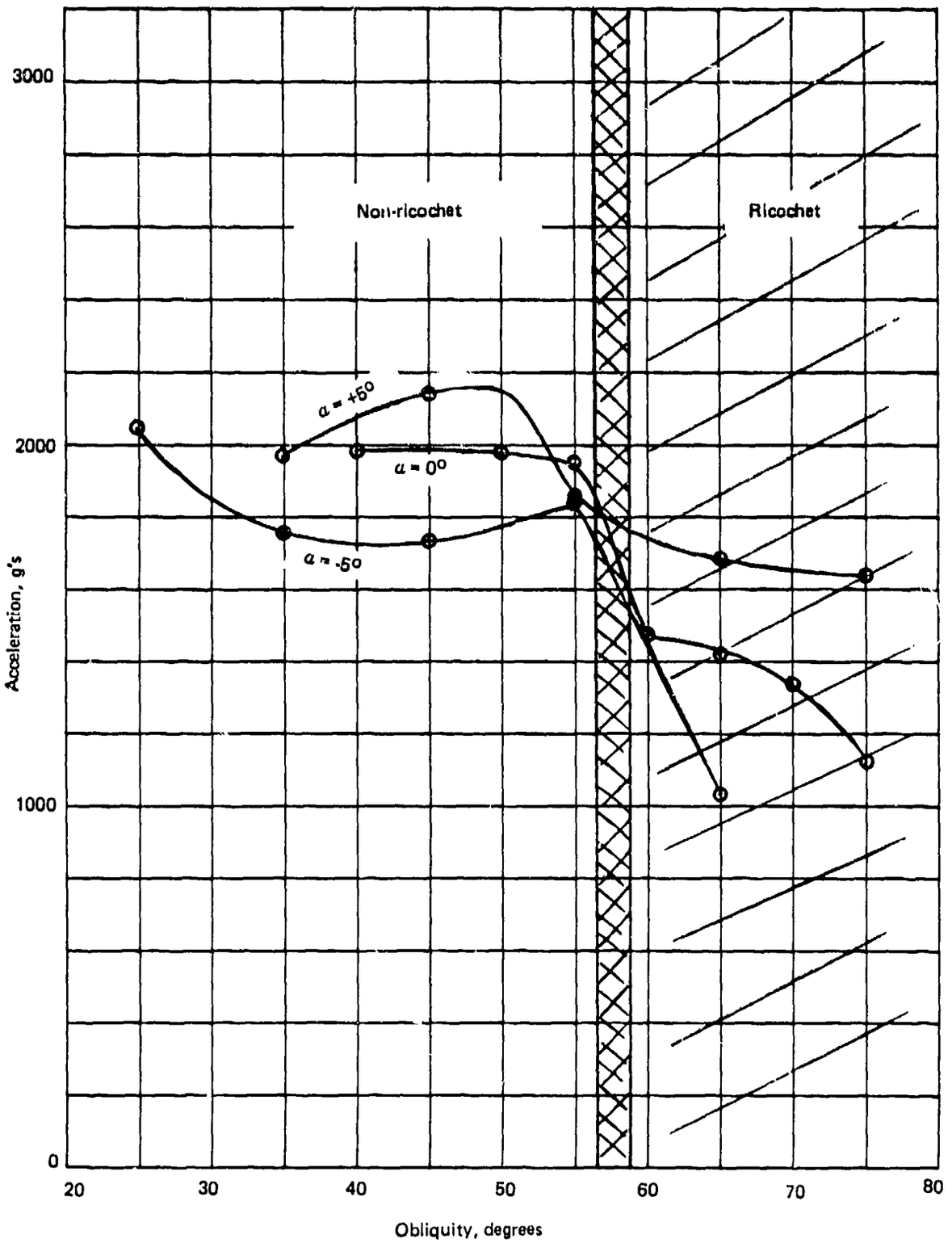

Figure 73. Axial acceleration: Mark 82

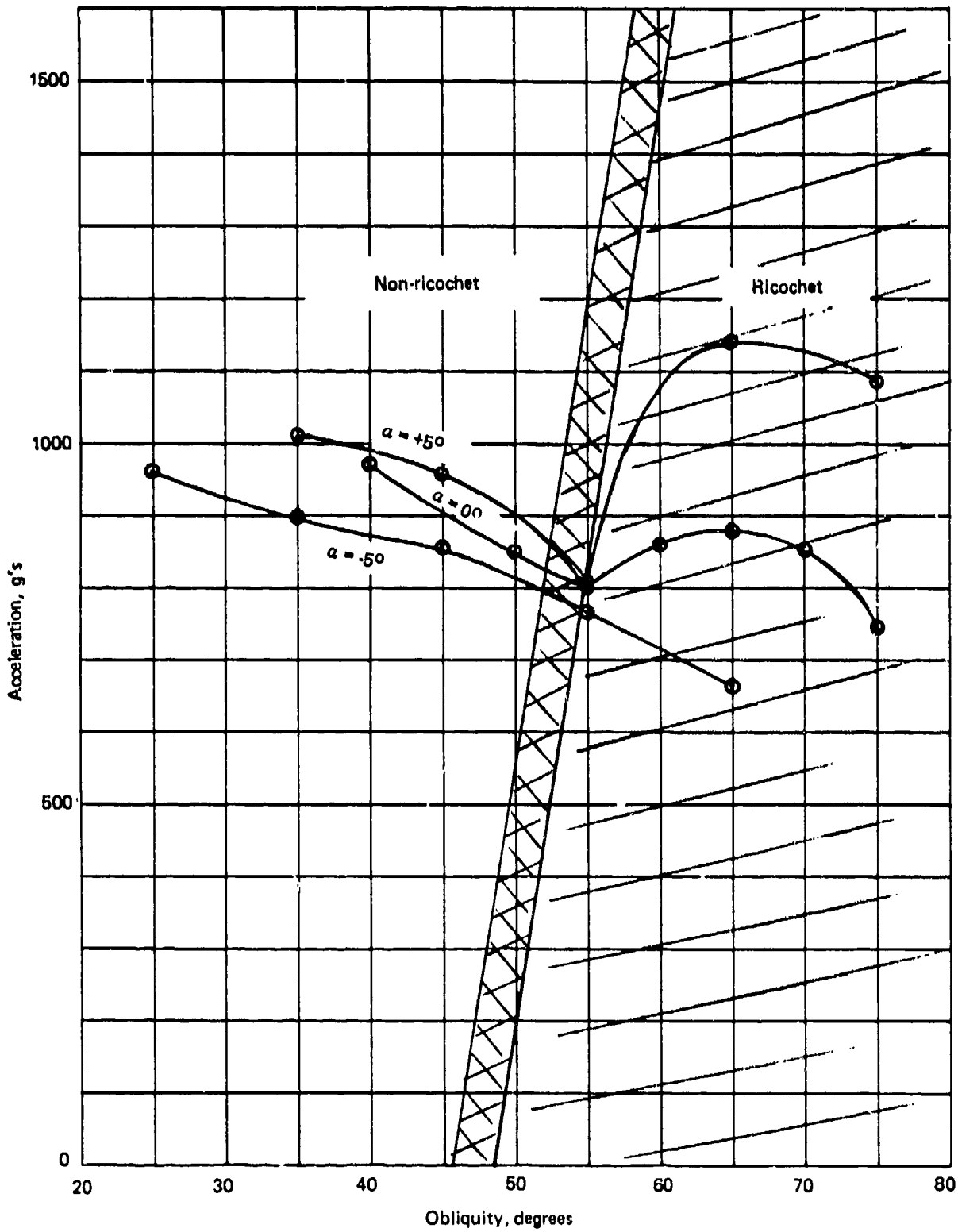

Figure 74. Axial acceleration Mark 84

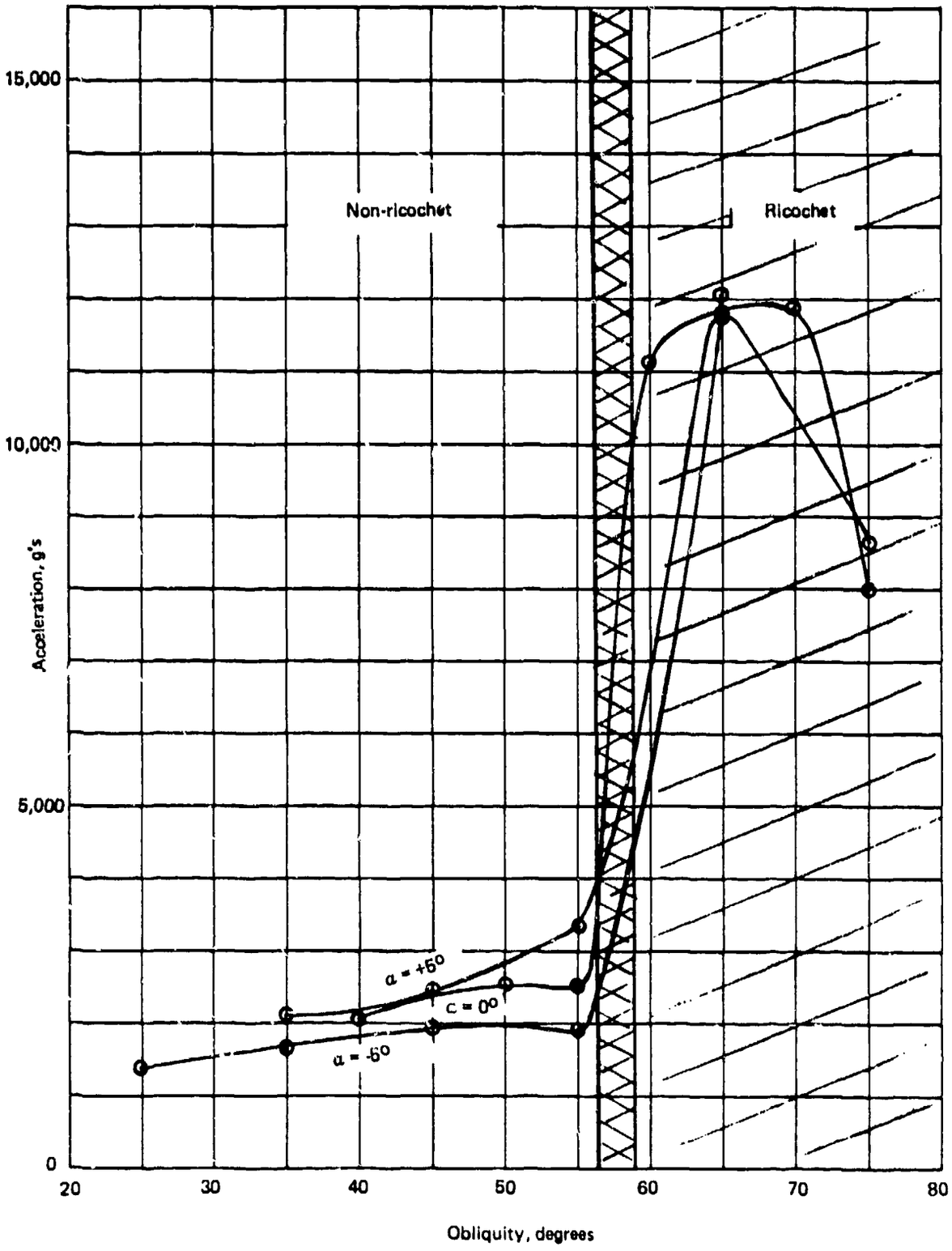

Figure 75. Lateral acceleration: Mark 82

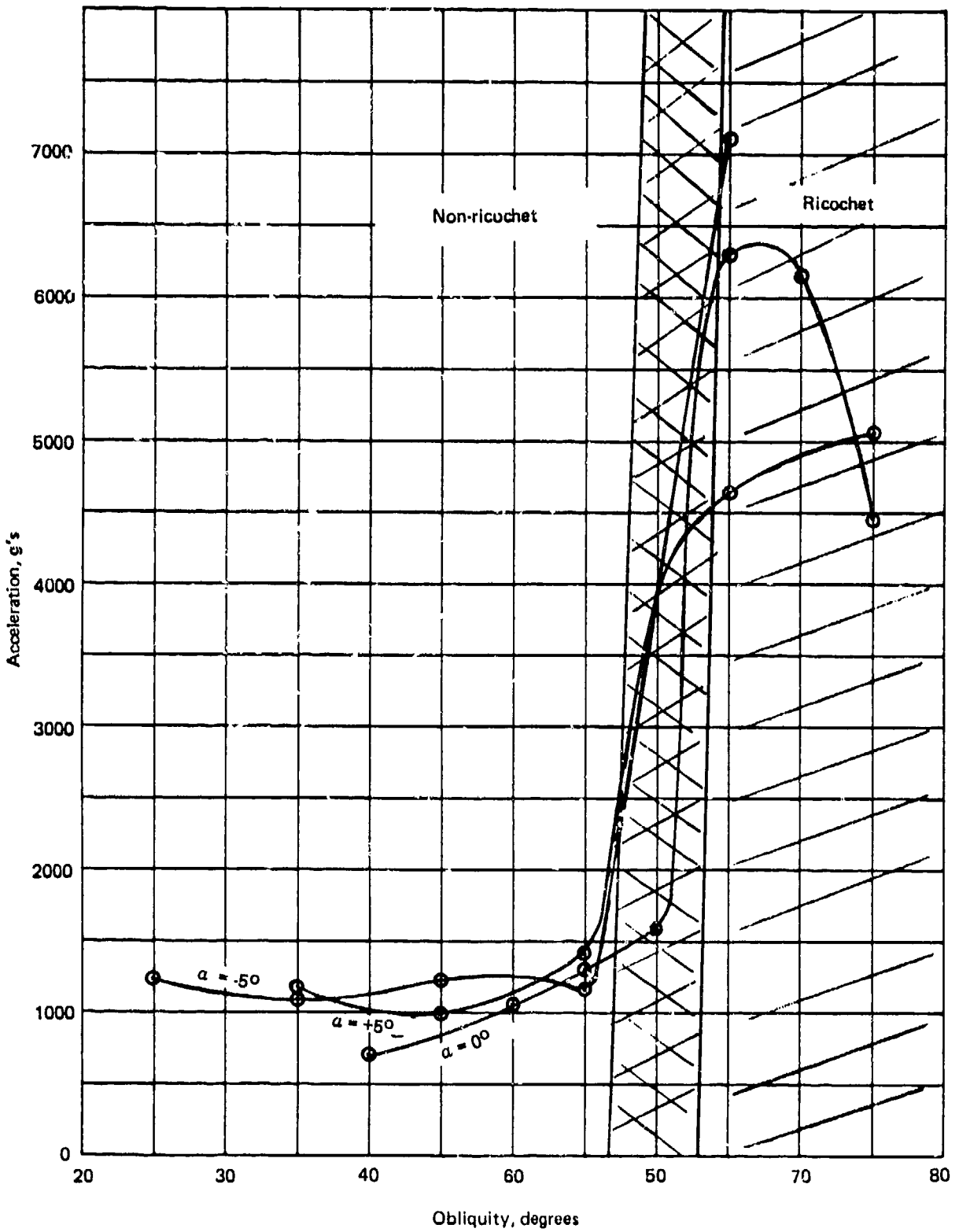

Figure 76. Lateral acceleration: Mark 84

Referring to the loading environment curves, it should be pointed out that after the onset of ricochet a severe and potentially destructive loading environment is applied to these warhead designs. This environment has been designated "tail slap" and is caused by excessive lateral loads being applied to the tail section of the warhead after the nose has bounced clear of the target. This type of loading has been observed to crush the back end of similar projectiles and could result in structural design integrity implications relative to the Mk 82 and 84. In the case of aft mounted fuzing systems this could cause problems relative to fuze functioning.

AVCO

SYSTEMS DIVISION
201 LOWELL STREET, WILMINGTON, MASSACHUSETTS 01887

APPENDIX A

9 June 1975
G500-75-DH-53

Major Todd Stong
Defense Nuclear Agency
Washington, D.C.

Dear Todd,

Enclosed you will find Avco's terradynamic performance predictions of the 1500 ft/sec Tonapa DEP Test. The structural resistance-to-penetration parameter " η " was based on a conversion process using the Cavity Expansion Theory with the basic data being supplied by WES. The inertial resistance-to-penetration was based on our own estimates of the characteristics of Welded Tuff.

Referring to Figure A-3, the estimated penetration depth is a little over 9 feet.

Accelerations are obtained from Figure A-4. Initial peak acceleration is on the order of 3700 g while the launch sabot is still attached. The slope to 4600 g is caused by the assumption that the sabot does not detach instantaneously.

Relative to the ongoing "Impact and Penetration Technology Program," Tests 3 and 4 were conducted this week (i.e., June 27th and 28th) and they both went well.

Test 3, which consisted of an impact velocity of 1500 ft/sec and an angle of attack (α) of 2 degrees produced stresses (based on strain gage readings) as expected in between those of $\alpha = 0^{o}$ and 5^{o}. Test 4, which consisted of an impact velocity of 1500 ft/sec and $\alpha = 10^{o}$ produced peak structural stresses of approximately 300,000 psi, again a nearly linear extrapolation of the other tests.

Now that the pressure is off (i.e., because of test setup requirements and transducer development efforts) we can reproduce the data from the four tests in hard copy for distribution to DNA and WES. This will be accomplished within the next week.

Very truly yours,

David Henderson
Senior Consultant Engineer

Enclosure

cc: Dr. Paul Hadala, Waterways Experimental Station, Vicksburg, Mississippi

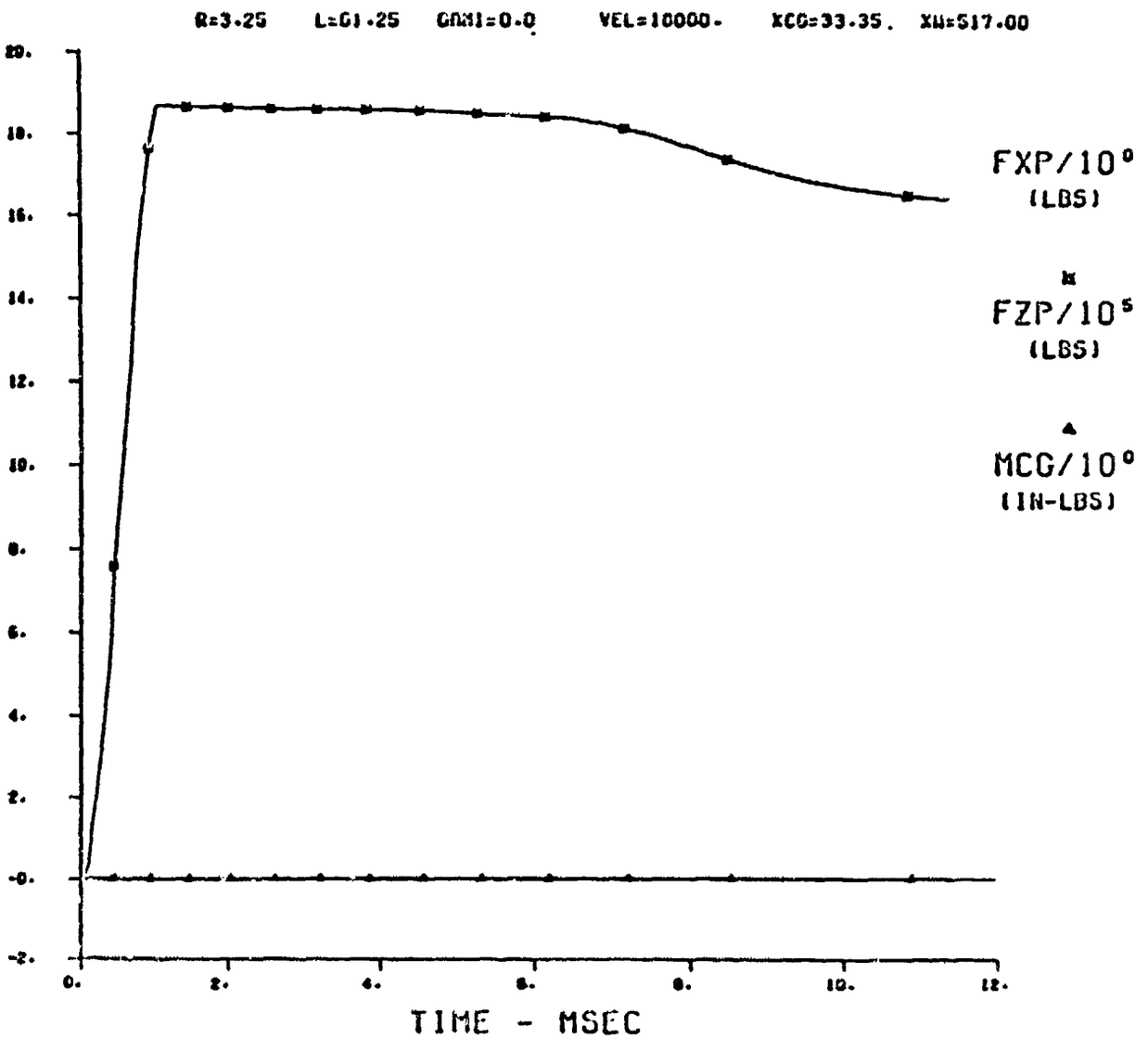

Figure A-1. Tonapa test prediction loads

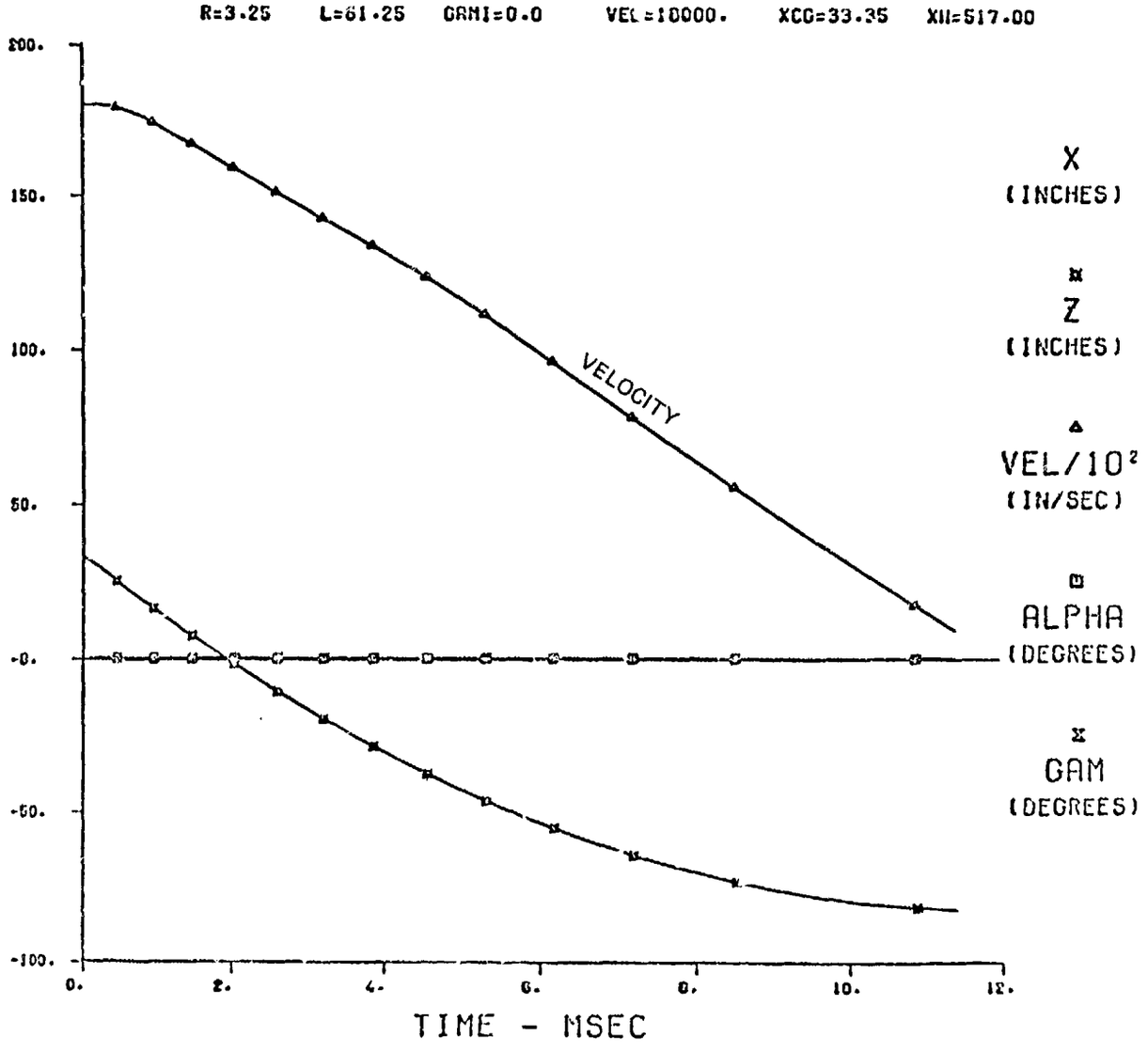

Figure A–2. Tonapa test prediction trajectory data

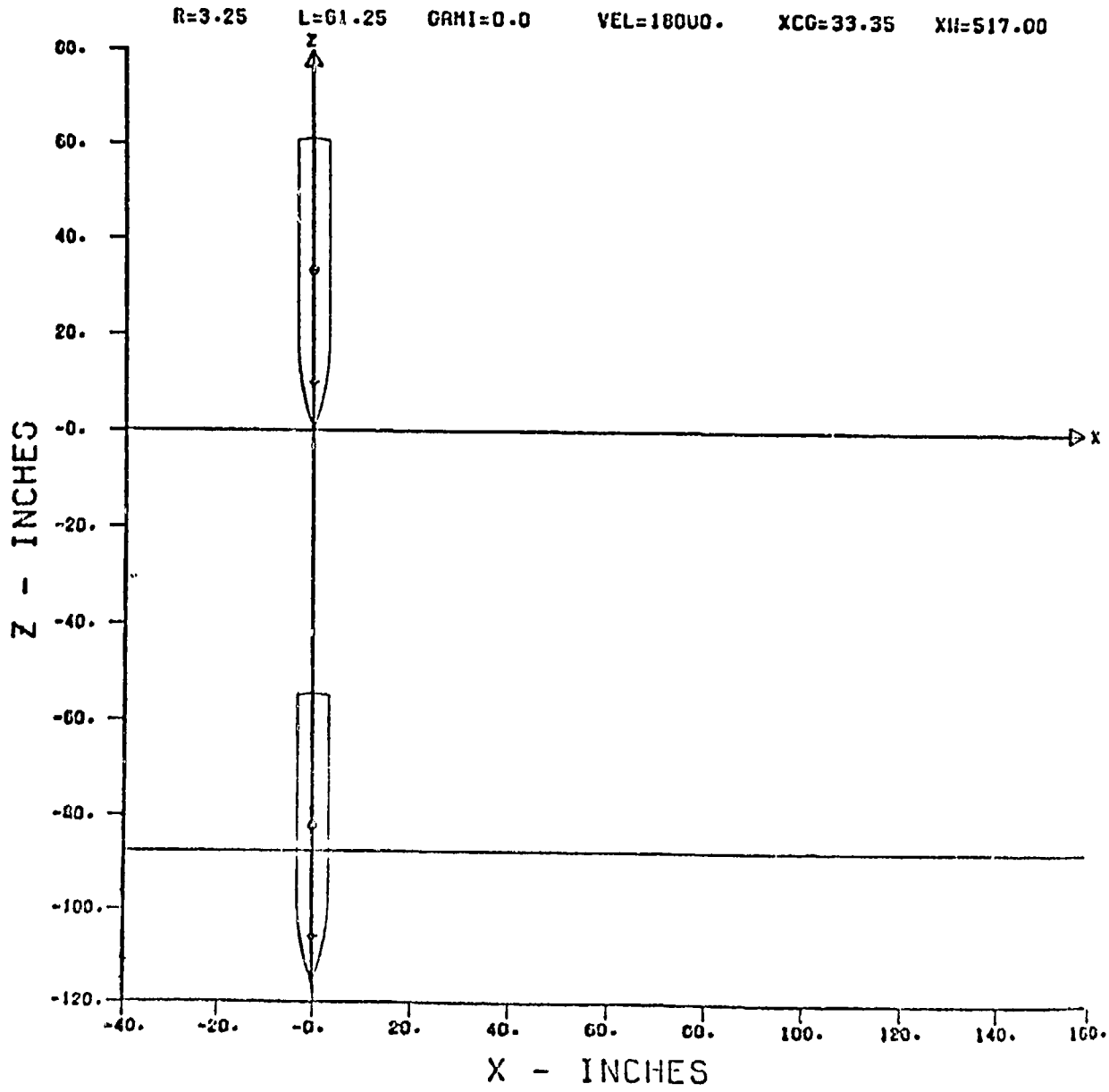

Figure A—3. Tonapa test prediction trajectory

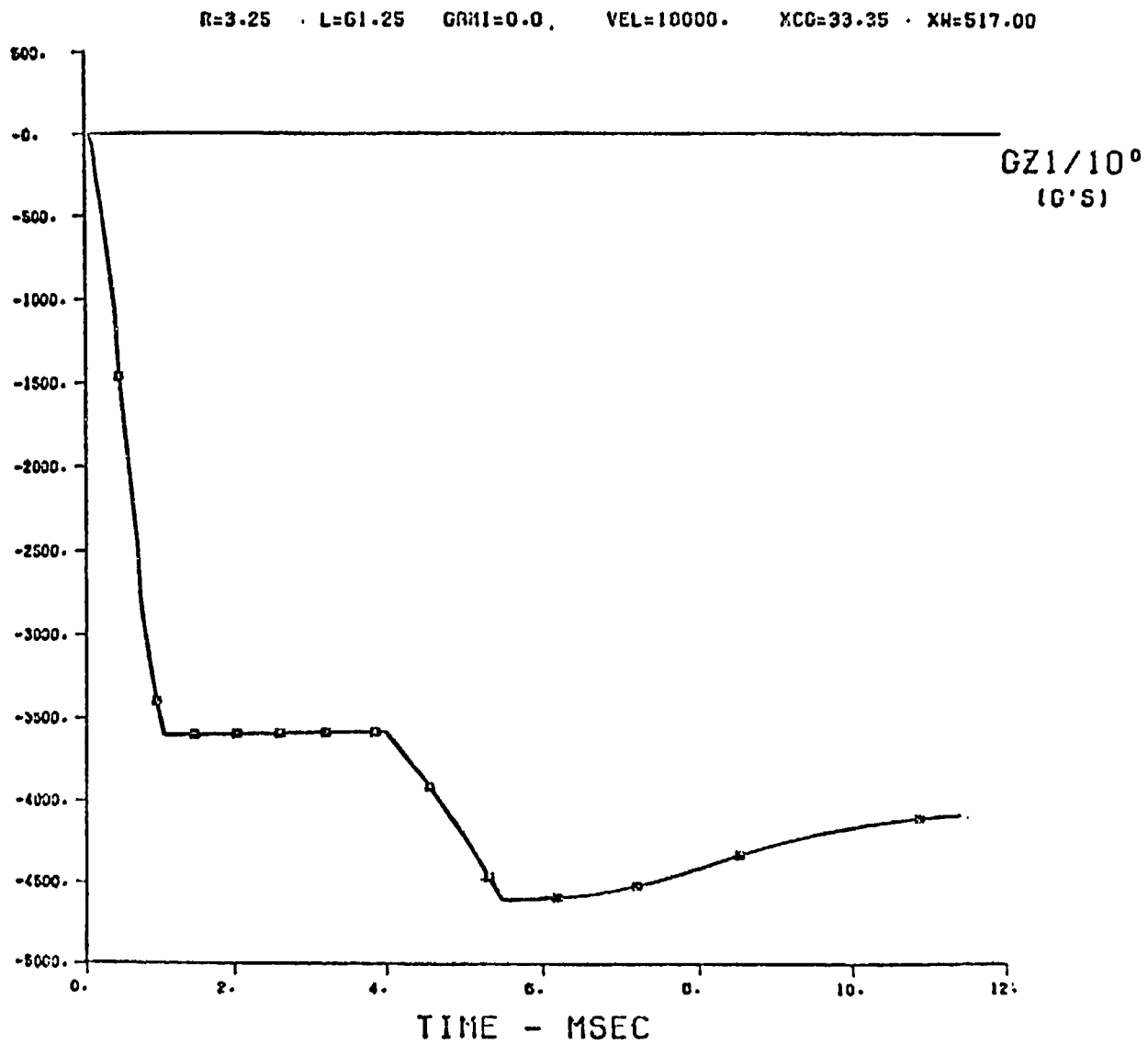

Figure A–4. Tonapa test prediction acceleration

DISTRIBUTION LIST

DEPARTMENT OF DEFENSE

Director
Defense Advanced Rsch. Proj. Agency
ATTN: Tech. Library

Director
Defense Civil Preparedness Agency
ATTN: Admin. Officer

Defense Documentation Center
12 cy ATTN: TC

Director
Defense Intelligence Agency
ATTN: DB-4C, Edward O'Farrell
ATTN: Tech. Library
ATTN: DT-2 Wpns. & Sys. Div.
ATTN: DI-7E
ATTN: Charles A. Fowler

Director
Defense Nuclear Agency
ATTN: SPAS
3 cy ATTN: TITL Tech. Library
5 cy ATTN: SPSS
ATTN: TISI Archives
ATTN: DDST

Commander, Field Command
Defense Nuclear Agency
ATTN: FCPR

Director
Interservice Nuclear Weapons School
ATTN: Doc. Control

Director
Joint Strat. Tgt. Planning Staff, JCS
ATTN: STINFO Library

Chief
Livermore Division Fld. Command, DNA
Lawrence Livermore Laboratory
ATTN: FCPRL

Under Secretary of Def. for Rsch. & Engrg.
ATTN: S&SS (OS)

DEPARTMENT OF THE ARMY

Dep. Chief of Staff for Rsch. Dev. & Acq.
ATTN: DAMA(CS), MAJ A. Gleim
ATTN: DAMA-CSM-N, LTC G. Ogden
ATTN: Tech. Library

Chief of Engineers
2 cy ATTN: DAEN-MCE-D
2 cy ATTN: DAEN-RDM

Deputy Chief of Staff for Ops. & Plans
ATTN: Dir. of Chem. & Nuc. Ops.
ATTN: Tech. Library

DEPARTMENT OF THE ARMY (Continued)

Chief
Engineer Strategic Studies Group
ATTN: DAEN-FES

Project Manager
Gator Mine Program
ATTN: E.J. Lindsey

Commander
Harry Diamond Laboratories
ATTN: DELHD-NP
ATTN: DRXDO-RBH, James H. Gwaltney

Commander
Picatinny Arsenal
ATTN: Ray Moesner
ATTN: Paul Harris
ATTN: Jerry Pental
ATTN: P. Angelloti
ATTN: B. Shulman, DR-DAR-1-C-FA
ATTN: Ernie Zimpo
ATTN: SMUPA-AD-D-M
ATTN: SMUPA-AD-D-A-7
ATTN: Marty Margolin
ATTN: SMUPA-AD-D-A
ATTN: Tech. Library

Commander
Redstone Scientific Information Ctr.
ATTN: Chief, Documents

Commander
U.S. Army Armament Command
ATTN: Tech. Library

Director
U.S. Army Ballistic Research Labs.
ATTN: G. Roecker
ATTN: G. Grabarek
ATTN: DRXBR-X
ATTN: J.H. Keefer, DRDAR-BLE
ATTN: A. Niccliazzi
ATTN: DRXBR-TB
ATTN: J.W. Apgar
2 cy ATTN: Tech. Library, Edward Baicy

Commander And Director
U.S. Army Cold Region Res. Engr. Lab.
ATTN: G. Swinzow

Commander
U.S. Army Comb. Arms Combat Dev. Acty.
ATTN: LTC Pullen
ATTN: LTC G. Steger

Commander
U.S. Army Engineer Center
ATTN: ATSEN-SY-L

Division Engineer
U.S. Army Engineer Div. Huntsville
ATTN: HNDED-SR

DEPARTMENT OF THE ARMY (Continued)

Division Engineer
U.S. Army Engineer Div. Missouri Rvr.
ATTN: Tech. Library

Commandant
U.S. Army Engineer School
ATTN: ATSE-TEA-AD
ATTN: ATSE-CTD-CS

Director
U.S. Army Engr. Waterways Exper. Sta.
ATTN: Guy Jackson
ATTN: William Flathau
ATTN: D.K. Butler
ATTN: P. Hadala
ATTN: John N. Strange
ATTN: Leo Ingram
ATTN: Tech. Library
ATTN: Behzad Rohani

Commander
U.S. Army Mat. & Mechanics Rsch. Ctr.
ATTN: Tech. Library

Commander
U.S. Army Materiel Dev. & Readiness Cmd.
ATTN: Tech. Library

Director
U.S. Army Materiel Sys. Analysis Acty.
ATTN: Joseph Sperazza

Commander
U.S. Army Missile Command
ATTN: J. Hogan
ATTN: F. Fleming
ATTN: W. Jann

Commander
U.S. Army Mobility Equip. R & D Ctr.
ATTN: Tech. Library
ATTN: STSFB-XS
ATTN: STSFB-MW

Commander
U.S. Army Nuclear Agency
ATTN: Tech. Library
ATTN: Doc. Control

Commander
U.S. Army Training And Doctrine Cmd.
ATTN: LTC J. Foss
ATTN: LTC Auveduti, COL Enger

Commandant
U.S. Army War College
ATTN: Library

U.S. Army Mat. Cmd. Proj. Mngr. for Nuc. Munitions
ATTN: DRCPM-NUC

DEPARTMENT OF THE NAVY

Chief of Naval Operations
ATTN: OP 982, LCDR Smith
ATTN: Code 604C3, Robert Piacesi
ATTN: OP 982, Lt Col Dubac
ATTN: CAPT Toole

DEPARTMENT OF THE NAVY (Continued)

Chief of Naval Research
ATTN: Tech. Library

Officer-In-Charge
Civil Engineering Laboratory
Naval Construction Battalion Center
ATTN: Tech. Library
ATTN: R.J. Odello

Commandant of the Marine Corps
ATTN: POM

Commanding General
Development Center
Fire Support Branch
ATTN: Lt Col Gaponski
ATTN: CAPT Hartneady

Commander
Naval Air Systems Command
ATTN: F. Marquardt

Commanding Officer
Naval Explosive Ord. Disposal Fac.
ATTN: Code 504, Jim Petrousky

Commander
Naval Facilities Engineering Command
ATTN: Tech. Library

Superintendent (Code 1424)
Naval Postgraduate School
ATTN: Code 2124, Tech. Rpts. Librarian

Director Naval Research Laboratory
ATTN: Code 2600, Tech. Library

Commander
Naval Sea Systems Command
ATTN: SEA-9931G
ATTN: ORD-033

Officer-In-Charge
Naval Surface Weapons Center
ATTN: M. Kleinerman
ATTN: Code WX21, Tech. Library
ATTN: Code WA501, Navy Nuc Prgms. Off.

Commander
Naval Surface Weapons Center
ATTN: Tech. Library

Commander
Naval Weapons Center
ATTN: Carl Austin
ATTN: Code 533, Tech. Library

Commanding Officer
Naval Weapons Evaluation Facility
ATTN: Tech. Library

Director
Strategic Systems Project Office
ATTN: NSP-43, Tech. Library

DEPARTMENT OF THE AIR FORCE

AF Armament Laboratory, AFSC
3 cy ATTN: John Collins, AFATL/DLYV
ATTN: Masey Valentine

AF Institute of Technology, AU
ATTN: ATTN: Library, AFIT Bldg. 640, Area B

AF Weapons Laboratory, AFSC
ATTN: SUL

Assistant Secretary of the Air Force
Research & Development
ATTN: Col R.E. Steere

Deputy Chief of Staff
Research & Development
ATTN: Col J.L. Gilbert

Commander
Foreign Technology Division, AFSC
ATTN: NICD Library

Hq. USAF/IN
ATTN: INATA

Hq. USAF/RD
ATTN: RDPM

Oklahoma State University
Fld. Off. for Wpns. Effectiveness
ATTN: Edward Jackett

Commander
Rome Air Development Center, AFSC
ATTN: EMTLD Doc. Library

SAMSO/RS
ATTN: RSS

DEPARTMENT OF ENERGY

Department of Energy
ATTN: Doc. Con. for Tech. Library

Division of Headquarters Services
ATTN: Doc. Con. for Class. Tech. Library

Department of Energy
ATTN: Doc. Con. for Tech. Library

Division of Military Application
ATTN: Doc. Con. for Test Office

University of California
Lawrence Livermore Laboratory
ATTN: Mark Wilkins, L-504
ATTN: Tech. Infor. Dept., L-3
ATTN: Jerry Goudreau

Los Alamos Scientific Laboratory
ATTN: Doc. Con. for Tom Dowler
ATTN: Doc. Con. for Reports Library

Sandia Laboratories
ATTN: Doc. Control for Tech. Library

DEPARTMENT OF ENERGY (Continued)

Sandia Laboratories
ATTN: Doc. Con. for William Caudle
ATTN: Doc. Con. for William Patterson
ATTN: Doc. Con. for John Ketzur
ATTN: Doc. Con. for 3141, Sandia Rpt. Coll.
ATTN: Doc. Con. for John Colp
ATTN: Doc. Con. for Walter Herrmann
ATTN: Doc. Con. for W. Altsmeirer

OTHER GOVERNMENT AGENCIES

NASA
Ames Research Center
ATTN: Robert W. Jackson

Office of Nuclear Reactor Regulation
Nuclear Regulatory Commission
ATTN: Robert Heineman
ATTN: Lawrence Shao

DEPARTMENT OF DEFENSE CONTRACTORS

Aerospace Corporation
ATTN: Tech. Info. Services

Agbabian Associates
ATTN: M. Agbabian

Applied Theory, Inc.
2 cy ATTN: John G. Trulio

Avco Research & Systems Group
ATTN: Pat Grady
ATTN: Research Library, A830 Rm. 7201
ATTN: David Henderson
ATTN: S. Skomp, J200

Battelle Memorial Institute
ATTN: Tech. Library

The BDM Corporation
ATTN: Tech. Library

The Boeing Company
ATTN: Aerospace Library

California Research & Technology, Inc.
ATTN: Tech. Library
ATTN: Ken Kreyenhagen

Civil/Nuclear Systems Corporation
ATTN: Robert Crawford

EG&G, INC.
ATTN: Tech. Library

Engineering Societies Library
ATTN: Ann Mott

General Dynamics Corporation
ATTN: Keith Anderson

General Electric Company
TEMPO-Center for Advanced Studies
ATTN: DASIAC

DEPARTMENT OF DEFENSE CONTRACTORS (Continued)

Georgia Institute of Technology
ATTN: S.V. Hanagud
ATTN: L.W. Rehfield

Honeywell, Incorporated
ATTN: T.N. Helvig

Institute for Defense Analyses
ATTN: IDA Librarian, Ruth S. Smith

Kaman Avidyne
Division of Kaman Sciences Corporation
ATTN: Tech. Library
ATTN: Norman P. Hobbs
ATTN: B.S. Crisclone

Kaman Sciences Corporation
ATTN: Library

Lockheed Missiles & Space Co., Inc.
ATTN: Tech. Library
ATTN: M. Culp

Lockheed Missiles & Space Co., Inc.
ATTN: Tech. Infor. Ctr. D/COLL

Martin Mariotta Corporation
ATTN: Al Cowen
ATTN: H. McQuaig
ATTN: M. Anthony

Morritt Cases, Inc.
ATTN: Tech. Library
ATTN: J.L. Morritt

University of New Mexico
Dept. of Campus Security and Police
ATTN: G.E. Triandafulidis

Nathan M. Newmark
Consulting Engineering Services
ATTN: Nathan M. Newmark
ATTN: W. Hall

Pacifica Technology
ATTN: G. Kent
ATTN: R. Bjork

DEPARTMENT OF DEFENSE CONTRACTORS (Continued)

Physics International Company
ATTN: Doc. Con. for Dennis Orphal
ATTN: Doc. Con. for Larry A. Behrmann
ATTN: Doc. Con. For Tech. Library

R & D Associates
ATTN: William B. Wright, Jr.
ATTN: Paul Rausch
ATTN: Arlen Fields
ATTN: Henry Cooper
ATTN: Cyrus P. Knowles
ATTN: Tech. Library
ATTN: Harold L. Brode
ATTN: J.G. Lewis

The Rand Corporation
ATTN: Tech. Library

Science Applications, Inc.
ATTN: Tech. Library

SRI International
ATTN: Jim Colton
ATTN: George R. Abrahamson

Systems, Science and Software, Inc.
ATTN: Tech. Library
ATTN: Edward Gaffney
ATTN: Robert Sedgewick

Terra Tek, Inc.
ATTN: Tech. Library

TRW Defense & Space Sys. Group
ATTN: Peter K. Dai, R1/2170
ATTN: Tech. Info. Center/S-1930

TRW Defense & Space Sys. Group
ATTN: E.Y. Wong 527/712

Weidlinger Assoc. Consulting Engineers
ATTN: J.M. McCormick
ATTN: Melvin L. Baron

Weidlinger Assoc. Consulting Engineers
ATTN: J. Isenberg